CRYOGENICS FOR PARTICLE ACCELERATORS AND DETECTORS

Ph. Lebrun, L. Tavian, G. Vandoni & U. Wagner

Lectures given at the CAS School on Superconductivity and Cryogenics
for Particle Accelerators and Detectors
Erice, Sicily, 8-17 May 2002

CONTENTS

FOREWORD

Cryogenics has become a key ancillary technology of particle accelerators and detectors, contributing to their sustained development over the last fifty years. Conversely, this development has produced new challenges and markets for cryogenics, resulting in a fruitful symbiotic relation which materialized in significant technology transfer and technical progress. This began with the use of liquid hydrogen and deuterium in the targets and bubble chambers of the 1950s, 1960s and 1970s. It developed more recently with increasing amounts of liquefied noble gases – mainly argon, but also krypton and even today xenon - in calorimeters. In parallel with these applications, the availability of practical type II superconductors from the early 1960s triggered the use of superconductivity in large spectrometer magnets – mostly driven by considerations of energy savings – and the corresponding development of helium cryogenics. It is however the generalized application of superconductivity in particle accelerators – RF acceleration cavities and high-field bending and focusing magnets – that has led to the present expansion of cryogenics, with kilometer-long strings of helium-cooled devices, powerful and efficient refrigerators and superfluid helium used in high tonnage as cooling medium.

This situation was well reflected over the last decades by the topical courses of the CERN Accelerator School (CAS). In 1988, CAS and DESY jointly organized the first school on Superconductivity in Particle Accelerators, held at Haus Rissen in Hamburg, where I shared the honor and duty of lecturing on cryogenics with Professor J.L. Olsen of ETH Zürich, while P. Seyfert of CEA Grenoble delivered an evening seminar on superfluidity. This successful school was reiterated in 1995, with cryogenics being addressed by Professor W.F. Vinen of University of Birmingham (superfluidity), as well as J. Schmid (thermodynamics and refrigeration) and myself (superfluid helium technology) of CERN. In the CAS School on Superconductivity and Cryogenics for Particle Accelerators and Detectors held in May 2002 in Erice, Sicily, I am particularly pleased to see a more complete syllabus in cryogenics, most of which is covered by CERN colleagues and published in this report. This is in my view, another sign of the development and vitality of this discipline at CERN, primarily in the LHC division which, by virtue of its mandate and competence, is presently building the largest helium cryogenic system in the world for the Large Hadron Collider and its experiments. I hope this report constitutes a useful source of information and updated reference for our staff dedicated to this formidable endeavour.

Philippe Lebrun

REFRIGERATION

U. Wagner
CERN, Geneva, Switzerland

Abstract
This introduction to cryogenic refrigeration is written in the frame of the CERN Accelerator School (CAS) Course on Superconductivity and Cryogenics. It consequently concerns refrigeration for cooling of superconductive devices with emphasis on liquid helium refrigeration. Following a general reminder of the thermodynamics involved, i.e. principally the first and second laws, the different thermodynamic cycles used to produce low temperatures are presented. Refrigerators working according to the different cycles are explained starting with the low-capacity range covered by cryocoolers and then concentrating on Claude-cycle refrigerators. The different thermodynamic and technological elements of a Claude-cycle refrigerator are discussed and an example for a large refrigerator used in an accelerator equipped with superconducting magnets is presented.

1. INTRODUCTION

The cryogenic temperature range has been defined as from -150 ˚C (-123 K) down to absolute zero (-273 ˚C or 0 K), the temperature at which molecular motion comes as close as theoretically possible to ceasing completely [1].

The application of cryogenics can roughly be separated into five major domains:

i) Liquefaction and separation of gases

ii) Storage and transport of gases

iii) Altering material and fluid properties by reduced temperature

iv) Biological and medical applications

v) Superconductivity

With the exception of the quest to get closer and closer to the absolute zero, in all the cases listed above cryogenics is a utility enabling the desired application or function. Since the first liquefaction of helium by Heike Kammerlingh Onnes in 1908, cryogenics has evolved in an engineering science combining different technologies in a "best compromise" to achieve a given goal. This should be remembered when reading the following paragraphs as several of the presented technological solutions are governed not only by the optimum achievable, in terms of e.g. efficiency or performance but as well by cost of investment and operation.

For particle accelerators, cryogenics is an ancillary technology for enabling the superconducting operation of accelerating or beam-positioning devices. Thus the choice of a cryogenic system is largely determined by the superconductors used.

1.1 Critical and operating temperatures of superconductors

In order to operate superconducting devices it is evident that the cooling agent used must have a temperature significantly below the temperature of superconductive transition, or critical temperature of the superconductor used. Table 1 lists the critical temperatures of some commercially available materials.

Table 1
Critical temperature of superconducting materials

Material	T_c [K]
Pb	7.2
Nb	9.2
Nb-Ti alloys	~ 9.6
Nb_3Sn	18.1
Nb_3Ge	23.2
$Y_1Ba_2Cu_3O_{7-x}$ (YBCO)	90
$BI_2Sr_2Ca_1Cu_2O$ (Bi2212)	80
$BI_2Sr_2Ca_2Cu_3O$ (Bi2223)	125

1.2 Properties of cryogenic fluids

The cryogenic fluid is both the working and cooling agent of the cryogenic system. To be considered "cryogenic" only those having a triple point below 100 K are considered, i.e. they are in either liquid or gaseous form below this temperature. Table 2 shows some properties of cryogenic fluids. The critical temperature of the fluid refers to the upper limit at which the liquid phase may appear.

Since the disappearance of liquid hydrogen bubble chambers, hydrogen is very little used as cryogenic cooling fluid and oxygen is never used due to the serious hazards implied. Neon though being an inert gas is very expensive and has therefore very rarely been considered up to now. Consequently the only fluids used are helium and nitrogen. The emergence of the high-Tc superconducting materials has opened the way to use nitrogen as cooling fluid. As the range of application using nitrogen is limited by its triple point still today the prevailing cryogen is helium.

Table 2
Property data of cryogenic fluids

Fluid		^4He	H_2	Ne	N_2	O_2
Normal boiling point	[K]	4.22	20.4	27.2	77.4	90.2
Critical temperature	[K]	5.20	33.2	44.4	126.	155.
Critical pressure	[MPa]	0.23	1.32	2.72	3.39	5.08
Triple point temperature	[K]	2.18*	14.0	24.6	63.1	54.4
Triple point pressure	[kPa]	5.04*	7.20	43.2	12.8	0.15
Liquid density at ambient pressure	[kg/m^3]	125.	70.8	1204.	808	1140
Vapour density at ambient pressure	[kg/m^3]	16.7	1.33	9.46	4.59	4.75
Normal density	[kg/m^3]	0.18	0.09	0.90	1.25	1.43

*: Lambda point

Helium shows the particularity that it has no triple point, it may solidify only at pressures above 2.5 MPa. The commonly quoted lambda point refers to the transition from normal to superfluid helium.

2. BASIC ENGINEERING THERMODYNAMICS

Cooling in a steady-state process is done by letting a working fluid undergo a series of cyclic thermodynamic transformations, called a thermodynamic cycle. The working fluid absorbs heat at low temperatures and rejects it at higher temperatures.

2.1 The Carnot factor

The Carnot factor is the predominant estimator for all low-temperature process considerations. It is named after Sadi Carnot, who in his "Réflexions sur la puissance motrice du feu" introduced first the concept that the work that can be extracted from a heat engine depends on the temperatures between

which this engine works. For a heat engine, the Carnot factor defines the maximum amount of work that can be extracted from a process operating between two temperature levels. For a heat pump, or a refrigerator, it defines the minimum amount of work necessary to extract heat at a low temperature and reject it at a higher one. In fact, the Carnot factor is a direct consequence of combining the first and second law of thermodynamics. Consider an open process removing heat from a given (cold) temperature level and rejecting it at a higher level as sketched in Fig. 1.
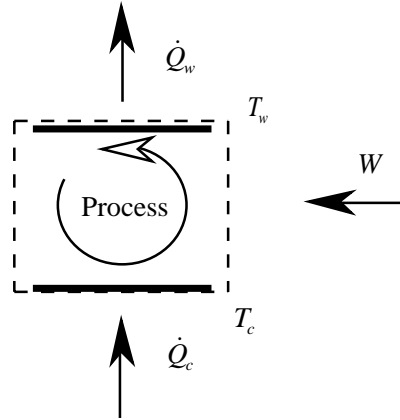

Fig. 1 Basic open process transporting thermal energy from any temperature to a higher temperature level.

The first law of thermodynamics expresses the conservation of energy.

$$\dot{Q}_w + \dot{Q}_c + W = 0 \tag{1}$$

The second law of thermodynamics defines that in any process the entropy is either constant (reversible process) or increased (irreversible process) but never diminished.

$$\frac{\dot{Q}_w}{T_w} + \frac{\dot{Q}_c}{T_c} \leq 0 \tag{2}$$

Combining equation (1) and (2) one can calculate the necessary power input into the process.

$$W \geq \dot{Q}_c \left(\frac{T_w}{T_c} - 1 \right) \tag{3}$$

The Carnot factor is defined as:

$$\left(\frac{T_w}{T_c} - 1 \right)$$

By convention heat or work is considered positive when entering the system and negative when leaving the system.

Fig. 2 shows the Carnot factor as function of the cold temperature with 300 K as warm reference temperature. It is quickly evident that the energy necessary to extract heat below 20 K increases rapidly with decreasing temperature. It is further not astonishing that for T -> 0 K the Carnot factor goes to infinity. Besides defining the minimum work necessary to extract heat in a reversible process, the Carnot factor clearly demonstrates why in any cryogenic system heat entering the low temperature level should be limited to the minimum. The refrigeration work in real systems is always above the limit given by the Carnot factor due to the inevitable irreversibilities.
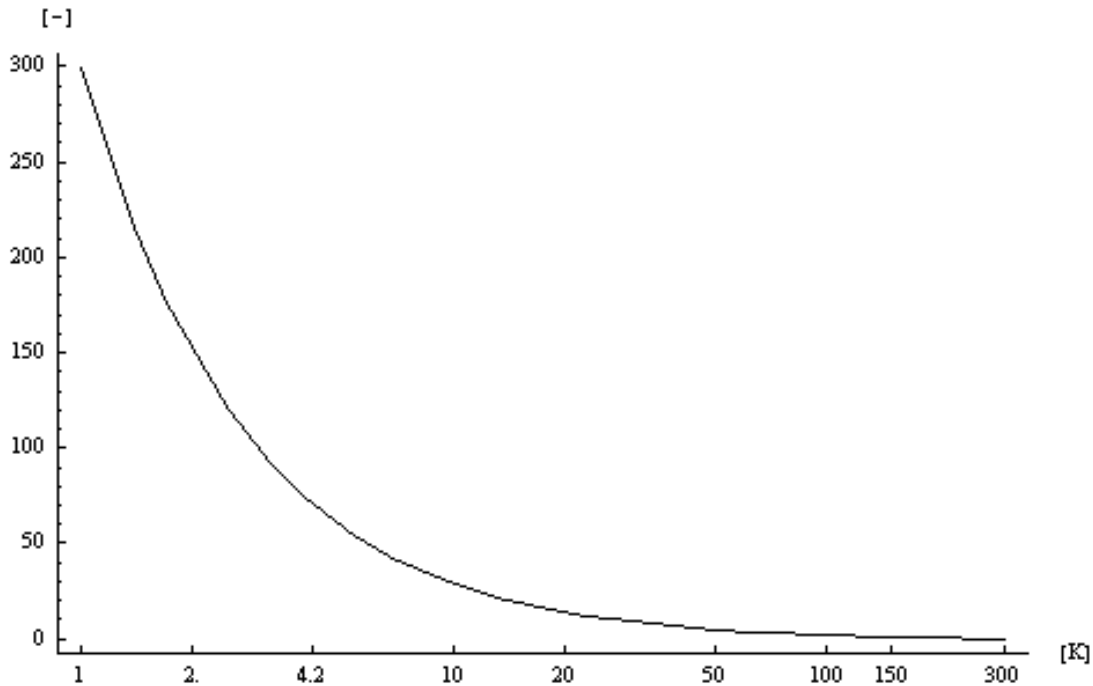
Fig. 2 Carnot factor as function of cold temperature for $T_W = 300$ K.

2.2 The T-s diagram

Within the number of different phase diagram for fluids, the temperature-entropy [T-s] diagram is the most practical to illustrate the different cycles used for the closed cryogenic processes.

In a T-s diagram the reversibly exchanged heat for any change of state is represented by the area under the path for the change of state. This allows to compare the heat exchanged for different process changes. Fig. 3 shows the commonly used T–s diagram issued by the National Bureau of Standards (NBS, now National Institute of Standards and Technology, NIST).

For low-temperature application it is may be convenient to use a T-s diagram with a logarithmic temperature scale. In this case for any ideal gas the isochors, isobars, and isenthalps are straight lines; moreover the isenthalps coincide with the isotherms. To go one step further, if the lines for constant enthalpy, pressure or volume are straight in a logarithmic T-s diagram for a real gas, on can deduce that in these areas the gas behaves like an ideal gas. Taking the logarithmic T-s diagram for helium, we quickly can establish that ideal gas laws are sufficient to calculate a process above a temperature of 10 K and an entropy of 13 J/g K covering a large part of any helium cycle. Close to the two-phase area and below 2.2 K helium becomes anything but ideal [2], detailed calculation of any process needs to relate of the real gas data. Another advantage of the logarithmic T-s diagram is that the cold area, i.e. the one of interest, is best represented. The disadvantage of the logarithmic temperature scale is that the area under the path for a change of state does not represent the reversibly exchanged heat. Fig. 4 shows a logarithmic T-s diagram in order to illustrate the statements above. The author agrees that this document, dated from 1941, is difficult to read and from a time prior to SI units. It is nevertheless the only such document he could lay hands on.

The world reference for the helium properties is NIST Technical note 1334 (1989) [3]. The property equations serving as basis for this note have been compiled into a program by its authors, and is commercially available [4].
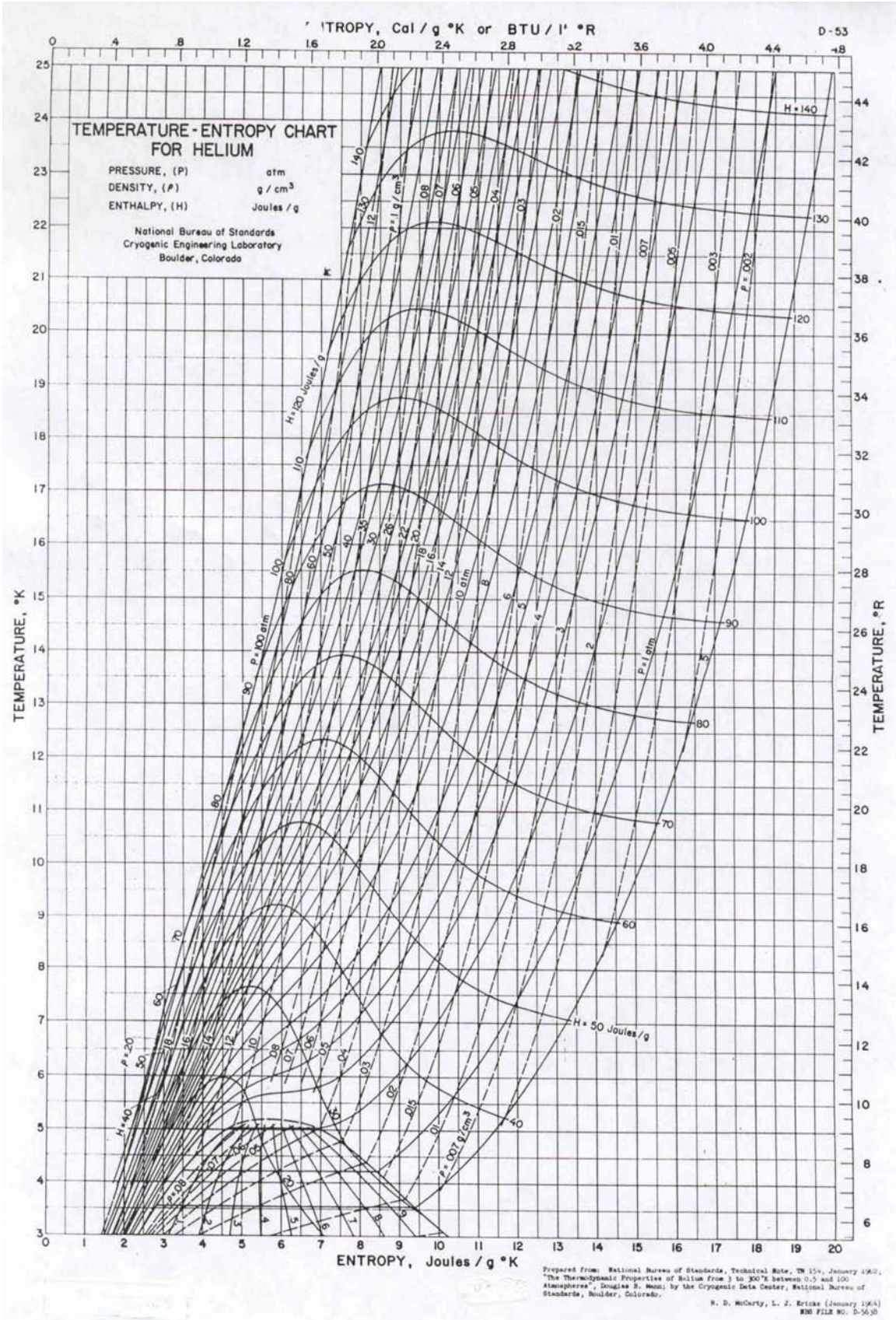
4

Fig. 3 T-s Diagram for helium (issued by NBS).

Fig. 4 LogT-s diagram for helium (issued by: Institut International du Froid).

The use of T-s diagrams for designing any process has significantly decreased since the widespread use of calculation software in combination with the property data. It should nevertheless be mentioned that the representation of a process in a T-s diagram considerably eases its understanding.

2.3   The basic cryogenic refrigeration cycles

All cycles listed below are "ideal" cycles, meaning they do follow ideal transformations that in reality can only be approximated. Some of these cycles are easier to realise with existing technology than others as it is possible to achieve nearly isobaric heat exchange, whereas it is very difficult to achieve any isentropic change of state. Of the multitude of possible thermodynamic cycles only those with frequent application in cryogenics are listed. Please note that some of these cycles may as well appear under a different name in literature; the identification used in this work corresponds to the most widespread in the cryogenic community as far as experienced by the author.

The <u>Carnot cycle</u> as the ideal cycle represents the reference to which any other process is measured. The process follows a sequence of isothermal expansion, isentropic compression, isothermal compression and isentropic expansion.

The <u>Stirling cycle</u> follows a sequence of isothermal expansion, isochoric compression, isothermal compression and isochoric expansion.

The <u>Ericsson cycle</u> follows a sequence of isothermal expansion, isobaric heating, isothermal compression and isobaric cooling.

Fig. 5 shows the these three cycles in a logarithmic T-s diagram for ideal gas. The necessary work input for all three cycles would in this case be equal, in other words all three cycles would have the some efficiency.
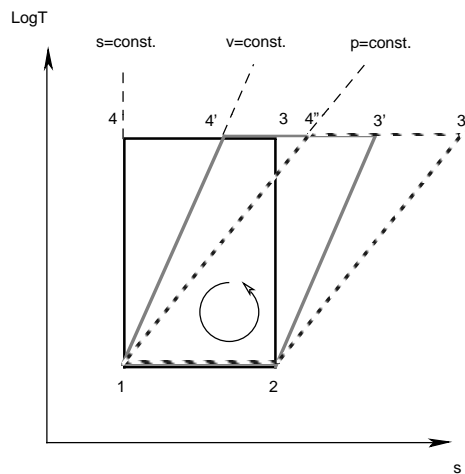
Fig. 5 Carnot cycle (1,2,3,4), Stirling cycle (1,2,3',4') and Ericsson cycle (1,2,3",4").

The <u>Brayton cycle</u>, follows a sequence of isentropic expansion, isobaric heating, isentropic compression and isobaric cooling.

Fig. 6 shows the Brayton cycle in comparison to the Ericsson cycle. In this comparison, the cooling capacity of the Brayton cycle is inferior to that of the Ericsson cycle though it is available at a lower temperature, the work input into the Brayton cycle is higher. These two aspects immediately qualify the Brayton cycle as less efficient. Though by definition less efficient then the three cycles shown in Fig. 5 , this cycle combines thermodynamic transformations that are easier to approximate in real systems, thus making it one of the references for cryogenic refrigeration.
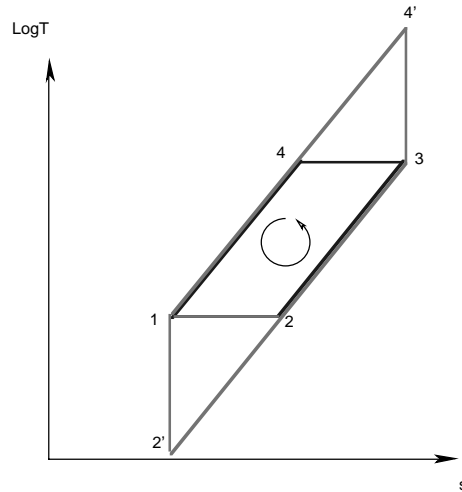
Fig. 6 Ericsson cycle (1,2,3,4) and Brayton cycle (1,2',3,4').

2.4   Real gas aspects

A real gas is characterised by the fact that $pV \neq RT$. In this case isenthalpic expansion, e.g. in a valve can produce cooling. This effect is called the Joule-Thomson effect and happens in a property region limited by the Joule-Thomson inversion curve that is dependent on temperature and pressure [5]. The two cycles listed below make use of this effect.
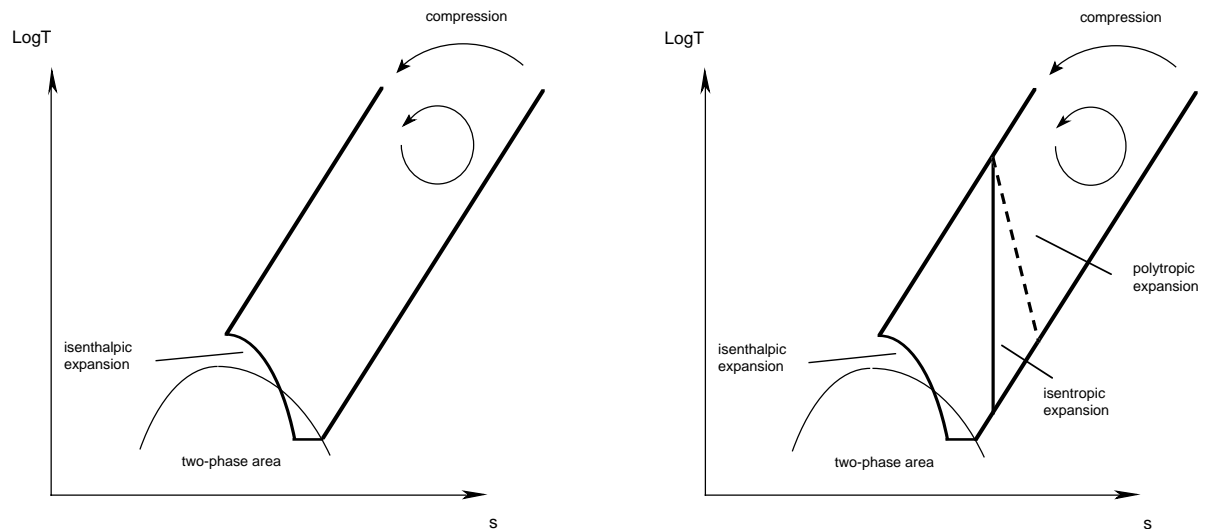
Fig. 7 Joule-Thomson cycle (left) and Claude cycle (right) for a real gas.

The Joule-Thomson (J-T) cycle combines isobaric cooling and heating with isothermal compression and isenthalpic expansion. For an ideal case the expansion would be isotherm, leading back to the Ericsson cycle.

The Claude cycle is in fact a combination of one (or more) Brayton cycles and a Joule–Thomson cycle at the cold end.

Fig. 7 shows these two cycles in an simplified logarithmic T-s diagram for real gas. The compression is not further qualified, and we concentrate only on the cycle part below atmospheric temperature. In the Joule-Thomson cycle the total amount of gas is cooled isobaric to a point close to

the two-phase zone. The isenthalpic expansion then results in the creation of a two-phase fluid. This cycle was first applied by Linde for the industrial liquefaction of air. In the Claude cycle, part of the gas is expanded at an intermediate temperature in an expansion machine that ideally would realise an isentropic expansion; in the real case the expansion is polytropic as sketched in Fig. 7. This cycle was used and patented by Claude for the liquefaction of air, leading to a considerably higher total efficiency than the Joule-Thomson cycle.

A process based on a pure Joule-Thomson cycle and starting from ambient temperature can only be used to liquefy a gas that has a Joule-Thomson inversion temperature above ambient. This is the case for nitrogen, oxygen and air. Helium, hydrogen and neon cannot be liquefied in a Joule-Thomson process as sketched. The first liquefaction process for helium by Kammerlingh Onnes used a cascade of Joule-Thomson cycles.

In a Claude cycle any gas can be liquefied; it is today the prevailing process arrangement for the liquefaction of helium. Though thermodynamically less efficient then the cycles listed in section 2.3, it is best adapted to technical realisation.

2.5 Cycle efficiencies

The efficiency of a cycle to produce cooling at liquid helium temperature determines the cost of operation for the refrigerator. As concerns the total cycle efficiency, two ways of calculation are commonly used, the Carnot efficiency and the exergetic efficiency. The latter can be directly derived from the Carnot efficiency and has the advantage of additionally providing a means to analyse any part of the process as concerns its contribution to losses.

2.5.1 Carnot efficiency

The Carnot factor as presented in section 2.1, defines the theoretical limit for an amount of energy to be injected in a cooling process. Consequently the efficiency of any process is expressed as efficiency relative to the Carnot factor or, in short, Carnot efficiency.

$$\eta_{carnot} = \frac{W_{carnot}}{W_{effective}} \cdot 100 \ [\%] \tag{4}$$

2.5.2 Exergetic efficiency

The concept of "énergie utilisable" was invented by Gouy in 1889 [6],the term "exergy" was coined by Rant in 1956 [7]. Exergy takes into consideration both the energy and its thermodynamic grade i.e. the Carnot factor based on T_W equal to the ambient temperature. Applying the equation (3) to a non-isothermal process between the two cold temperatures T_{c1} and T_{c2} and assuming no irreversibility, yields:

$$W_{\min} = \int_{T_{C1}}^{T_{C2}} d\dot{Q}_C \left(\frac{T_W}{T} - 1 \right) \tag{5}$$

Assuming further that we have a working fluid to which the heat is transferred at the relevant temperature level, again without irreversibility i.e. no temperature difference and no pressure losses, we can write for this fluid:

$$W_{\min} = -T_W \int_{T_{C1}}^{T_{C2}} \frac{d\dot{Q}_C}{T} + \int_{T_{C1}}^{T_{C2}} d\dot{Q}_C \tag{6}$$

9

Respectively:

$$W_{\min} = -T_W \int_{T_{C1}}^{T_{C2}} dS + \int_{T_{C1}}^{T_{C2}} T dS \tag{7}$$

For the case of a steady-state fluid process, that is often considered for a process definition, and by using the specific properties of state at the inlet and outlet of the considered cooling process one can transform equation (7) to:

$$W_{\min} = -T_W \dot{m}(s_{T_{C2}} - s_{T_{C1}}) + \dot{m}(h_{T_{C2}} - h_{T_{C1}}) \tag{8}$$

Equation (8) defines the exergetic capacity the fluid absorbs, i.e. the exergetic capacity required to cool the process considered. T_W in this case represents the reference temperature on which finally all heat and work absorbed by the process will be rejected as heat flow. For our earthbound system this is the ambient temperature, usually set to 300 K.

In other words the exergetic capacity describes the necessary effort to change in any thermal process the temperature as compared to the natural equilibrium temperature given by our earthbound environment.

The specific exergy, defined as:

$$e = -T_{ambient}s + h \tag{9}$$

is a combined property of state once $T_{ambient}$ is defined.

It is very convenient to calculate the exergetic capacity of any cooling process using the inlet and outlet conditions of the cooling fluid taking the heat. It equals the refrigeration capacity multiplied by the Carnot factor. Exergetic efficiency can be calculated for any part of a process by comparing the exergy flow balance on the input and output boundaries.

$$\eta_{exergetic} = \left| \frac{\sum\limits_{output\ boundary} \dot{m}(-T_{ambient}s + h)}{\sum\limits_{input\ boundary} \dot{m}(-T_{ambient}s + h)} \right| 100\ [\%] \tag{10}$$

The absolute value is necessary as exergy, like energy is defined positive when flowing into the boundary, and negative when flowing out.

As electrical power is defined as pure exergy, it has the same "value" independent of the temperature where it is used, the exergetic efficiency for a total process can therefore be written as:

$$\eta_{exergetic} = \left| \frac{\sum\limits_{cooling\ boundary} \dot{m}(-T_{ambient}s + h)}{P_{electric\ input}} \right| 100\ [\%] \tag{11}$$

An exergy analysis determining the exergetic losses for a process and its different parts is an excellent tool for cycle analysis. The sum of the losses for the different parts equals the total loss and the contribution of the individual losses to the total can therefore be quantified.

2.5.3   Achieved efficiencies in cryogenic equipment

Fig. 8 shows a large number of realised cryogenic refrigeration systems plotted with their Carnot efficiency versus refrigeration capacity at 4.5 K. It is significant to note, that the efficiency increases with refrigeration capacity and seems not dependent on the technical solution.

The reason for this behaviour may be explained by the combination of several factors, both technological and commercial. Technologically the larger the equipment the higher individual efficiency, especially for rotating machines like turbo-expanders. The incentive to spend more on equipment in order to save on operation increases with the absolute value of the power consumption. Moreover, the relative increase in investment cost for a more efficient machine is smaller for a large refrigerator.

The plot shown in Fig. 8 must be understood under these two aspects, it does not represent a law of physics. Experience nevertheless show that the tendency shown in the graph is universal.

It should be mentioned at this point that any helium refrigerator represents a complex system combining different technologies in a "best compromise" following the taste of the designer and the requirements of the user for whom it was built. Both of which may influence the efficiency of the installation in one way or other.
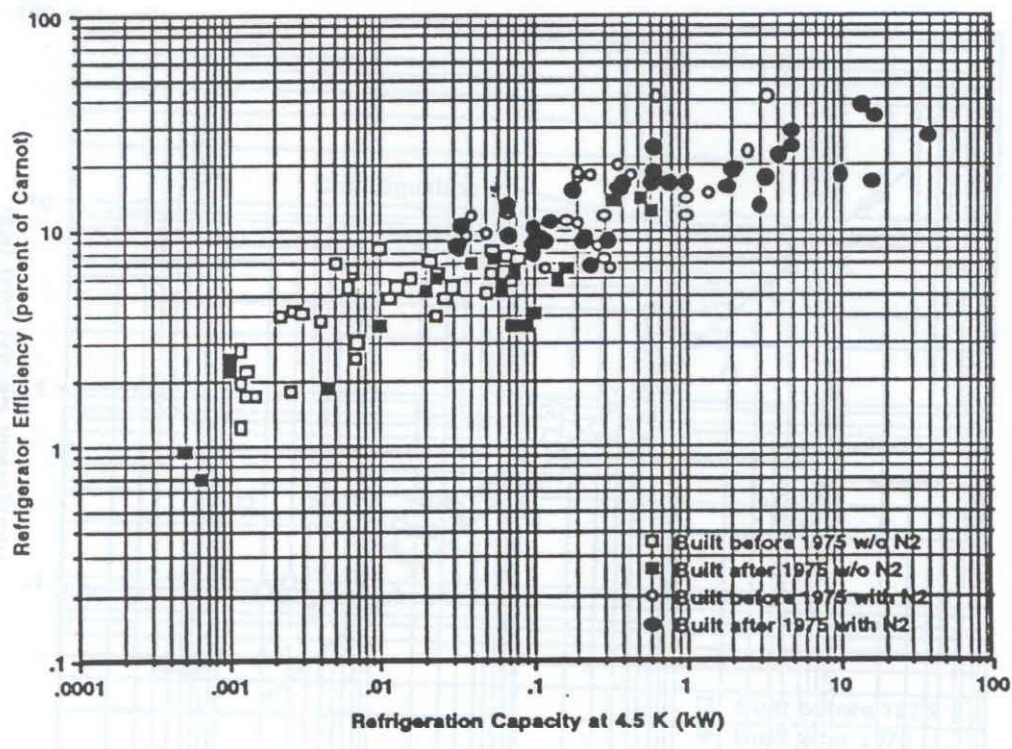
Fig. 8 Efficiency of cryogenic refrigeration systems (from [8]).

2.6   Liquefaction and refrigeration

The two terms of liquefier and refrigerator are often used for the same type of cryogenic machinery. The two processes of liquefaction and refrigeration are in fact basically different. A "pure" refrigerator delivers only isothermal cooling capacity at the liquid temperature of the working fluid. A liquefier uses its cooling capacity to cool a part of the working fluid from ambient to its boiling point and

supply this in liquid form as the final product of the process. The two process variants are sketched in Fig. 9.
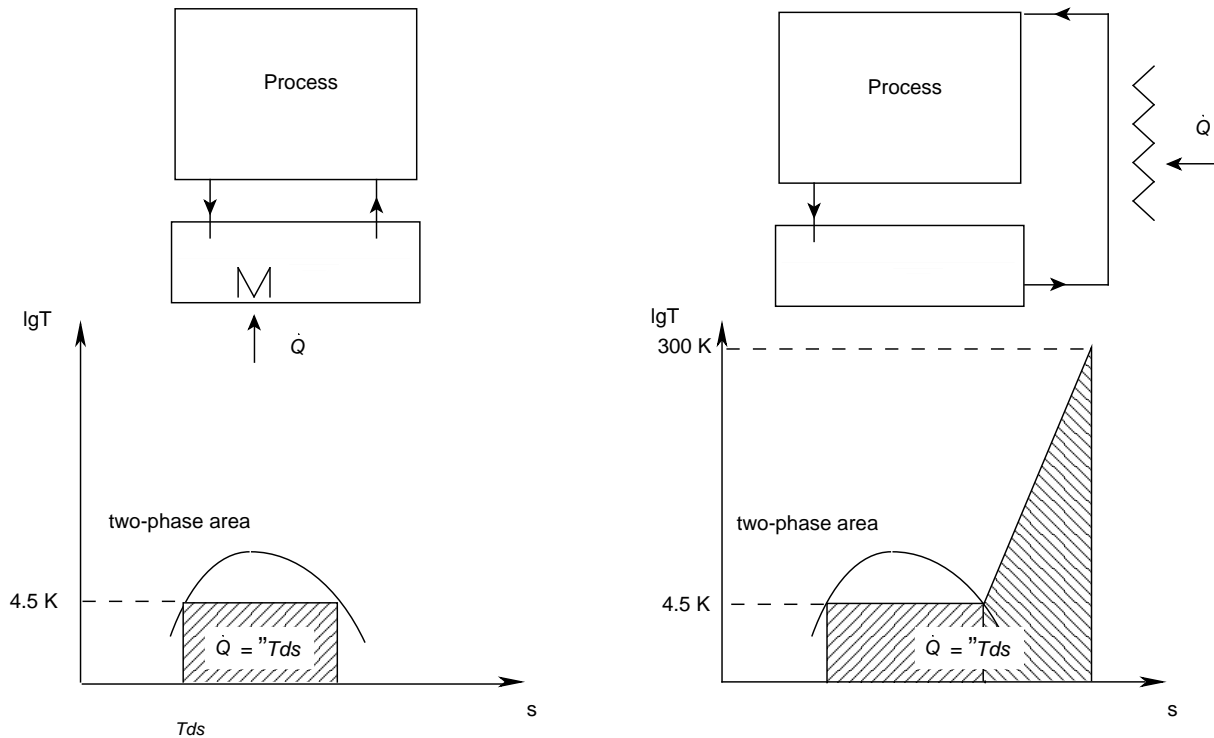
Fig. 9 Comparison of cryogenic refrigeration (left) and liquefaction (right).

Remembering the remark from section 2.2 we may identify that the reversibly exchanged heat for a given mass flow is considerably higher for a liquefier than for a refrigerator.

2.7   Equivalent isothermal capacity

Following the Carnot factor it is evident that the effort necessary to extract heat at low temperatures is strongly temperature dependent. For pure isothermal cooling in a two-phase bath it is evident to relate cooling capacity and cooling temperature. For non-isothermal cooling, like for liquefaction, this becomes more difficult. In order to compare capacities of cryogenic machines the equivalent capacity was introduced, expressing the total cooling capacity as equivalent isothermal refrigeration at 4.5 K.

For practical reasons for pure liquefiers one refers to the capacity rather by defining the liquefaction flow either in volume flow or mass flow.

The equivalent capacity represents an exergy calculation for the different cooling capacities referred to the exergetic capacity of pure refrigeration at 4.5 K. If we can compare the exergetic capacity necessary to liquefy one g/s of helium from 300 K to 4.5. K with the same exergetic capacity for pure refrigeration at 4.5 K.

Table 3 shows the property data for helium at 4.5 K vapour, 4.5 K liquid and conditions. The exergetic capacity for the liquefaction of 1 g/s helium can be calculated to: 6754 W. For the same exergetic capacity we may evaporate 5.47 g/s of liquid helium which would have an isothermal cooling of 103 W. One may therefore roughly say that 1 g/s of liquefied helium needs an equivalent effort as isothermal cooling of 100 W.

Table 3
Property data for helium to define the equivalent capacity of liquefaction and refrigeration

Temperature [K]	Pressure [kPa]	Entropy [kJ/kg K]	Enthalpy [kJ/kg]	Exergy [kJ/kg]
300	100	31.61	1574	-7910
4.5 (vapour)	100	8.067	30.47	-2390
4.5 (liquid)	100	3.893	11.64	-1156

3.   COOLING METHODS

For an experimentalist having e.g. a small sample to cool to low temperatures the choices for supplying the cooling are the following:

i)   Buying liquid helium, use it to cool the sample and let it evaporate to atmosphere.

ii) Buying liquid helium, recover the evaporated gas and return this in compressed form to the vendor.

iii) Buying gaseous helium and a refrigerator producing cooling capacity in closed cycle

These three simple cases change the necessary infrastructure for cryogenics considerably. In the first case one may install one big central dewar storing the helium from which one fills smaller, transportable dewars that supply the experiment cryostat. In the second case this equipment is increased by a recovery system, usually using balloons, a purification unit and a compression system with high pressure gas tanks. In the last case one may find a whole range of systems from compact cryocoolers supplying cooling to a small experiment over an installation with central liquefier, storage dewar, transport dewars, recovery and purification system, to a dedicated refrigerator for any large experiment including cryogenic distribution system with liquid helium transfer lines, recovery systems, purification systems and gas storage.

Cryogenic installations may become specialised systems of their own requiring considerable investment and operating cost. For anybody approaching this problem for the first time it is therefore recommended to ask for advice at institutions where such an infrastructure already exists.

The following chapters describe the principle machinery of cryogenic cooling equipment emphasising on helium refrigeration systems down to 4.2 K. As concerns systems using nitrogen as cooling agent a very common equipment are Stirling refrigerators for a midrange capacity of about 20 kilowatt at 80 K. Otherwise liquid nitrogen is a comparably cheap, widely available fluid generally used in open circuit, i.e. returning the evaporated gas to atmosphere where it originated.

4.   CRYOCOOLERS

Cryocooler is the common name for refrigerators with small capacity ($\leq$ 10 W at 4.5 K). These refrigerators are very compact and avoid the need of extensive systems. A typical example for commercial use are the magnetic resonance imaging (MRI) systems where a cryocooler covers the heat losses of the liquid helium cryostat. A wide range of cryocoolers has been developed. The most common on the market are still Gifford-McMahon-type refrigerators. In recent years the development of pulse tube cryocooler made impressive progress and this equipment will become more and more frequently used.

This course is held within the frame of the CERN Accelerator School. For particle accelerator devices, cryocoolers are in general not applicable as they lack the necessary capacity, especially concerning liquefaction. The selection below is therefore mainly intended to demonstrate the application of different cycles and in order to remind that for the small capacity range this equipment may be advantageously chosen.

4.1 Stirling cryocoolers

Though these machines are not widely used as cryocoolers the realised performance ranges from less than one watt to some tens of kilowatts at a temperature of 20 K to 80 K.

The Stirling cycle is realised following the simplified process in Fig. 10. The numbering of the different process stages follows that of the Stirling cycle in Fig. 5.
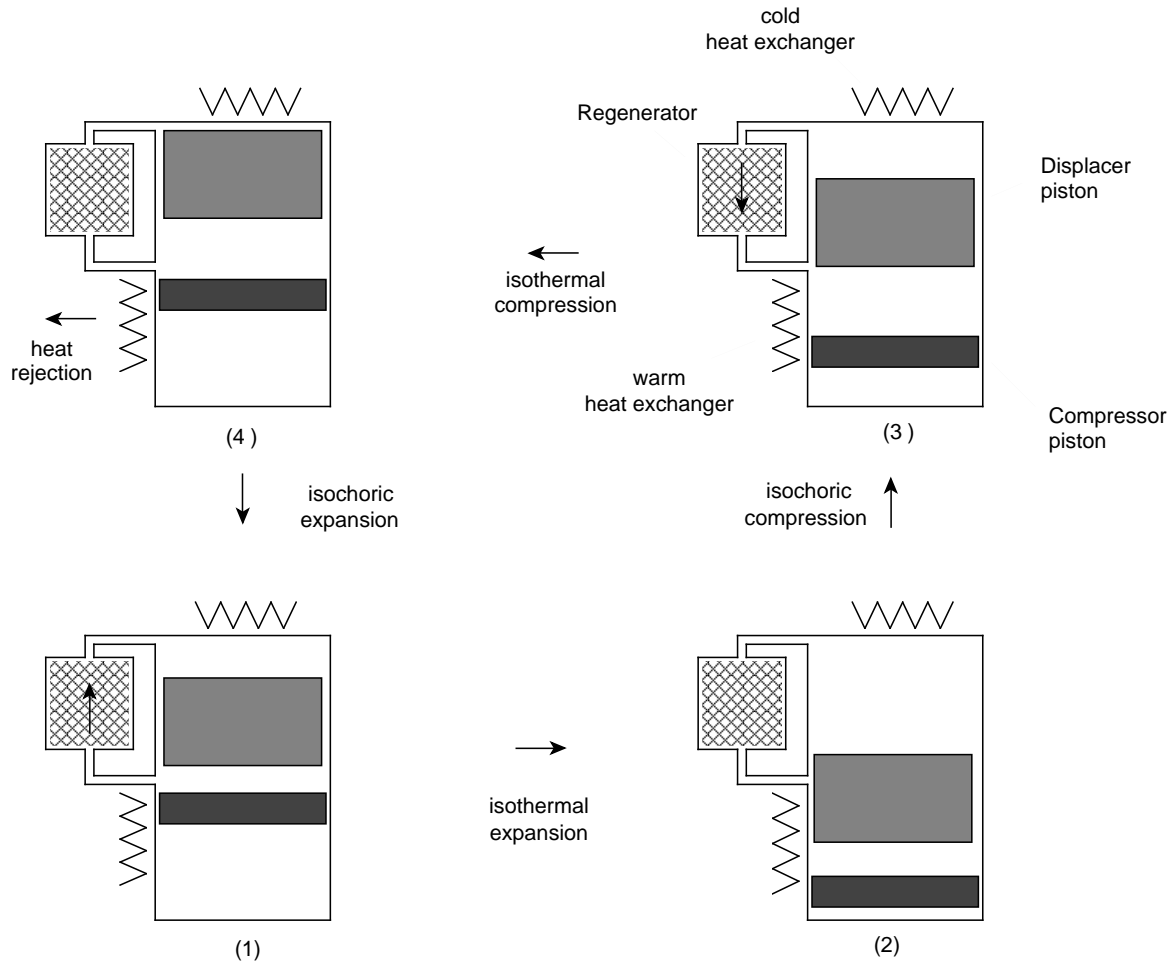
Fig. 10 Operation of a Stirling cycle refrigerator.

Between stage (1) and (2) the displacer piston and the compressor piston move down cooling the gas volume above the displacer piston and allowing heat to be absorbed and the cold heat exchanger. From stage (2) to stage (3) the displacer piston moves up pushing cold gas through the regenerator and warming the gas up while cooling the regenerator material. From stage (3) to stage (4) the displacer piston and the compressor piston move up heating the gas volume between the two pistons and
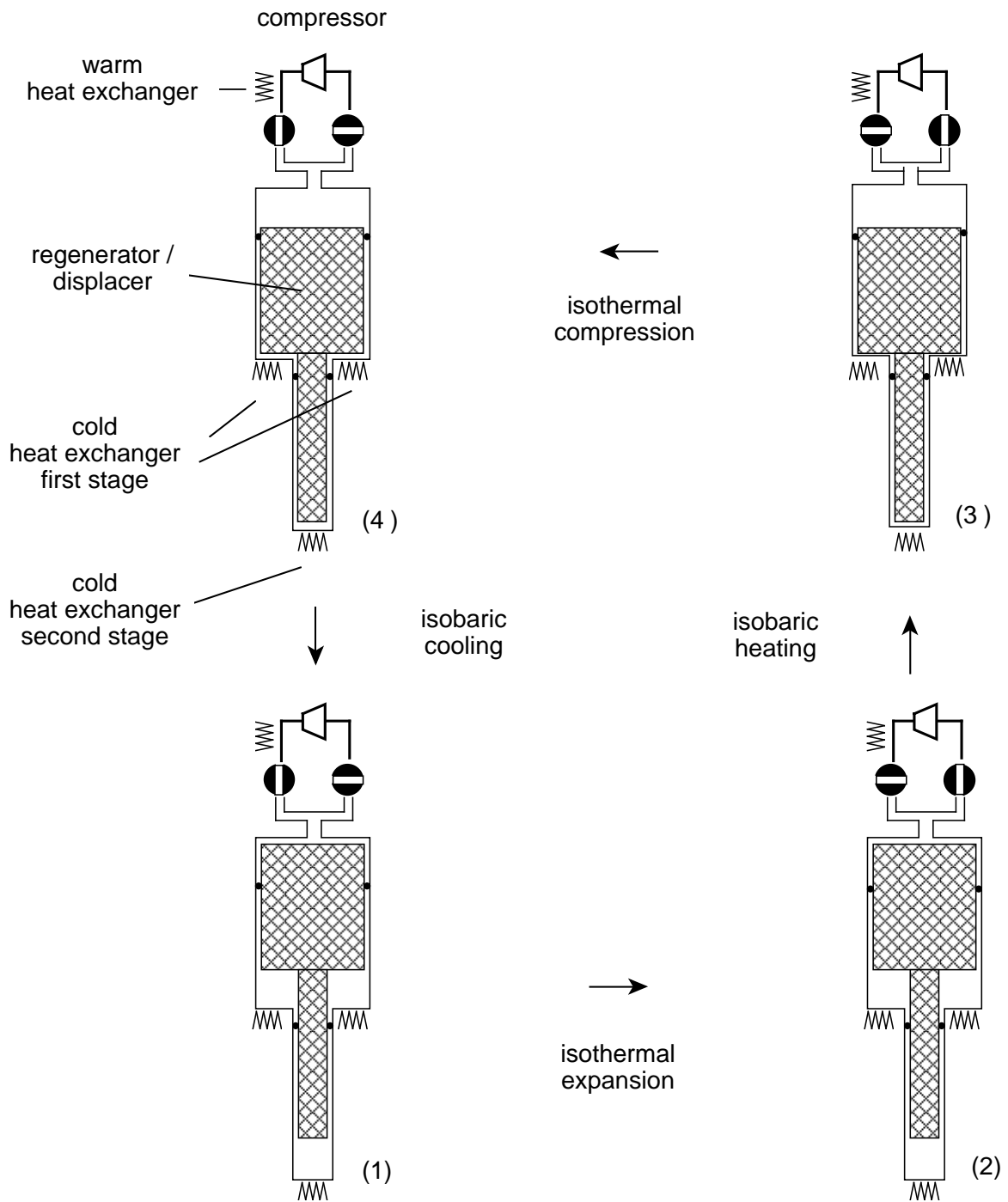
Fig. 11 Operation of a Gifford-McMahon refrigerator.

allowing heat rejection at the warm heat exchanger. Finally from stage (4) to stage (1) the displacer piston moves down, pushing the warm gas between the pistons back through the regenerator and cooling the gas while heating the regenerator material.

One may notice that the movement of the two pistons can be achieved by a phase angle of 90 degrees. This can be realised either by the geometry of the crank shaft or by separating the cylinder in two volumes arranged with orthogonal axes.

4.2 Gifford-McMahon cryocoolers

Gifford-McMahon cryocoolers are designed as two-stage Ericsson refrigerators. Their useful operation temperature is at about 10 K for the second stage and 50 K for the first stage. The different steps of the process can be followed in Fig. 11. The numbering of the different process stages follows that of the Ericsson cycle in Fig. 5.

Between stage (1) and (2) the regenerator is at the upper position and the gas pressure is lowered from high pressure to low pressure by opening the low-pressure valve. Heat can be absorbed on the two temperature level heat exchangers. From stage (2) to stage (3") the regenerator is lowered, displacing and heating the gas from bottom to top and cooling the regenerator material. From stage (3") to stage (4") the whole volume is pressurised by opening the high-pressure valve. Finally between stage (4") and stage (1) the regenerator is moved up, displacing the gas down and cooling it, while heating the regenerator material. The heat rejection is done at ambient temperature at the compressor exhaust.

4.3 Pulse-tube refrigerators

Pulse tube refrigerators have seen an impressive development during the last ten years, reaching temperatures down to a record 2.2 K. Nowadays it is possible to buy compact pulse tube systems delivering about one watt at 4.5 K and about 20 W at 50 K.
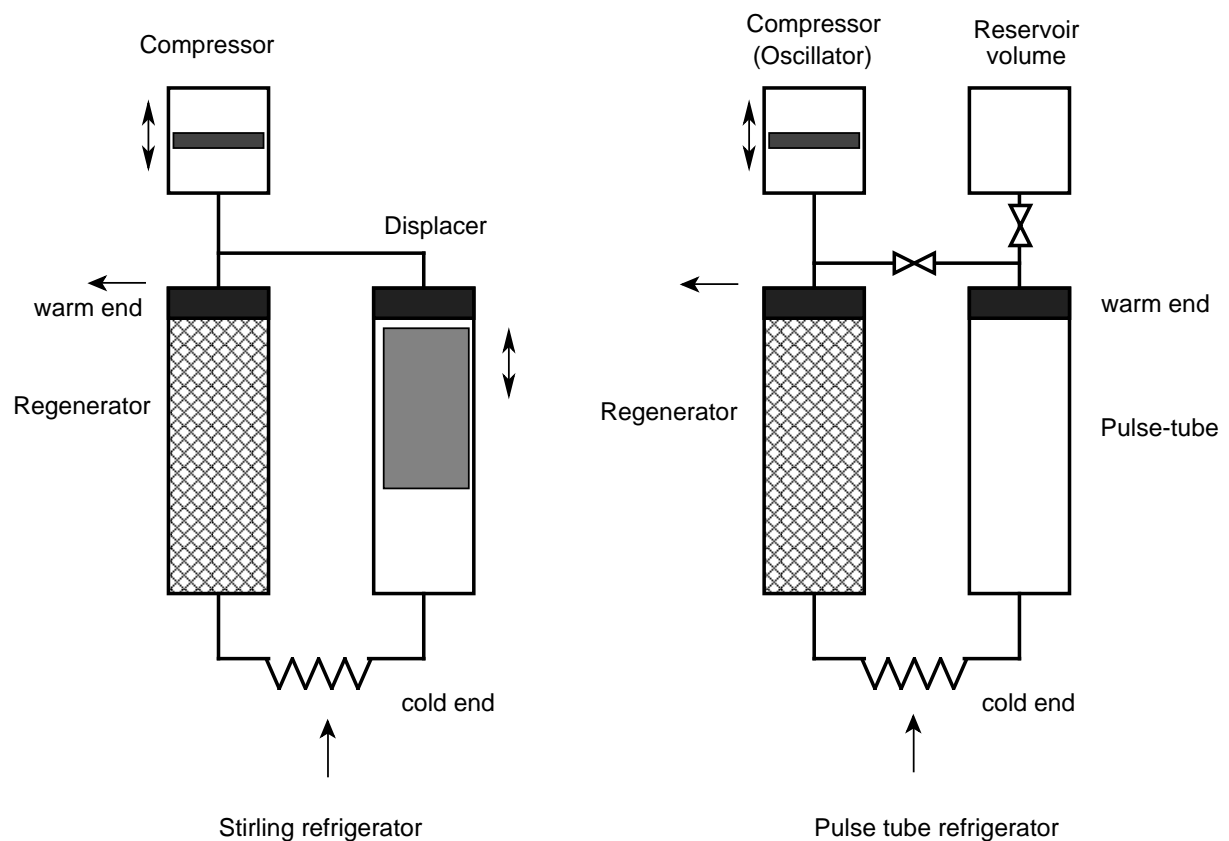
Fig. 12 Pulse-tube refrigerator compared to Stirling refrigerator.

The process can be compared to a Stirling cycle according to Fig. 12. The function of the displacer is replaced by the oscillating gas volume in the pulse tube, once correct calibration of the orifices that connect the pulse-tube to the reservoir volume and the oscillating source yield a phase angle of 90 degrees between the pressure wave of the oscillator and in the pulse-tube.

Pulse-tube refrigerators have a distinctive advantage as they need no moving parts in the cold area. For small capacity applications down to 4.5 K these devices will certainly be increasingly used in the future.

5.   CLAUDE-CYCLE REFRIGERATORS

All refrigerators using helium as working fluid are based on the Claude cycle if their range of capacity exceeds that provided by the cryocoolers. Up to a wide range of capacity, one usually finds two Brayton stages combined with one J-T stage. Fig. 13 shows the typical process for such a refrigerator in a simplified T-s Diagram on the left side and the arrangement of the main process elements on the right side. The basic thermodynamic elements of the cycle and some rules for calculation are listed in the sections below.
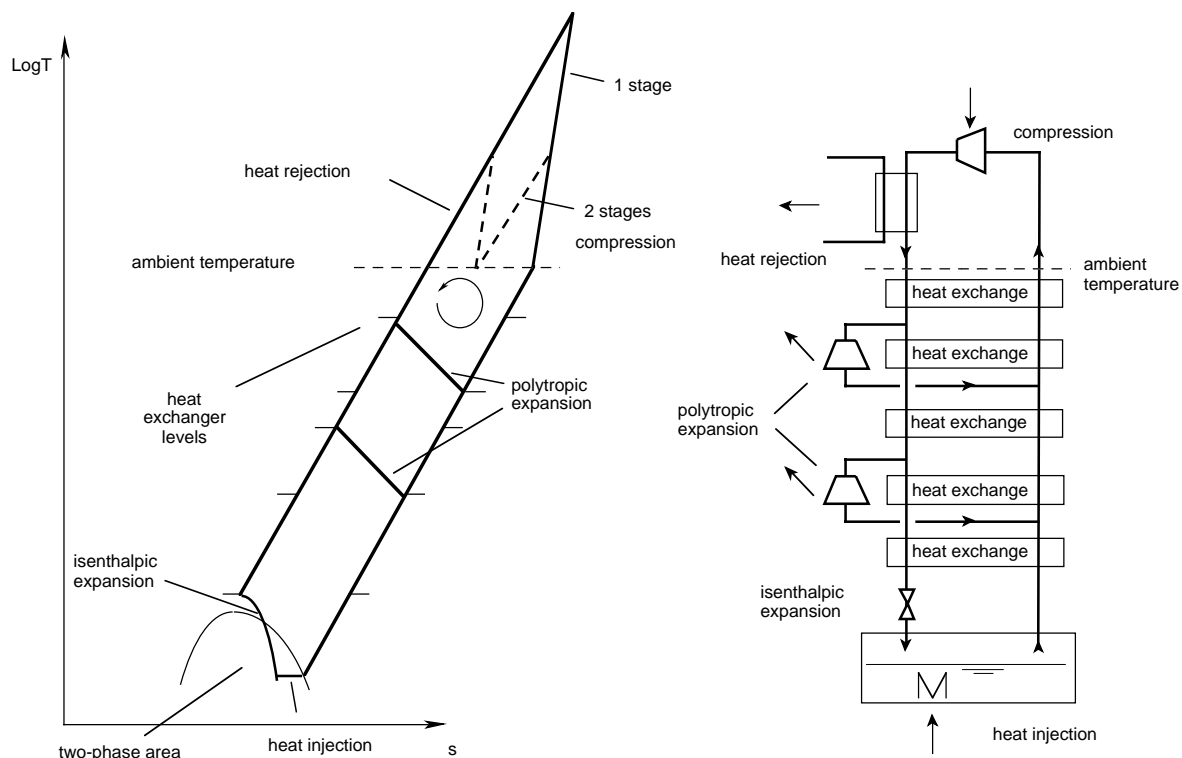
Fig. 13 Typical helium refrigerator cycle combining two Brayton stages and one Joule-Thomson stage.

5.1   Compression at ambient inlet temperature

The work input necessary for the refrigeration process is all injected during the compression of the helium gas. Compression above ambient temperature would ideally be isothermal. Fig. 13 shows a polytropic compression, as can be achieved by a compressor without integrated cooling. Comparing the different area in the T-s diagram covered by single-stage and two-stage compression, the advantage of multi-stage compression is clearly illustrated. An increasing number of compression stages would gradually approach the isothermal limit.

Comparing the necessary compression work with the one for the isothermal compression leads to the isothermal efficiency of the compression stage. This expresses the "quality" of the compression.

The isothermal work input is defined by:

$$T \cdot \Delta S \quad \text{or} \quad \dot{m} \cdot T \cdot \Delta s \tag{12}$$

17

In the case of an ideal gas such as helium at ambient temperature, this can be written as:

$$m \cdot T \cdot R \cdot \ln \frac{p_{out}}{p_{in}} \tag{13}$$

with p_{out} and p_{in} being the outlet discharge and inlet pressure of the compression stage.

The isothermal efficiency is consequently defined as:

$$\eta_{isothermal} = \frac{\dot{m} \cdot T_{suction} \cdot R \cdot \ln {p_{out}}/{p_{in}}}{P_{el}} \tag{14}$$

5.2 Heat rejection to ambient

The recooling of the compressed fluid to ambient temperature, in general via the intermediate cooling medium water, represents the rejection of the total heat entering the cycle plus the work necessary for compression.

5.3 Heat exchange

Besides the heat exchange for the heat rejection above, the isobaric cooling and heating is approximated in the process heat exchangers exchanging heat between the two fluid streams. In order to limit the entropy generation i.e. irreversibility losses, any heat exchange should ideally be done without temperature difference and pressure loss. Both goals are impossible to reach in the real case. One may "classify" the heat exchange process by calculating the exergetic efficiency of the heat exchanger balance following equation (10), or one may calculate the exergetic capacity created by summing up the individual exergy flows, and by this calculate the losses created by the heat exchange. The process of heat exchange is thermodynamically rather complex. Several characteristic figures for the classification and calculation of heat exchangers exist, like efficiency of the heat exchanger, the overall heat transfer coefficient times area (UA-value) and the Number of Transfer Units (NTU value). All these characteristic values only consider the thermal exchange performance but no losses created by friction.

The author considers the NTU value as most informative for cryogenic applications and therefore only this is explained below.

Fig. 14 shows the temperature profile along the heat exchanger length for a balanced flow of two ideal gas streams. Following this sketch one can write for the heat transferred:

$$\dot{Q} = \dot{m}_W \cdot c_{p\,W} \cdot (T_{W1} - T_{W2}) \tag{15}$$

$$\dot{Q} = \dot{m}_C \cdot c_{p\,C} \cdot (T_{C1} - T_{C2}) \tag{16}$$

Defining the heat capacity flow as:

$$C = \dot{m} \cdot c_p \tag{17}$$

equations (15) and (16) can be reformulated to:

$$\dot{Q} = C_W \cdot (T_{W1} - T_{W2}) \tag{18}$$

$$\dot{Q} = C_C \cdot (T_{C1} - T_{C2}) \tag{19}$$
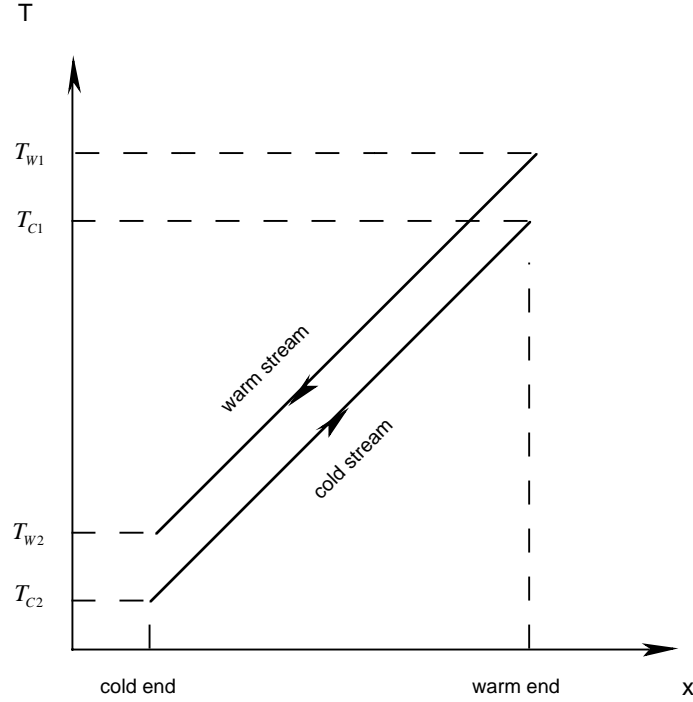
Fig. 14 Heat exchange of two equal flows of ideal gas.

This implies that the heat exchanger is thermally insulated to the environment which is sufficiently well achieved by placing it inside a vacuum insulated cold box. The transferred heat may also be expressed by using the overall heat transfer coefficient U, the exchanger area to which this coefficient is referred, A and the mean logarithmic temperature difference, which in this case equals the temperature difference of the two streams in any cross section of the exchanger.

$$\dot{Q} \; = \; U \cdot A \cdot \overline{\delta T} \tag{20}$$

With C_{min} being the smaller of the two values C_C and C_W, the NTU is a dimension less value defined as:

$$NTU \; = \; \frac{U \cdot A}{C_{\min}} \tag{21}$$

Or in general form as:

$$NTU \; = \; \int \frac{U(T) \cdot dA}{C_{\min}(T)} \tag{22}$$

For an ideal gas case with constant c_p, we can following the equations above write:

$$NTU \; = \; \frac{\Delta T_{Stream}}{\overline{\delta T}} \tag{23}$$

Where ΔT_{stream} represents the temperature difference of the stream with the smaller mass flow. In the case of a balanced heat exchanger, i.e. the mass flows of both streams are equal, the temperature differences are equal as well.

The NTU gives therefore a ratio between the temperature difference between the two streams and the one of which each stream can be cooled or heated. A standard NTU for the warm-end heat

exchanger in a modern refrigerator would be around 25. In other words with a temperature of 5 K between the two streams one may cool or heat either stream for a temperature difference of 125 K. The inverse calculation can be done defining the characteristic NTU of a heat exchanger for which the performance is known. It should be remembered that ideal gas condition can be assumed in a helium refrigerator down to a temperature of 20 K for the common pressure range of up to 2.0 MPa.

5.4 Expansion machines

In the example of Fig. 13 two stages of expansion machines are used, a typical compromise between efficiency and cost for a common refrigerator for capacities up to 2 kW at 4.5 K.

Ideally the adiabatic expansion would also be isentropic; in real machines isentropic transformations can only be approximated. In analogy to what has been written for the compression, one defines an isentropic efficiency for the expanders in order to define their quality of thermodynamic performance.
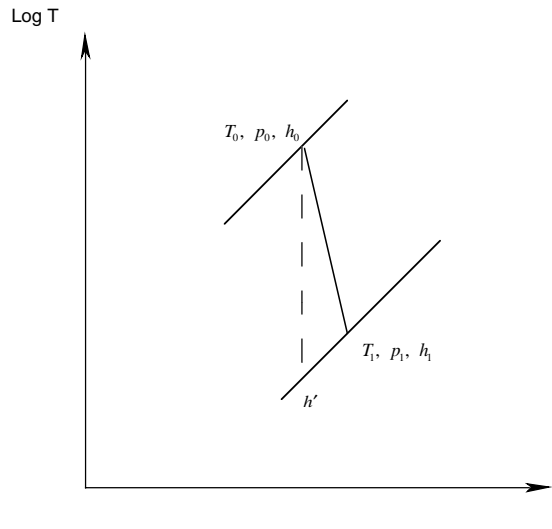
Fig. 15 Polytropic expansion compared to isentropic expansion.

Following the nomenclature of Fig. 15, the isentropic efficiency is defined as:

$$\eta_{isentropic} = \frac{h_0 - h_1}{h_0 - h'} \cdot 100 \ [\%] \tag{24}$$

It compares the maximum possible isentropic enthalpy drop for a given pressure difference, to the actually achieved enthalpy drop. Using ideal gas equations we can write for the isentropic efficiency:

$$\eta_{isentropic} = \frac{T_0 - T_1}{T_0(1 - \frac{p_1}{p_0}^{\frac{\gamma-1}{\gamma}})} \cdot 100 \ [\%] \tag{25}$$

The capacity extracted during the expansion process equals:

$$\dot{Q}_{exp} = \dot{m} \cdot (h_0 - h_1) \tag{26}$$

or, again considering ideal gas and introducing isentropic efficiency:

$$\dot{Q}_{exp} = \dot{m} \cdot c_p \frac{\eta_{isentropic}}{100} \cdot T_0(1 - \frac{p_1}{p_0}^{\frac{\gamma-1}{\gamma}}) \tag{27}$$

The work extracted by the expanders is dissipated as heat at ambient temperature resulting in a pure loss for the refrigerator process. Ideally this work should be recovered to compress the gas. Considering that even in big helium refrigerators using more than two expansion stages the work dissipated from the expansion of the gas amounts to only about 2% of the work input into the compressors, the technical effort to recover this is not considered worth the possible gain in efficiency. For Brayton cycles working for air or nitrogen the work from the gas expansion is usually recovered as compression work above ambient temperature.

5.5 Isenthalpic (Joule-Thomson) expansion

Isenthalpic expansion can be performed in any thermally isolated restriction. In general this is represented by a valve. If this expansion takes place in the property region where the Joule-Thomson effect produces cooling, the valve is called Joule-Thomson (J-T) valve. Thermodynamically this expansion is a pure loss. It would be more efficient to use an expansion machine instead. Due to its simplicity the J-T valve remains a common process element. Fig. 16 shows a sketch of a process combining a Joule-Thomson expansion and a heat exchanger.

A simple energy balance immediately shows that the heat that can be absorbed in the helium bath is equal to:

$$\dot{Q} = \dot{m} \cdot \Delta h \tag{28}$$

With Q and Δh as indicated in Fig. 16.
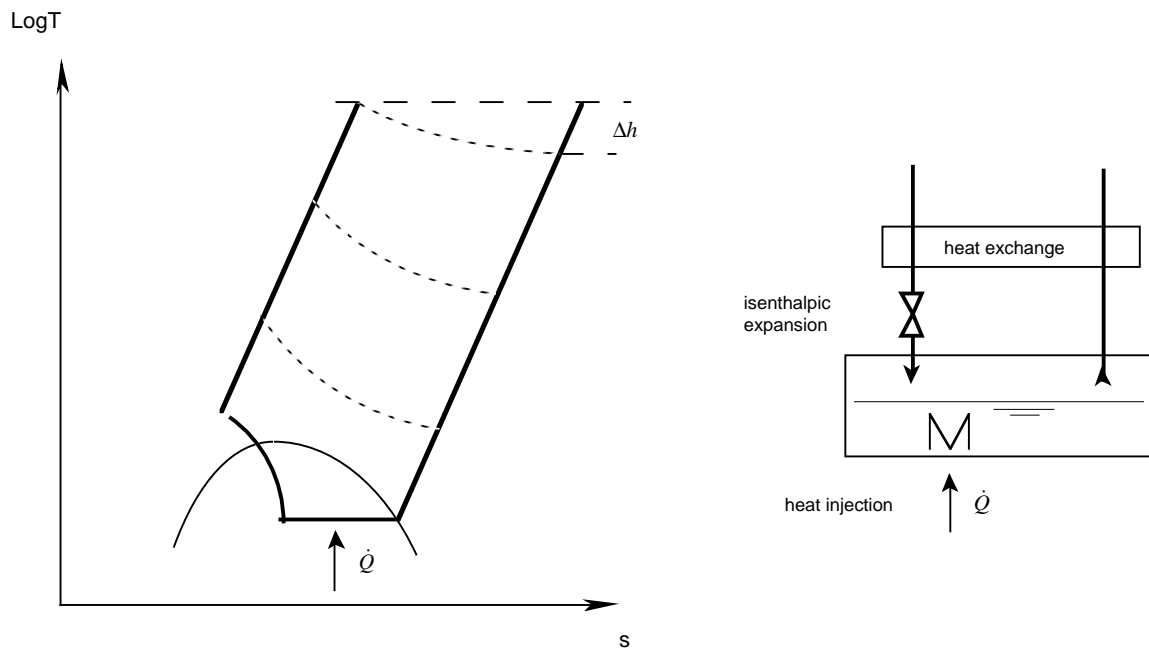
Fig. 16 Joule-Thomson stage.

Fig. 16 further sketches the isenthalpic lines of the non-ideal gas in the property region where Joule-Thomson cooling happens. One can imagine the whole system at the same upper temperature and then cooling down following the sketched isenthalpic lines. This may illustrate that no gas that has ideal behaviour at room temperature can be cooled, or liquefied by a pure Joule-Thomson cycle as already mentioned in section 2.4. Table 4 lists the maximum inversion temperatures for some gases. It should

be noted that close to the maximum inversion temperature this effect is very small. For helium it becomes exploitable below 20 K.

Table 4
Maximum Joule-Thomson inversion temperature for some gases

Gas	Maximum Joule-Thompson inversion temperature [K]
Helium	43
Hydrogen	202
Neon	260
Air	603
Nitrogen	623
Oxygen	761

5.6   The phase separator

A two-phase vessel allowing the flow of liquid helium to be separated is integral part of any refrigerator. It may be incorporated in the refrigerator cold box, it may be a storage or transport dewar or it may be formed by the cryostat housing the load to be cooled. Due to the small difference in specific weight between liquid and vapour of helium (see Table 2) the separation of the two phases is not trivial. The design of the phase separator should avoid returning liquid droplets back into the process heat exchangers, as this would decrease their performance and consequently the performance of the refrigerator or liquefier.

6.   BASIC COMPONENTS OF A REFRIGERATOR

Whereas in chapter 5 the different process elements were presented concerning their thermodynamic characteristic, here we will introduce the basic technical and mechanical aspects of the elements used for Claude-cycle refrigerators.

6.1   Cycle compressors

Cycle compressors for helium work from about ambient temperature and pressure, to pressures between 1.0 MPa and 2.0 MPa. The suction pressure is selected to be just above ambient level in order to avoid the intake of air impurities in case of small leaks in the system. The discharge pressure is generally not defined by the process in the refrigerator, that could profit from higher pressure ratios, but by the mechanical limits of the equipment in the refrigerator or the compressor itself. Common pressure ratios for Claude-cycle refrigerators are 16 to 20.

Due to the properties of helium its compression is accompanied by a high temperature rise. A pressure ratio of 16 would in an ideal isentropic compression process generate a temperature ratio of 3, i.e. the helium temperature would rise up to 900 K. Any deviation from the ideal increases this temperature difference. This must be considered when designing compressors for helium refrigeration.

Two types of compressors are generally used in helium refrigerators, piston compressors or screw compressors.

6.1.1   Piston compressors

Piston compressors for helium refrigeration are "dry" compressors, i.e. no lubricating agent is used for the piston-cylinder in order to prevent contamination of the process gas.

Small units may use synthetic (PTFE) piston rings that need regular replacement, bigger compressors usually use a labyrinth seal. Due to the high temperatures generated by the compression, a compressor has several pistons on one crankshaft, compressing the gas in series with a pressure

ration of about 2 to 3. After each compression stage the gas is re-cooled in a gas-to-water heat exchanger. Due to the change in volumetric flow accompanied with the increasing pressure for each stage, the piston diameter decreases from low-pressure to high pressure stage.

The isentropic efficiency of the compression process is between 60 % and 70 %. The total isothermal efficiency of these machines is usually around 55%.

For Claude-cycle refrigerators piston compressors have been replaced by screw compressors mainly because these are more compact.

6.1.2   Oil-lubricated screw compressors

The compression process in a screw compressor is shown in Fig. 17. The gas volume is enclosed in the screw pitch and continuously compressed until it is expelled. Though not evident at first sight, a screw compressor is a volumetric machine. Oil is injected at a pressure above discharge pressure and is mainly needed to ensure the gas-tightness for the compression process. The injection of oil has a secondary effect as some of the compression heat is exchanged between oil and gas so that the discharge temperatures are considerably lower than for a piston compressor thus getting closer to isothermal. A single screw may therefore easily reach compression ratios of 10 or higher.

The disadvantage of these machines is the presence of oil in contact with the helium as this creates an undesired contamination of the gas. The oil must therefore be removed by a series of coalescing filters and a final adsorber with activated charcoal filling. Only synthetic oil with low vapour pressure may be used in order to achieve an oil content in the range of parts per billion after the oil removal system. Though the cooling by oil during the compression process can decrease the compression work, the mechanical losses of the machine result in typical isothermal efficiencies of about 50%, comparable of those of a piston compressor.
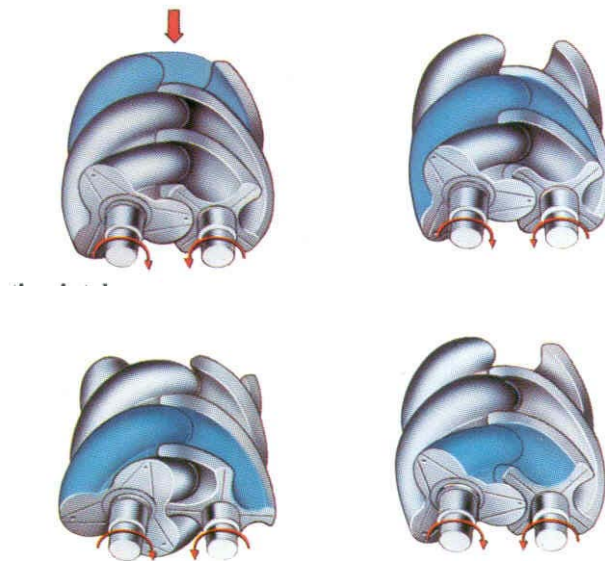
Fig. 17 Compression process in a screw compressor (courtesy of AERZENER MASCHINENFABRIK).

6.2   Process heat exchangers

As this chapter concentrates on Claude-cycle refrigerators, only recuperative heat exchangers are considered.

As process heat exchangers one commonly define those that exchange heat between the different helium flow in the process below ambient temperature. The heat exchangers serving to reject the heat and work to ambient temperature are not considered.

A multitude of engineering solutions exist for the process heat exchangers especially for small capacity refrigerators. The general interest is reaching high thermal performance, i.e. large NTU-values and in the same time staying comparably compact in order to limit the size of the refrigerator cold box. This leads to heat exchangers having a large specific exchange surface, i.e. a large exchange surface per unit volume. This again consequently leads to the distribution of the different flow streams on several channels inside a heat exchanger. The heat exchanger design has to carefully consider an equal distribution of the flow over the different channels as any imbalance would degrade the thermal performance.

For refrigerators with capacities above 100 W at 4.5 K commonly only two types of heat exchangers are used, coiled fin-tube exchangers and aluminium plate-fin heat exchangers.

6.2.1   Coiled fin-tube heat exchanger

It consists of copper tubes with copper fins on the outside of the tube. The fins may be rolled on the tube or soldered on it. The finned tube is then wound around a mandrel or pipe in one or several layers. The whole assembly is then fitted into another tube of appropriate diameter.

The leads to a two-flow heat exchanger where the warm high-pressure stream flows inside the copper tube and the cold low pressure flows around the finned outer space.

These heat exchangers are by their geometry limited to small volume flows which confines them to smaller refrigerators or to the low-temperature end of the refrigerator. It is further difficult to use them for more than two streams at different pressure, a feature that might be required in big refrigerators (> 1 kW at 4.5 K).

6.2.2   Aluminium plate-fin heat exchanger

Aluminium plate-fin heat exchangers are composed by stacking layers of corrugated sheets, forming the fins, between flat sheets thus forming one stream channel. The core of this kind of heat exchanger then consists of a multitude of these channels. The whole arrangement is brazed under vacuum. Fig. 18 shows a typical arrangement of this kind of heat exchanger. The construction allows to incorporate a large number of streams at different pressures in one block. These units can operate at pressures up to 6 MPa and temperatures between 340 K and 2 K. With a specific heat exchanger surface of up 1000 m2/m3 these exchangers are very compact and efficient.

6.3   Expansion machines

6.3.1   Piston expanders

The first expansion machines used for helium refrigeration were reciprocating piston expanders that are still used today in some applications.

The isentropic efficiency that can be reached by these expanders typically ranges from 75% to 82%. Fig. 19 shows a principle scheme of such expanders. Their use is limited by the maximum volume flow they can treat. The sealing packing of piston expanders require regular replacement in order to limit the leakage losses. The energy extracted form the gas is recovered in an electric generator working as a brake.
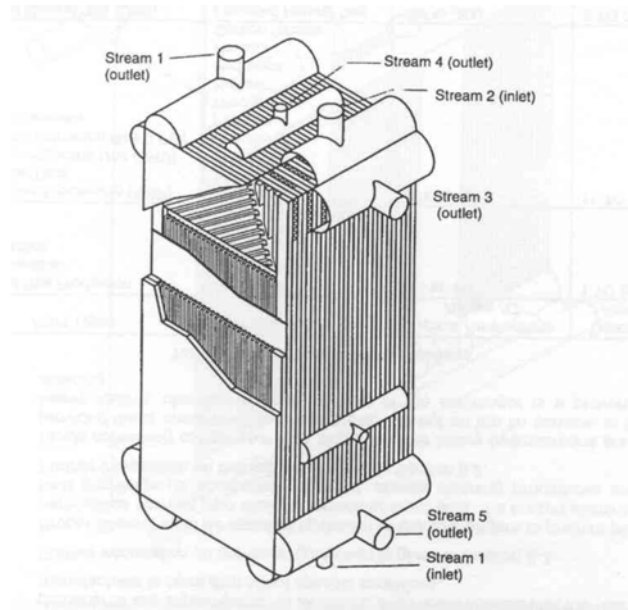
Fig. 18 Plate-fin heat exchanger (courtesy of Linde AG).
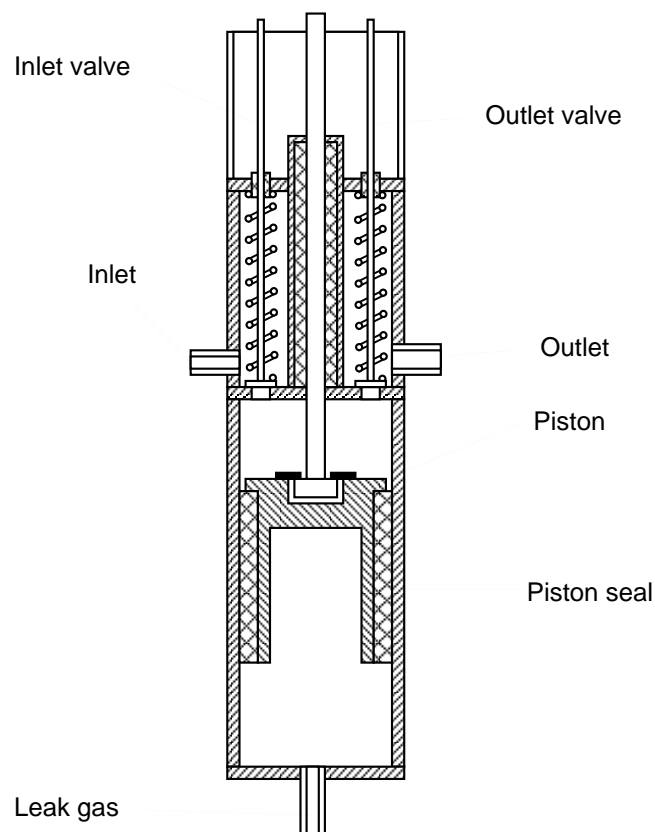
Fig. 19 Schematic view of a piston expander.

6.3.2 *Turbine expanders*

In turbine expanders the recovery of the work from the expansion of gas is done via a gas compressor mounted on the same shaft as the turbine wheel. The characteristic figure for the hydrodynamic

reaction process is the blade-jet-speed ratio, comparing the speed of the turbine blades at the gas inlet with the theoretical maximum speed to which the gas can be accelerated by isentropic expansion. An example of a turbine expander is shown in Fig. 20. The turbines have a maximum efficiency for a blade-jet-speed ratio of 0.55 to 0.7 depending on the wheel geometry.

The blade speed is defined by:

$$u \;=\; D\pi f \tag{29}$$

The jet speed by:

$$c \;=\; \sqrt{2(h_0 - h')} \tag{30}$$

For a "typical" turbine having a wheel diameter of 50 mm and running with inlet temperature at 80 K, inlet pressure 1.6 MPa and outlet pressure of 0.4 MPa, the optimum rotation speed would be 2300 Hz. Theses speed ranges cannot be handled by conventional bearings. The expansion turbines therefore use gas or oil bearings. As oil bearings have the inherent risk to contaminate the cold process parts only turbine expanders with helium gas bearings are used nowadays.

The obtainable isentropic efficiency of such expanders depends on their size i.e. the volume flow treated and typically ranges from 65 % for small expanders to 80 % for larger units.
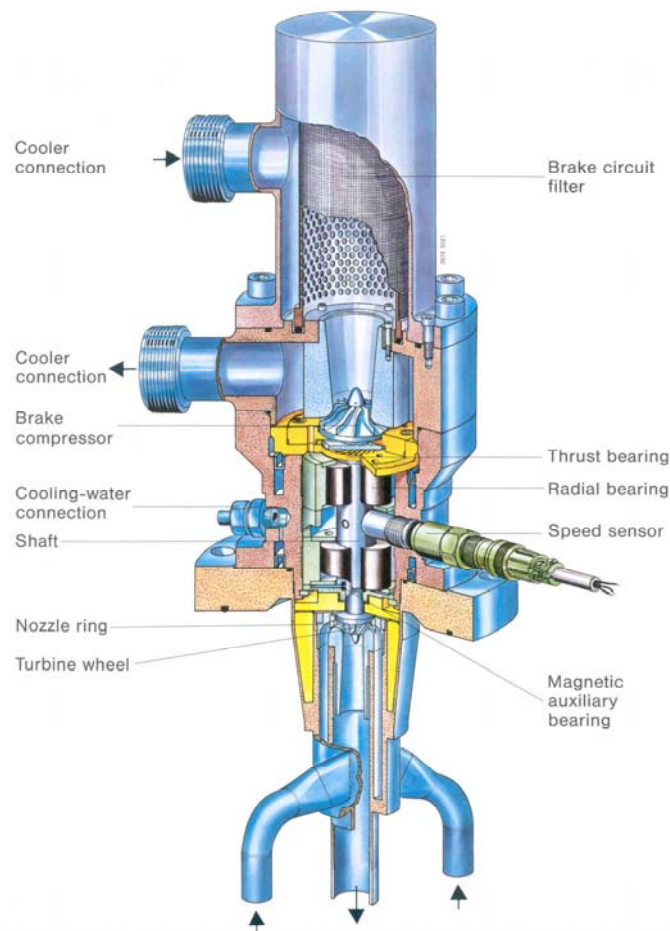
Fig. 20 Dynamic gas bearing turbine (courtesy of Linde Kryotechnik AG).

7. A LARGE CLAUDE-CYCLE REFRIGERATOR: HERA AT DESY, HAMBURG

Chapter 5 explained a standard Claude-cycle refrigerator with two expanders and a J-T valve For the range of equivalent capacity of 50 W to 1000 W at 4.5 K these cycles are commonly applied as being a good compromise between investment cost (equipment cost) and operation cost (efficiency) for higher capacities it is of advantage to design more complicated Claude-cycles with more expanders and a more sophisticated flow distribution in the heat exchangers.

As an example for a refrigerator designed for an accelerator using superconducting magnets the refrigerators for the HERA machine are selected as their process design has been well presented in several publications [9, 10] and especially in [11] a detailed exergy analysis was published,

Table 5
Design capacity for one HERA refrigerator

Cryogenic load		Process design capacity
Refrigeration at 4.3 K	[W]	6875
Vapor superheating at 0.11 MPa	[W]	275
Liquefaction at 4.3 K	[g/s]	22.5
Refrigeration at 40 K to 80 K	[W]	22000

The designed capacity for each HERA refrigerator is given in Table 5 showing a typical mixed duty including isothermal refrigeration and liquefaction at liquid helium temperature, in this case 4.3 K, and a non-isothermal refrigeration load for the cooling of thermal shields below 80 K. In order to calculate the equivalent capacity it is necessary to know that for refrigeration and liquefaction at 4.3 K subcooled helium at 4.5 K and 0.4 MPa is supplied and the vapour is returned at 0.11 MPa. The refrigeration at 40 K is supplied at a pressure of 1.8 MPa and returned at 1.7 MPa. Using the helium property data, one calculates a total exergetic capacity of 799 kW, equivalent to 12.2 kW isothermal refrigeration at 4.5 K.
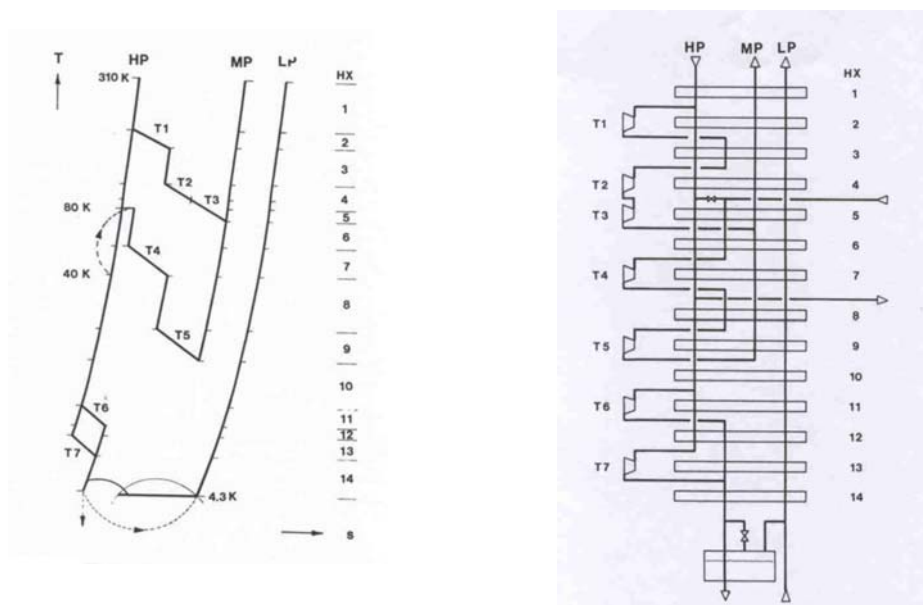
Fig. 21 T-s diagram and simplified process flow diagram of the HERA refrigerators [from 11].

Fig. 21 shows the T-s diagram and the simplified process flow diagram for one HERA refrigerator. The Claude-cycle process may be compared with the one sketched in Fig. 13; it looks much more complicated, though it can quickly be reduced to a cycle with two Brayton stages including turbines T1, T2 and T3 in series for the first stage and turbines T4 and T5 for the second. Instead of expansion through a J-T valve the HERA cycle uses expansion in two turbines, T6 and T7 operating in parallel on slightly different temperature levels. The basic features of the Claude cycle from Fig. 13 are kept in the HERA design, though the arrangement allows a higher efficiency of the refrigeration process.

In [11] a detailed exergy analysis of the process is presented, identifying the loss contribution of the individual process elements. The result is given in form of exergy flow diagrams that are shown in Figs 22 and 23. One notices the important contribution to the overall loss by the helium compressors, and of the compression system in general where only about 50% of the exergy is passed to the cryogenic part of the process. This is given by the machines used for the helium compression and represents a figure that is generaly valid for any Claude-cycle process. As this figure could not be improved the designer of the refrigeration cycle made an effort to improve the cryogenic part of the process which is reflected in the T-s diagram. The cold box efficiency in this case is about 56% which can be considered as a very good value obtained in large refrigerators. Limit values that have been reached in comparable machines are about 60% exergetic efficiency.
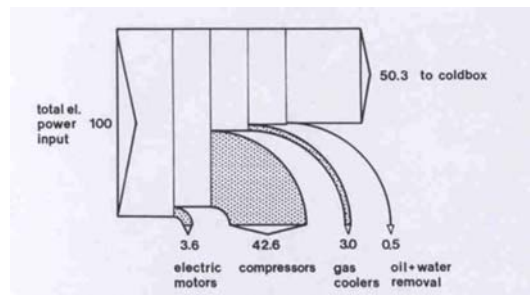
Fig. 22 Exergy flow diagram of the compressor station for the HERA refrigerators [from 11].
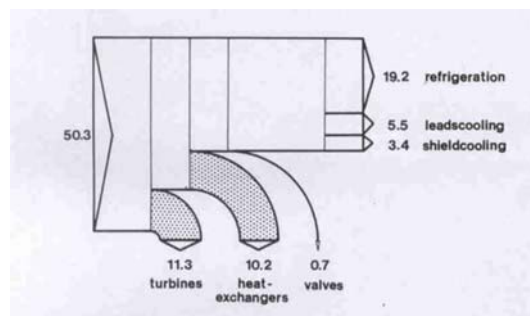
Fig. 23 Exergy flow diagram of the cold box for the HERA refrigerators [from 11].

The final exergetic efficiency delivered at the cold box boundary is 28.1% corresponding to an electrical power input of 2.84 MW into the system in the design case.

8.   CRYOGENIC SYSTEMS

In the previous chapters helium refrigerators with various sizes and process cycles were presented stressing the emphasis on Claude-cycle refrigerators and their process elements typical for accelerator requirements. Such refrigerators are no stand-alone elements but are part of the cryogenic system that comprises:

i) The refrigerator itself including a compressor station with one or several compressors and an oil removal system in case oil lubricated compressors are used, and a cold box housing all the equipment of the process.

ii) A system to distribute the cold cryogen to the different users comprising vacuum insulated transfer lines and distribution valve-boxes. Depending on the extent of such a system it may be as costly as the refrigerator.

iii) Cryostats housing the cold load to be cooled.

iv) Instrumentation and process control for each sub unit and for the overall system .

This usually leads to a cryogenic system of extended complexity and hence cost, both in investment as in operation and maintenance [12].

9.   CONCLUSIONS

The aim of the present article is to give a modest introduction into the physical background and technical realisation of helium refrigerators and liquefiers. Though the thermodynamics involved have been well established for over a century, the realisation of especially larger units with their complex and often mainly empirically understood machinery can still today represent a considerable challenge. As many other fields of engineering, cryogenic refrigeration requires a combination of practical experience and know-how with thorough understanding of the physics involved in order to successfully design efficient systems.

Mainly used as a service technology the basic functioning of cryogenic refrigeration should as well be understood by a user of cryogenic services in order to comprehend reactions, response times and particularities proper to such a system.

REFERENCES

[1]   "Cryogenics" Encyclopædia Britannica http://search.eb.com/eb/article?eu=28520 [Accessed July 2, 2002].

[2]   W. Vinen, Physics of Superfluid He, Proc. CAS School on Superconductivity and Cryogenics for Particle Accelerators and Detectors, Erice, Sicily, 8-17 May 2002.

[3]   V. Arp and R.D. McCarty, Thermophysical properties of helium4 from 0.8 to 1500 K with pressures to 2000 MPa, NIST technical note 1334 (1989).

[4]   HEPAK (© copyright Cryodata Inc.) Helium property program written by V. Arp, R.D. McCarty and B.A. Hands.

[5]   W. Vinen, Survey of Basic Thermodynamics, Proc. CAS School on Superconductivity and Cryogenics for Particle Accelerators and Detectors, Erice, Sicily, 8-17 May 2002.

[6]   G. Gouy, Sur les transformations et l'équilibre en thermodynamique, C. R. Acad. Sc., Gauthiers-Villars, Paris (1889).

[7]   Z. Rant, Exergie, ein neues Wort fur technische Arbeitsfahigkeit, Forsch.-Ing.-Wes. Nr. 22 (1956).

[8]   R. A. Byrns and M.A. Green, An Update on estimating the cost of Cryogenic Refrigeration, Adv. Cryo. Eng. 43B (1998) 1661.

[9]   G. Horlitz, Refrigeration of a 6.4 km Circumference 4.5 Tesla Superconducting Magnet Ring System for the Electron-proton Colllider HERA, Proc. ICEC 10, Butterworth (1984) 377.

[10] H.R. Barton et al., Central refrigeration System for the Superconducting HERA Proton Magnet Ring, Proc. Worklshop on Superconducting Magnets and Cryogenics, Brookhaven National Laboratory (1984).

[11] B. O. Ziegler, Second Law Analysis of the Helium Refrigerators for the HERA Proton Magnet Ring, Adv. Cryo. Eng. <u>31</u> (1986) 693.

[12] S. Claudet, Ph. Gayet, Ph. Lebrun, L. Tavian and U. Wagner, Economics of Large Helium Cryogenic Systems: experience from Recent Projects at CERN, Adv. Cryo. Eng. <u>46A</u> (2000).

BIBLIOGRAPHY

B.A. Hands, Cryogenic Engineering, Academic Press (1986).

K.D. Timmerhaus and Th. F. Flynn, Cryogenic Process Engineering, Plenum Press (1989).

S. W. van Sciver, Helium Cryogenics, Plenum Press (1986).

J. G. Weisend II, Handbook of Cryogenic Engineerring, Taylor and Francis (1998).

HEAT TRANSFER

G.Vandoni
CERN, European Organization for Nuclear Research, Geneva, Switzerland

Abstract
Distribution of refrigeration power and limitation of heat leaks at every temperature stage, required by thermodynamic effectiveness, involve a careful analysis of heat transfer in a cryogenic environment. We review here the fundamental laws of the three modes of heat transfer focusing onto cryogenic operation conditions, and give useful data and examples of practical application for cryostat design.

1. INTRODUCTION

Thermodynamics' first and second laws introduce us to the concepts of heat Q [J] and temperature T [K]. Heat transfer is the energy interaction between two systems driven by their respective temperature difference. The objective of the study of heat transfer is to describe precisely how the temperature difference governs the rate of energy transfer, but it is again thermodynamics which identifies two classes of objectives in cryogenic engineering practice. Consider the efficiency of a thermodynamic engine, or the quantity of work W required to extract a quantity of heat Q produced at temperature T and rejected at a temperature T_a:

$$W \geq Q\left(\frac{T - T_a}{T}\right) \tag{1}$$

with the equality sign applying to the Carnot cycle. As a consequence of (1), both the capital and the operational cost of a cold installation will be determined by the heat loads on the system, with an increasingly high thermodynamic "value" for decreasing heat sink temperature. In other words, the lower the temperature, the smaller the heat loads on a cold system have to be maintained. One objective of thermal design will then be to work out the most effective **thermal insulation**, to reduce the heat transfer rate $\dot{q}$ between two temperature extremes T_A and T_B, which generally are fixed.

On the other hand, in a large system, to extract heat at a long distance from the refrigeration plant, refrigeration power must always be produced at a temperature lower than that of the furthest location. The additional temperature drop ΔT implies an increase ΔW in refrigeration power, or an increase in entropy generation. In the design of heat exchangers and sinks one will therefore aim at **enhancing heat transfer**, to evacuate the heat flux $\dot{q}$, this time usually a fixed quantity, across a minimized temperature difference T_A-T_B.

An extended treatment of heat transfer is beyond the scope of these lectures: specialized literature can be found in the bibliography. Limiting us to an introduction to cryogenic heat transfer, we shall review the fundamental laws and present materials' properties and examples of practical use for application to cryostat design.

There are three basic mechanisms for transferring heat: **conduction**, **convection** and **radiation**. In conduction, heat is transported inside solids or fluids at rest by atomic scale processes. In convection, macroscopic movement of a fluid produces the heat transfer. Finally, in radiative heat transfer, energy is transported by electromagnetic radiation, emitted by any surface at $T > 0$ K, without need of matter's support. Fig. 1 shows the temperature dependence of the three mechanisms (conduction and convection only for fluids and gases) below ambient temperature.

The basic laws for the flow of heat $\dot{Q}$ through an area A or onto a surface A in the three modes are:

Fourier's law for conduction $\qquad\qquad \dot{Q} = -kA\,grad\,T$ (2)

General convection law, free or forced $\quad \dot{Q} = hA(T_w - T_f)$ (3)

Stefan-Boltzmann's law for radiation $\quad \dot{Q} = \sigma\varepsilon A(T_h^4 - T_c^4)$ (4)

where k is the thermal conductivity of the medium, h is the heat exchange coefficient, T_w the wall and T_f the fluid temperature, $\sigma = 5.67 \cdot 10^{-8}$ W m^{-2} K^{-4} Stefan-Boltzmann's constant, ε an effective emissivity, T_h the warm surface and the T_c the cold surface temperature.

For a small ΔT, linearisation of the three laws permit to develop the analogy with an electrical circuit, where ΔT is the equivalent of the electrical potential difference and $\dot{Q}$ the equivalent of the electrical current. The thermal impedance R_{th} defined by this analogy, $R_{th} = \Delta T / \dot{Q}$, allows to describe complex systems for numerisation or to simplify them for qualitative evaluation.
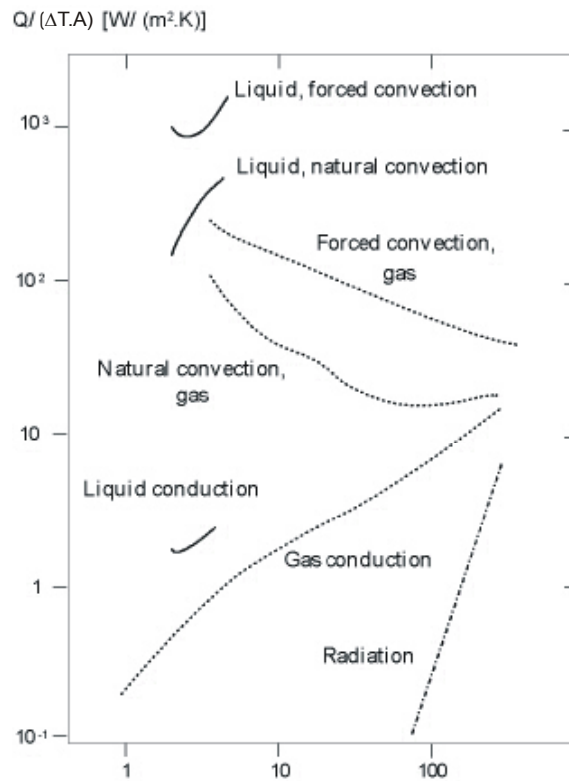

Fig. 1 Typical heat transfer rate per unit surface and temperature interval at temperature T, exchanged by **radiation**, by **conduction** through helium between two walls separated by 1cm, or by **convection** in helium around a horizontal stick of 1cm diameter.

2. CONDUCTION

2.1 General law

In most cases, the thermal conductivity k depends on temperature, resulting in Fourier's law being non-linear. In the one-dimensional case of time-independent heat flow through a cross section $A(x)$ over a length L, between T_h and T_c, integration of (2) yields:

$$\dot{Q} = \int_{T_c}^{T_h} k \, dT \Big/ \int_0^L \frac{dx}{A} = \frac{A}{L} \int_{T_c}^{T_h} k \, dT \tag{5}$$

Thermal conductivities and their integrals can be found in literature for most structural materials. We give some useful ones in Table 1. They clarify the important gain in thermal losses which can be obtained by heat interception at intermediate temperature: depending on the material, the thermal conductivity integral between liquid nitrogen temperature and liquid helium temperature is a factor three to twenty smaller than the integral between ambient and liquid helium temperature.

Energy conservation in an infinitesimal volume, together with Fourier's law, permits us to write the one-dimensional differential equation of general conduction for time-dependent heat flow with heat source $\dot{Q}_h$:

$$\frac{\partial}{\partial x}\left(k \frac{\partial T}{\partial x} \right) + \dot{Q}_h = \rho C \frac{\partial T}{\partial t} \tag{6}$$

with ρ density and C specific heat of the solid. The first term accounts for longitudinal conduction, the second, for internal heat sources, and the third, for thermal inertia. We define the heat diffusivity $D = k/\rho C$, which allows to evaluate the characteristic propagation time τ of a thermal perturbation. Being r_o a characteristic dimension of the body, for instance the diameter of a sphere cooled through its surface, then the propagation time τ is $\tau \approx r_o^2/D$. We can now distinguish between an "early" regime, $t << \tau$, when a large temperature gradient exists in the external layers of the object while the internal temperature remains unperturbed, and a "late" regime, $t >> \tau$, when the internal body temperature is equal to the surface temperature and T evolves only with time. The advantage of this approach is that the late regime can be described by a simple exponential variation of the temperature with time,

$$T(t) - T_\infty = (T_o - T_\infty) \exp(-\beta t) \tag{7}$$

with time constant $\beta = 1/R_{th}C_{th}$, R_{th} being the thermal impedance of the surface, for instance $R_{th} = 1/hS$ for convective cooling, and $C_{th} = \rho CV$ the thermal inertia of the body.

Under some circumstances, not only the late regime, but the whole temperature history of the body may be described by (7). This happens when the internal thermal resistance of the body is much smaller than that at the surface, i.e. when the temperature difference established inside the body is always much smaller than the temperature difference between the surface of the body and its volume. Equating the surface heat flux

$$\frac{\dot{Q}_{surf}}{A} = h\Delta T_S \tag{8}$$

and the internal heat flux

$$\frac{\dot{Q}_{vol}}{A} = \frac{k\Delta T_{vol}}{r_o} \tag{9}$$

we see that the condition of $\Delta T_{vol} << \Delta T_{surf}$ leads to $Bi = hr_o/k << 1$. The number Bi is called Biot number. The quantity of heat released by the body upon cooling, for instance transmitted to a cooling fluid, is equal to the decrease in internal energy of the body. Equation 7 constitutes a useful approximation of the thermal equilibrium for any body.

2.2 Conduction in solids

Heat carriers in solids are delocalized electrons and phonons, the elementary excitations of the atomic lattice. At low temperature, the thermal conductivity associated with phonons varies with T^3, whereas for electrons, it varies linearly with T. Generally, good electrical conductors are also good thermal conductors, although the best thermal conductors, diamond and sapphire, are electrical insulators. Heat transmission at low temperature is hindered by electron-defect and phonon-defect scattering, limiting the mean free path of the heat carriers: as a result, a pure metal is a better conductor than its alloys. Treatments modifying the defect's content of a metal affect its thermal conductivity: cold work reduces it, annealing enhances it. At higher temperature, it is electron-phonon and phonon-phonon scattering which limit the mean free path, such that the differences between pure metals and dilute ones vanish.

Wiedemann-Franz-Lorenz's law yields an acceptable estimate for the thermal conductivity of pure metals at low temperature, based on the free electron approximation:

$$\rho_{el}k = LT \tag{10}$$

where L is the Lorenz constant, $L = 2.445 \cdot 10^{-8}$ W$\cdot\Omega\cdot$K^{-2}. For some metals, a more precise description of thermal conductivity over a broad temperature range has been developed by NBS [18,19]. Here, the thermal conductivity $k(T)$ is parametrized by the RRR value, the ratio between the electrical resistivity at ambient temperature and at 4 K. The RRR parameter accounts both for chemical impurities and for extended lattice defects. Since the measurement of the RRR is more straightforward than that of ρ, this parametrisation proves very useful for practice.

Table 1
Thermal conductivity integrals for some structural materials

T2	Copper ETP	Aluminium 1100	Austenitic st.steel	Glass	PTFE	G10 Composite	Graphite
[K]	[W cm^{-1}]	[W cm^{-1}]	[W cm^{-1}]	[mW cm^{-1}]	[mW cm^{-1}]	[mW cm^{-1}]	[W cm^{-1}]
10	33.2	6.1	0.0293	6.81	4.4	0.31	0.025
20	140	27.6	0.163	20.2	16.4	1.56	0.15
30	278	59.2	0.424	36.8	32.3	4.23	0.48
40	406	96.2	0.824	58.6	50.8	9.04	1.1
50	508	134	1.35	84.6	71.6	17.1	2.9
60	587	170	1.98	115	93.6	29.3	4.6
70	651	202	2.70	151	116	48.4	6.9
80	707	232	3.49	194	139	67.5	9.8
90	756	258	4.36	240	163		13
100	802	284	5.28	292	187	130	22
120	891	330	7.26	408	237		32
140	976	376	9.39	542	287		45
160	1060	420	11.7	694	338		59
180	1140	464	14.1	858	390		74.
200	1220	508	16.6	1030	442	900	99
250	1420	618	23.4	1500	572		133
300	1620	728	30.6	1990	702	2650	251

For superconductors, the thermal conductivity in the normal state is essentially electronic, and hence varies linearly with temperature. Below the transition temperature, however, the thermal conductivity is determined entirely by phonons, varying with T^3. A ratio of $k_{normal}/k_{supra} = 45/T^2$ is obtained for Pb and of $1/T^2$, for In.

Fig. 2 displays the diffusivity for some structural materials. Since the specific heat usually decreases faster than the thermal conductivity, at low temperature the time to reach thermal equilibrium decreases markedly. The diffusivity of copper, equal to $D = 1.12 \cdot 10^{-4}$ m^2/s at ambient temperature, increases to $D = 2.2$ m^2/s at low temperature, that of stainless steel increases from $4 \cdot 10^{-6}$ m^2/s at ambient temperature to $1.4 \cdot 10^{-5}$ m^2/s at low temperature.
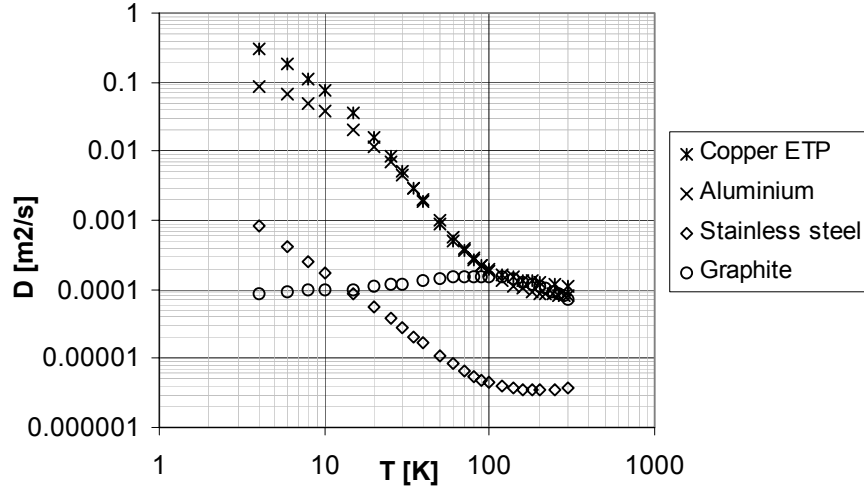
Fig. 2 Thermal diffusivity of selected materials.

The specific heat, needed for the calculation of the thermal diffusivity, can often be approximated by the Debye function, which describes the heat capacity per kilogram mole C_v in terms of Debye temperature θ_D.

$$C_V = 9R\left(\frac{T}{\theta_D}\right)^3 \int_0^{\theta_D/T} \frac{x^4 e^x}{(e^x - 1)^2} dx \tag{11}$$

Values of the Debye temperature for several materials are given in Table 2.

Table 2
Debye temperature for some elements and materials.

Material	θ_D [K]	Material	θ_D [K]
Aluminium	385	Iron	460
Carbon (graphite)	760	Nickel	440
Copper	310	Niobium	265
Gold	180	Titanium	355
Indium	105	Quartz	255

2.3 Conduction in gases and fluids

Heat transmission between two surfaces separated by gas obeys two different regimes according to the ratio between the mean free path of gas molecules λ and the distance L between the two surfaces. For $\lambda \ll L$, the *viscous* regime, heat transmission is described in terms of thermal conduction k, which is independent of pressure. The heat flux is therefore inversely proportional to wall distance. Decreasing the residual gas pressure, the *molecular* regime is reached as $\lambda \gg L$. The molecules travel undisturbed from the warm to the cold surface and heat transfer becomes proportional to residual gas pressure and independent of wall distance.

Kinetic gas theory predicts the mean free path at temperature T [K], pressure p [Pa] and viscosity μ [Pa.s], for a gas of molar mass M [g/mole] as being equal to:

$$\lambda = 115 \cdot \frac{\mu}{p} \sqrt{\frac{T}{M}} \tag{12}$$

Table 3
Mean free path at 300 K for different gases, in [cm]

[Pa]	1×10^{-6}	1×10^{-4}	1×10^{-2}	1	100
Ar	6300	63	0.63	6.3×10^{-3}	6.3×10^{-5}
Air	6100	61	0.61	6.1×10^{-3}	6.1×10^{-5}
N2	6000	60	0.60	6.0×10^{-3}	6.0×10^{-5}
He	1.77×10^{4}	177	1.77	1.77×10^{-2}	1.77×10^{-4}

In the viscous regime, the thermal conductivity coefficient, given in table 4 for different gases under atmospheric pressure, is

$$k = \frac{1}{3} \rho \left(\frac{8RT}{\pi M} \right)^{1/2} \lambda C_V \tag{13}$$

Table 4
Thermal conductivity k [W cm^{-1} K^{-1}] as a function of temperature under atmospheric pressure for several gases.

T [K]	^{4}He	H_2	O_2	N_2	Ar
300	$1.56 \ 10^{-3}$	$1.92 \ 10^{-3}$	$2.63 \ 10^{-4}$	$2.60 \ 10^{-4}$	$1.8 \ 10^{-4}$
80	$0.64 \ 10^{-3}$	$0.60 \ 10^{-3}$		$0.76 \ 10^{-4}$	$0.6 \ 10^{-4}$(90 K)
20	$0.26 \ 10^{-3}$	$0.16 \ 10^{-3}$			
5	$0.10 \ 10^{-3}$				

In the molecular regime, Kennard's law permits describes the heat transfer between two surfaces at temperature T_1 and T_2:

$$\dot{Q} = A_1 \alpha \left(\frac{\gamma+1}{\gamma-1} \right) \left(\frac{R}{8\pi} \right)^{1/2} \frac{p}{\sqrt{MT}} (T_2 - T_1) \tag{14}$$

with $\gamma = C_p/C_v$, R the ideal gas constant, A_1 the surface receiving the heat flow and α an accommodation coefficient. The latter parameter, ranging between 0 and 1, defines the degree of thermal equilibrium between the gas molecules and the walls, and for simple geometries it takes a form analogous to the effective emissivity of radiation heat transfer:

$$\alpha = \frac{\alpha_1 \alpha_2}{\alpha_2 + \alpha_1(1-\alpha_2)\dfrac{A_1}{A_2}}$$

(15)

Close to condensation temperature, $\alpha = 1$, a value which can be used for practical purposes for most common gases. Light gases, however, may have much lower α values, as shown in Table 5. In particular, the low accommodation coefficient of helium is responsible for the smaller heat transfer for helium with respect to hydrogen, in spite of its higher intrinsic thermal conductivity.

Table 5
Accommodation coefficients for some gases

T [K]	Helium	Hydrogen	Air
300	0.3	0.3	0.8-0.9
76	0.4	0.5	1
20	0.6	1	-

In general, liquids are bad thermal conductors, with the important exception of superfluid helium. Conductivities of some liquids are listed in Table 6.

Table 6
Thermal conductivity for some common cooling fluids [mW/cm.K].

Water at 300 K	6
Oil at 300 K	1.3
Nitrogen at 77 K	1.38
Helium at 4.2 K	0.27

2.4 Contact resistance

When the apparent contact surface A_C between two solids is traversed by a heat flow $\dot{Q}$, a temperature discontinuity ΔT appears. The thermal boundary resistance R_H per unit area is defined as:

$$R_H = \frac{\Delta T}{\dot{Q}/A_C}$$

(16)

Two reasons explain why a contact resistance appears. On one hand, due to microscopic roughness, the two surfaces only touch at a limited number or spot-like points. On the other hand, phonon scattering occurs at the interface due to acoustic mismatch between dissimilar materials. Obviously, the contact resistance depends strongly on surface preparation, and can be decreased by applying an appropriate filler, for instance indium, vacuum grease, solder, or simply a thin plate of copper, between the two surfaces.

Some general trends are observable in contact heat resistance [21]:

a) *Contact resistance is inversely proportional to applied force and not to local pressure.* The contact conductance is actually almost independent of the apparent contact area, because the average contact spot size is approximately constant. Thus, increasing the load only changes the number of contact spots. In a first-order approximation, the slope of the contact conductance versus applied force is linear; saturation is reached at about 30 N at 300 K for Cu, Al, brass and stainless steel. However, cycling loading experiments always result in hysteresis, due to plastic deformation of the local contact spots.

b) For contacts made in electrically conducting materials, the thermal conductance can be inferred from the electrical resistance.

c) Contact conductance is approximately proportional to T^n (n = 3 for insulators, 1 < n < 2 for metals) at liquid helium temperature. With increasing temperature, $K_H(T)$ becomes rather linear with T and above 200 K tends to a temperature independent value.

d) The thermal contact resistance is, in a crude approximation, proportional to the ratio of thermal conductivity to the microhardness.

Very complete reviews of contact resistance measurements are given in [20] and in [21].

2.5 Thermal Switches

Applications requiring a rapid cooldown but necessitating thermal isolation at operating conditions may make use of thermal switches, connecting the body with a refrigeration source. Some possible implementation techniques are given below:

a) Exchange gas: A gas which is non-condensable at the operation temperature is introduced, then pumped away once the operation temperature is reached. Since the volumes to be pumped may be large, this technique is rather lengthy.

b) Heat exchanger: The thermal contact is given by a small pipe in insulating material, filled with gas. Once equilibrium is reached, the pipe is evacuated. Small volumes reduce pumping times.

c) Superconducting switch: The thermal conductivity of some superconductors (Pb, In) is much larger in the normal state than in the superconducting state. Switching between the normal and the superconducting state is obtained by applying a magnetic field larger than the critical field to a superconductor strip inserted in a coil.

d) The thermal conductivity of polycristalline graphite varies with T^3 up to 100 K, where it attains a value of 100W/m.K, a strong variation which can be exploited for thermal switching.

3. RADIATION

3.1 General laws

Any surface at finite temperature absorbs and emits energy in the form of electromagnetic radiation, depending on wavelength and direction. For an incident light flux P, a fraction *a* is absorbed, a fraction *t* (transmissivity) traverses the body, and a fraction *r* (reflectivity) is reflected back. Energy conservation requires the sum *a* + *t* + *r* to be equal to 1.

A body is called black when its surface absorbs all of the incident flux, i.e. no energy crosses the body or is reflected back. Per definition, the absorptivity *a* is then equal to 1. The best real-life approximation of a black-body is a hole on the surface of a hollow cavity: radiation reaching the hole is trapped in the cavity and eventually absorbed after successive reflections on its walls.

The electromagnetic energy flux [W/cm^3] emitted per unit wavelength and surface by a black-body in the hemisphere as a function of wavelength is described by Planck's law:

$$E_{b,\lambda} = \frac{C_1 \lambda^{-5}}{\exp(C_2 / \lambda T) - 1} \tag{17}$$

The energy flux spectrum features a maximum for a wavelength which depends on temperature according to Wien's law:

$$\lambda_{max} = \frac{2898}{T} \ [\mu m/K] \tag{18}$$

At $T = 300$ K, the maximum energy flux is emitted at a wavelength of 10 μm, situating the radiation spectrum relevant for cryogenics in the far-infrared domain. For comparison, the sun emitting in the visible light range has a surface "black-body" temperature of above 5500 K.

Integrating Planck's law over all wavelengths, we obtain Stefan-Boltzmann's law, describing the total hemispherical emissive power, emitted in all directions by a black-body at temperature T:

$$E_b = \sigma T^4 \tag{19}$$

with $\sigma = 5.67 \ 10^{-8}$ Wm^{-2}K^{-4}.

The net heat transfer rate between two black surfaces is obtained by computing the radiation emitted by the first surface and intercepted by the second one, and subtracting the radiation emitted by the second surface and intercepted by the first. We get:

$$\dot{Q} = \sigma A_1 F_{12} (T_2^4 - T_1^4) \tag{20}$$

where F_{12} , the geometric view factor, is the ratio between the radiation leaving A_1 and being intercepted by A_2 and the radiation leaving A_1 in all directions. By definition, F_{12} is equal to the integral of the solid angle under which surface 1 sees surface 2. Values for several geometries are available in literature [4].

The intensity of radiation emitted at temperature T by a real surface is only a fraction of the corresponding intensity for a black-body. For example, relative to the energy flux $E_{b,\lambda}(\lambda,T)$ emitted by a black-body, a real surface emits directional, monochromatic radiation $E_\lambda(\lambda,T,\phi,\theta)=\varepsilon(\lambda,T,\theta) E_{b,\lambda}(\lambda,T)$ where $\varepsilon(\lambda,T,\theta) = 1$ is termed monochromatic directional emissivity. The total hemispherical emissivity ε of a real surface is defined by

$$\dot{q} = \sigma \varepsilon T^4 \tag{21}$$

The complicated function of direction and wavelength which usually is $\varepsilon(\lambda,T,\theta)$ can be approximated by considering it as being independent from wavelength (*grey-body*) and from direction (*diffuse body*). For a diffuse-grey body, Kirchhoff's law applies, stating that the absorptivity $\alpha(T)$ and the emissivity $\varepsilon(T)$ are equal. In practice, this law is used to estimate α from ε, provided that the incident radiation and the absorbing surface have the same temperature.

Within the diffuse-grey body approximation, we have now all the ingredients to write the expression for the radiative heat exchanged between two real enclosed surfaces A_1 and A_2 at temperature T_1 and T_2 and emissivity ε_1 and ε_2 , facing each other with a geometrical view factor F_{12} :

$$\dot{q} = \frac{\sigma(T_2^4 - T_1^4)}{\dfrac{1-\varepsilon_1}{A_1 \varepsilon_1} + \dfrac{1}{A_1 F_{12}} + \dfrac{1-\varepsilon_2}{A_2 \varepsilon_2}} \tag{22}$$

We can interpret this expression considering the blackbody emissive power difference $\sigma(T_2^4 - T_1^4)$ to act as a potential difference and the heat flux as a net current. The total resistance in the denominator is constituted by three resistances in series, the first and last being surface resistances to black-body radiation emission, and the intermediate being the purely geometrical resistance between two black bodies. Eq. 22 may be rewritten as

$$\dot{q} = \sigma \varepsilon_{12} (T_2^4 - T_1^4) \tag{23}$$

with ε_{12} an effective emissivity accounting for the emissivities of the two surfaces and their mutual view factor. Table 7 displays the value of ε for some common geometries.

Table 7
Effective emissivity for particular two-surface enclosures: cylinders and spheres may not be concentric.

Parallel plates ($A_1 = A_2 = A$)	$\dfrac{\varepsilon_1\varepsilon_2}{\varepsilon_2 + (1-\varepsilon_2)\varepsilon_1}$
Annular space between long cylinders or spheres ($A_1 < A_2$)	$\dfrac{\varepsilon_1\varepsilon_2}{\varepsilon_2 + \dfrac{A_1}{A_2}(1-\varepsilon_2)\varepsilon_1}$

Notice that if $A_1 \ll A_2$, or if $\varepsilon_2 \sim 1$, the effective emissivity reduces to ε_1. In this particular case, black-body radiation "fills" the cavity between the two surfaces and is collected by A_1 proportionally to its emissivity. Values of ε_{12} for particular surface conditions are given in [24] in this book.

3.2 Emissivity and materials

For real materials, emissivity depends on wavelength and direction, two facts neglected in the diffuse-grey body approximation. As an example, the emissivity of metals increases sharply above 60° angle of incidence. However, many real surfaces satisfy reasonably well the diffuse-grey approximation and hence Kirchhoff's law. The hemispherical emissivities of some structural materials are given in Table 8. We observe that clean, well-polished metallic surfaces have small emissivities, whereas non-metallic surfaces have high emissivities. In general, the best reflectors are also good electrical conductors. Actually, the emissivity and the electrical resistance of an ideal metal are related by Drude's law:

$$\varepsilon(\lambda, T) = 0.365\sqrt{\frac{\rho(T)}{\lambda}} \tag{24}$$

The emissivity varies also with temperature: for metals, it decreases with decreasing temperature and is almost proportional to T at cryogenic temperature. For non-metals, the emissivity may decrease or increase with temperature, and in particular it increases with decreasing temperature for organic materials.

The emissivity of a coating is related to its surface resistance and not to the bulk resistance and it is worth noticing that the latter is strongly determined by the thickness of the film[1]. Reflectivity close to 1 is attained at cryogenic temperatures only for a film thickness above 40nm. Anodized aluminum has an emissivity close to 0.8. The emissivity of a superconductor is close to the one it has in its normal state. Finally, let's observe that the brilliant aspect a surface might display for visible radiation is not necessarily indicative of a low emissivity in the far-infrared region.

---

[1] Actually, the electron mean-free path is then largely determined by the distance between the two boundary surfaces, sort of macroscopic defects of the system.

Table 8
Emissivity of various materials as a function of temperature [9] [16].

Temperature [K]	4	20	80	300
Copper mechanically polished	0.02		0.06	0.1
Copper black oxidized				0.8
Gold			0.01	0.02
Silver	0.005		0.01	0.02
Aluminium electropolished	0.04		0.08	0.15
Aluminium mechanically polished	0.06		0.1	0.2
Aluminium with 7μm oxide				0.75
Magnesium				0.07
Chromium			0.08	0.08
Nickel			0.022	0.04
Rhodium			0.08	
Lead	0.012		0.036	0.05
Tin	0.012		0.013	0.05
Zinc			0.026	0.05
Brass, polished	0.018		0.029	0.035
St.steel 18-8	0.2		0.12	0.2
Glass				0.94
Ice				0.96
Oil paints any color				0.92-0.96
Silver plate on copper		0.013	0.017	
Aluminium film 400A on Mylar			0.009	0.025
Aluminium film 200A on Mylar			0.015	0.035
Nickel coating on copper		0.027	0.033	

3.3 Thermal radiation insulation: multi-layer insulation

"Floating", i.e. solely radiation cooled, reflective screens, interposed between a warm and a cold surface, effectively reduce radiative heat flow between the two surfaces. Assuming the same emissivity ε for the two juxtaposed surfaces and the n screens, it is easy to demonstrate that the heat flux is reduced by a factor $(n + 1)$. A larger reduction is obtained with one single screen cooled at sufficiently low temperature, for instance by the vapor escaping from a cold bath. The concept of floating radiative screens is implemented in multi-layer insulation (MLI), an assembly of reflective films (usually aluminium or aluminized polyester film) separated by insulating spacers (polyester, glass-fiber nets or paper), operated under vacuum. Heat transmission through MLI can be seen as the parallel acting of solid conduction and radiation, resulting in an apparent conductivity:

$$k_{eff} = k_1 T + k_2 T^3 \tag{25}$$

The actual performance of real MLI depends on layer density, with a minimum at 10-20 cm^{-1}. Fig. 3 shows the heat flux as a function of number of layers for a layer density of 15 cm^{-1}. Residual gas pressure affects the performance, as shown in Fig. 4. In practice, with some caution heat fluxes as low as 0.5-1 W.m^{-2} are achieved in vacuum for boundary temperature 300 K and 80 K and 25-100 mW.m^{-2} for boundary temperature 80 K and 4 K. Actual performance depends on field installation, where care has to be exerted to ensure low packing and avoid holes and bad joints which strongly compromise the efficiency of MLI. For complete application data and empirical formulas, see [22].
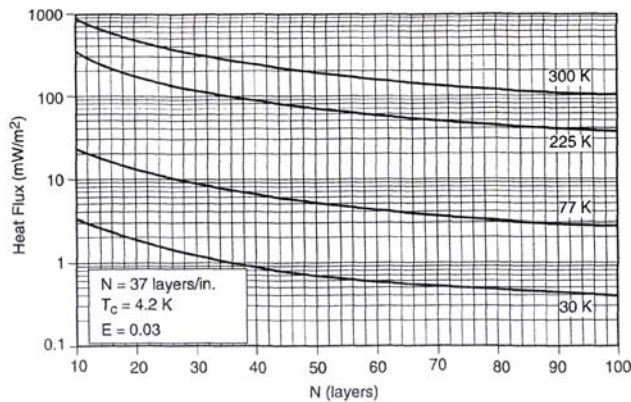
Fig. 3 Heat flux versus number of layers for different warm boundary temperatures, cold boundary 4.2 K, packing density 15 cm^{-1} [22].
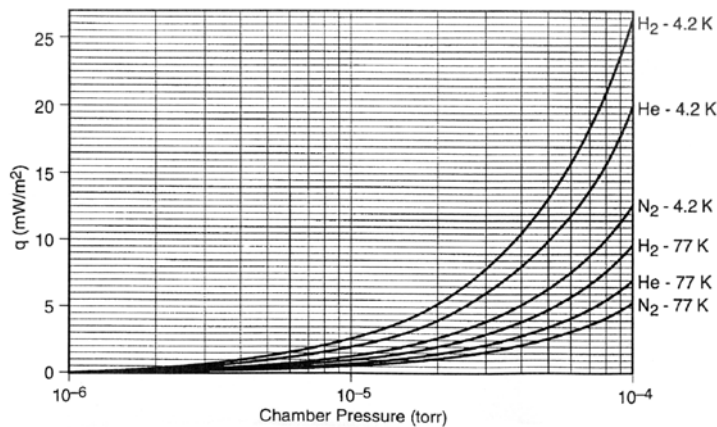

Fig. 4 Gas conduction versus chamber pressure for various interstitial gases and cold boundaries, hot boundary 300 K, 37 layers, 15 cm^{-1} [22].

3.4 Screening of holes

A discontinuity in an intermediate radiation screen behaves as a blackbody at the temperature of the warm surface behind the screen; even a small hole has then a large impact on the cold losses. Depending on the respective areas and temperatures of hole and screen, it may be interesting to blacken the screen, for example by anodisation, to absorb radiation from the hole instead of redirecting it onto the cold parts. When low losses are sought, care should be applied to pipes, e.g. pumping lines, connecting directly the cold core to ambient: to reduce the waveguide effect for 300 K radiation to the cold parts, black radiation screens are inserted in the tube in correspondence of a heat sink.

3.5 Passive cooling by radiators

Electromagnetic radiation towards a cold screen is exploited to obtain contact-less passive cooling of devices having a sufficiently large surface-to-volume ratio, provided the surface emissivity of devices and screen can be made close to 1. Black silicone paints compatible with high vacuum are available from space industry, and were for instance exploited for purely radiative cooling of mobile pick-up electrodes for the CERN antiproton collector [23]. Similar techniques are applied for cooling in space applications, where the cold source is the cosmic background radiation at 2.7 K. Simultaneous screening of the solar radiation has then to be ensured.

4. CONVECTION

Boiling, water

Boiling organic liquids

Condensation, water vapors

Condensation, organic vapors

Liquid metals, forced convection

Water, forced convection

Organic liquids, forced convection

Gases 200atm, forced convection

Gases 1atm, forced convection

Gases, natural convection

$$1 \qquad 10 \qquad 10^2 \qquad 10^3 \qquad 10^4 \qquad 10^5 \qquad 10^6$$
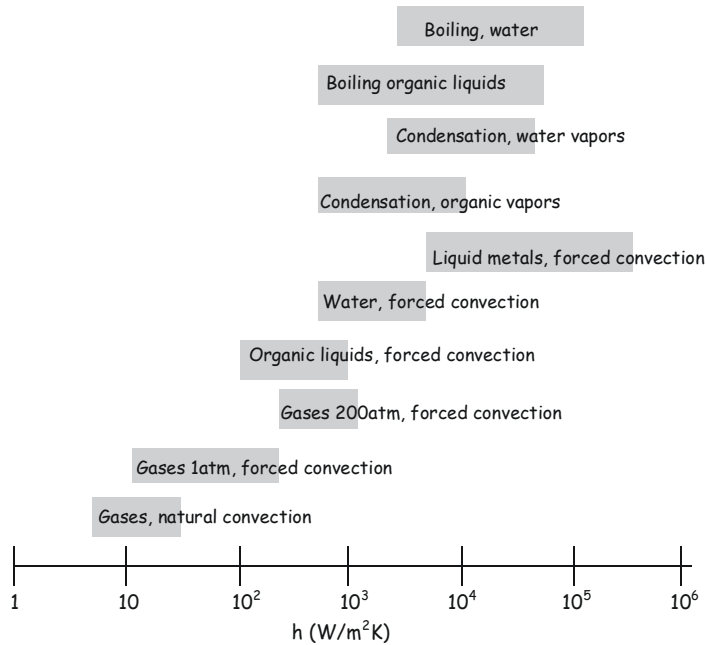
h (W/m^{2}K)

Fig. 5 Effect of fluid type and flow regime on the convection heat transfer coefficient.

Owing to the variety and complexity of problems encountered in convection, it is impossible to treat the subject here in detail. We will restrain us to how convection problems are solved through dimensionless groups describing fluid and flow properties, and give useful relations valid in the most common cryogenic cases.

The general law of convection heat transfer has the simple form:

$$\dot{q} = h(T_s - T_f) \qquad (26)$$

where T_f is the temperature in the bulk of the fluid (internal flow) or at infinite distance from the wall (external flow) and T_s the temperature of the surface in contact with it. The engineering problem consists in determining the exchange coefficient h. Fig. 5 displays ranges of h for fluid types and flows.

4.1 Dimensionless numbers and their physical interpretation

Convection exchange is characterized by the Nusselt number Nu, which compares h with that of purely conductive exchange; a characteristic dimension is chosen as an estimate of the thickness of the perturbed fluid layer.

The Reynolds number, comparing destabilizing inertia forces with stabilizing viscous forces, characterizes the flow regime: below a critical value, the flow is laminar, above, it becomes turbulent. Although the value of the critical Re separating laminar from turbulent flow depends also on the roughness of the tube, for most purposes a value of $Re = 2000$ is taken as the upper limit for laminar flow, and $Re = 10^4$ as the lower limit for turbulent flow. The heat transfer is small in the laminar regime, because of the small layer conduction and large in the turbulent one, due to the reduced dimension of the boundary layer. The Prandtl number, comparing the mass diffusion in the fluid with the heat diffusivity, is a characteristics of the fluid. Typically, $Pr = 0.7$ for a gas, but also for normal liquid helium; further, $Pr = 7$ for water at 20°C, $Pr = 2.5$ for nitrogen at 77 K. The Grashof number, which appears in the description of natural convection, compares the buoyancy, due to gravity, with the viscous forces. Temperature differences along a vessel wall cause local flows due to density

differences, which in turn enhance the heat transfer. The magnitude of *Gr* indicates whether these local fluid flows are laminar or turbulent, with the associated low or high heat transfer rate. In cryogenic problems, large *Gr* and hence large heat transfer rates are to be expected, because of the large volume expansivity β.

Table 9
Dimensionless groups and their physical interpretation.

Group	Name	Definition	Physical interpretation
Re	Reynolds	$\dfrac{\rho V d}{\mu}$	$\dfrac{inertia\ force}{viscous\ force}$
Pr	Prandtl	$\dfrac{\mu C_p}{k}$	$\dfrac{momentum\ diffusivity}{thermal\ diffusivity}$
Nu	Nusselt	$\dfrac{hd}{k}$	$\dfrac{convection\ exchange}{conduction\ exchange}$
Gr	Grashof	$\dfrac{\beta g \Delta T d^3 \rho^2}{\mu^2}$	$\dfrac{buoyancy\ force}{viscous\ force}$
Ra	Rayleigh	*Gr Pr*	
d = characteristic dimension, ex. tube diameter or hydraulic diameter, μ = dynamic viscosity, β = coefficient of volume expansion, k = thermal conductivity, ΔT = temperature difference, ρ = density, C_p = specific heat at constant pressure, h = heat transfer coefficient			

4.2 Natural convection

Natural convection occurs when the fluid movement has its origin in the expansion and ascension of heated sections of fluid. The useful dimensionless groups are *Nu*, *Pr* and *Gr*. A relation of the type *Nu = f(Gr,Pr)* permits to calculate the exchange coefficient *h*. Empirical forms

$$Nu = a(GrPr)^n = a\,Ra^n \qquad (27)$$

where the Rayleigh number *Ra = Gr Pr* appears, have been developed for several typical configurations, some of which are displayed in Table 10.

Table 10
Empirical relations for natural convection in some typical configurations

Configuration	Regime	Limits	a	n
vertical, free surface	laminar	$5.10^3 < Ra < 10^9$	0.59	¼
	turbulent	$10^9 < Ra < 10^{13}$	0.13	1/3
horizontal, free surface		$Ra < 10^3$	1.18	1/8
	laminar	$10^3 < Ra < 2.10^7$	0.54	¼
	turbulent	$2.10^7 < Ra < 10^{13}$	0.14	1/3

The characteristic dimension *d* to use in the calculation is:

the diameter	for a horizontal cylinder
the height	for vertical plates or cylinders
the smallest exchange dimension	for horizontal planes
the distance between walls	for enclosures

In the case of a common gas, it is easy to see that the exchange factor h is proportional to the square root of pressure, $h \sim p^{1/2}$, and inversely proportional to the square root of temperature, $h \sim T^{-1/2}$. Useful formulas valid for air close to ambient conditions, with d in [m], are given below:

for vertical plates $$h = 1.4 \left(\frac{\Delta T}{d}\right)^{1/4} \qquad [\text{Watt m}^{-2}\,\text{K}^{-1}] \tag{28}$$

for horizontal plates $$h = 1.3 \left(\frac{\Delta T}{d}\right)^{1/4} \qquad [\text{Watt m}^{-2}\,\text{K}^{-1}] \tag{29}$$

For free convection in cold gaseous helium at 1 bar, a Nusselt number ~3.65 can be assumed.

4.3 Monophase forced convection

Three dimensionless numbers are applied in problems of forced convection: *Nu, Re* and *Pr*. A relation of the type $Nu = f(Re,Pr)$ permits to infer h, the exchange coefficient. Empirically, a variety of relations of the type

$$Nu = f(Re,Pr) = a\,F\,Re^m\,Pr^n \tag{30}$$

have been established for the most usual cases. We give in Table 11 those which are more often used in cryogenic problems, valid for flow parallel to the duct.

Table 11
Empirical relations for mono-phase forced convection in some typical configurations.

Configuration	Regime	Limit	a	m	n	F
horizontal plate	laminar	$10^3 < Re < 10^5$	0.66	½	1/3	1
	turbulent	$3 \cdot 10^5 < Re$	0.036	0.8	1/3	1
horizontal tube or annular space	laminar	$10^3 < Re < 2.1 \cdot 10^3$ $Re\,Pr\,d/L > 10$	1.86	1/3	1/3	$(d/L)^{1/3}$
	turbulent	$10^4 < Re < 1.2 \cdot 10^5$ $Re Pr\,d/L > 2.4 \cdot 10^5$	0.023	0.8	0.33	$1 + (d/L)^{0.7}$

The relation describing exchange in *laminar* flow inside a horizontal tube takes the name of **Sieder & Tate** formula, the one valid for *turbulent* flow is the well-known **Colburn** formula.

The pressure drop along a segment L of a tube is determined by the friction force:

$$\frac{dp}{dx} = \frac{\rho v^2}{2}\frac{4f}{d} \tag{31}$$

with v flow velocity, f Fanning friction factor, and d hydraulic diameter, defined as $d = 4A/p$, where A is the cross section of the duct and p its wetted perimeter. The relation between Re and f depends on the flow regime, on the geometry of the cross section of the duct, but also on the roughness of the

surface. Three useful relations for flow inside a duct of circular or annular cross section and smooth surface, are

laminar $\qquad Re < 2000 \qquad\qquad f = \dfrac{16}{Re} \qquad\qquad$ Poiseuille law $\qquad\qquad$ (32)

turbulent $\qquad 2 \cdot 10^3 < Re < 2 \cdot 10^4 \qquad f = 0.079\,Re^{-0.25} \qquad$ Blasius law $\qquad\qquad$ (33)

$\qquad\qquad\quad 2 \cdot 10^4 < Re < 10^6 \qquad f = 0.046\,Re^{-0.2} \qquad\qquad\qquad\qquad$ (34)

An exchange problem in forced convection is solved by first determining the flow character from the calculation of Re, then Pr from the fluid characteristics, and then choosing the appropriate correlation formula for Nu. In case of doubt about the importance of natural convection, the calculation of the Gr or Ra might be helpful.

4.4 Convection with change of phase
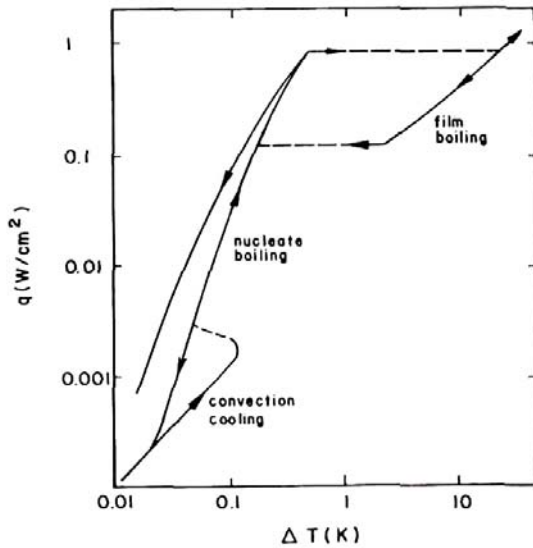
4.4.1 Boiling heat transfer or pool boiling

Fig. 6 Boiling heat transfer to liquid helium [8]

Boiling heat transfer occurs when the temperature of a solid surface is sufficiently higher than the saturation temperature of the liquid in contact with it. The heat flux versus temperature difference features a strongly non-linear behavior with hysteretic features. With increasing temperature difference, after a first regime where natural convection increases heat transfer, nucleate boiling appears, in which vapor bubbles are generated locally on the surface. The ascending currents promote heat transfer. A maximum is reached at the peak-nucleate boiling flux (PNBF), above which individual bubbles merge into a continuous film, which strongly limits the heat transfer. If the temperature difference is decreased from above the film-boiling crisis, recovery to nucleate boiling does not occur on the same portion of the curve. Fig. 6 illustrates boiling heat transfer to liquid helium. The PNBF at the normal boiling point amounts to 1 Wcm^{-2} for helium and 10 Wcm^{-2} for nitrogen, with respective excess temperatures of 1 K and 10 K. For water, a heat flux of 100 Wcm^{-2} is obtained at 30 K excess temperature. In saturated superfluid helium, in spite of an exceptionally high heat conduction, owing to the small density of the liquid and the slope of the vapor pressure curve, the

heat transfer switches to film boiling at heat flux values not much higher than those of normally boiling helium. A positive consequence of the existence of a maximum heat flux in pool boiling is the limit it sets on the heat release from a warm object, like a quenching magnet, or in the cooling of a nitrogen spill on human skin.

4.4.2 Two-phase convection and instabilities

In two-phase convection, both natural and forced, the actual heat transfer rate is due to a combination of bubble formation and motion near the walls and the direct sweeping of the heated surface by the fluid. Due to significant density changes in the two-phase regime, or to pressure-drop change, instabilities and oscillations may occur. A guiding map to instabilities can be found in [6]. The frequency of oscillations may vary from 1/20 Hz to some hundreds of Hz. In the near-critical phase-space region, density-wave type oscillations may appear. Pressure waves increase locally the heat transfer rate, create an expansion of the fluid, decrease thereby its conductivity and hence the heat transfer rate. Oscillations may be avoided by applying the following practical rules:

- always maintain a low vapor quality throughout the flow

- avoid large differences in elevation along the circuit, which enhance natural buoyancy

- avoid downstream flow restrictions, which are destabilizing, and introduce upstream flow restrictions, which are stabilizing both on density-wave oscillations and on pressure-drop oscillations.

4.5 Refrigeration properties of cryogens

Table 12
Refrigeration properties of helium, nitrogen and water.

		He	N_2	H_2O
Normal boiling point	[K]	4.2	77	373
Critical temperature	[K]	5.2	126	647
Critical pressure	[bar]	2.3	34	221
Liquid density/ Vapor density*		7.4	175	1600
Heat of vaporisation*	[Jg^{-1}]	20.4	199	2260
Liquid viscosity*	[μPa s]	3.2	152	283
Enthalpy increase between T_1 and T_2	$T_1 = 4.2$ K	384	-	-
	$T_2 = 77$ K			
[Jg^{-1}]				
	$T_1 = 77$ K	1157	228	-
	$T_2 = 300$ K			
*at normal boiling point				

In particle accelerators and detectors, the most common cryogens are nitrogen and helium, whose properties are listed in Table 12. They are characterized by the small gap in thermodynamic phase-space separating relevant operation domains. Consequently, the properties of the liquid and vapor phase in cryogenic systems are much closer to each other than is the case, for instance, for water. The latent heats of vaporization are low, the liquid and vapor density are similar, the liquid viscosity is low. A large enthalpy can be absorbed in cold vapor between the normal boiling point and ambient for helium, and to a lesser extent, for nitrogen. This refrigeration capacity proves very advantageous to cool structural elements and thermal shields.

Fig. 7 Phase-diagram of helium; usual operating domains are shown hatched.

The phase diagram of helium is shown on Fig. 7. Instead of a triple point, a phase transition into a superfluid state appears. The transition leads to a macroscopic quantum state in which the liquid features unusual transport properties: an exceptionally high heat conductivity and a very low viscosity. The transition is a second-order one, i.e., no latent heat is associated to it. A peak appearing in the specific heat across the phase transition has given the transition line the name of lambda-line. Superfluid helium physics is presented in [8] and in this school, ref.[14], while superfluid helium technology is illustrated in [14bis].

Table 13
Comparison of operation domains of helium refrigeration.

Phase-diagram domain	Advantages	Drawbacks
Saturated normal helium bath	Monovariant: constant T independent of heat load	Large inventory Nucleate boiling crisis
Forced flow of saturated helium	Good heat transfer Small liquid inventory Joule-Thomson cooling	Flow instabilities Limited working range in T and p
Forced flow of supercritical helium	Easy modelling Small inventory No instabilities	Bivariant High pressure operation Joule-Thomson heating
Saturated superfluid helium bath	Low temperature operation Excellent heat transfer	Dielectric breakdown Sub-atmospheric operation Large gas volume
Pressurized superfluid helium bath	Low temperature operation Excellent heat transfer Large heat capacity	Cost of refrigeration Subatmospheric piping

Typical working domains of helium, highlighted on Fig. 7, are summarized in Table 13. *Saturated normal helium* is a monovariant system, where the pressure above the bath determines the equilibrium temperature. Operating in *supercritical helium* permits to avoid two-phase problems like instabilities in the circuits, however, as a bivariant system, its temperature will depend on applied heat

load. The use of *saturated superfluid helium* is undermined by the risk of dielectric breakdown and operation at subatmospheric pressure; *pressurized superfluid helium*, usually at atmospheric pressure or slightly above, is more advisable for cooling devices.

4.6 Thermal shielding potential of cold vapor

Taking advantage of the large enthalpy stored in the gases evaporating from a bath, the heat inleak is reduced by vapor-cooling cryostat necks, supports, current leads. In the case of a support or neck of length L and cross section A, assuming perfect exchange between it and the escaping gas (i.e., identical temperature of gas and wall), the heat balance equation yields

$$k(T)A\frac{dT}{dx} = \dot{Q} + \dot{m}C_p(T - T_1)$$ (35)

where Q is the residual heat inleak from the element into the liquid, at temperature T_1. If the regime is self-sustained, i.e., the evaporation of the liquid is entirely due to residual heat inleak, then

$$\dot{Q} = L_v\dot{m}$$ (36)

Integration of eq.35 yields

$$\dot{Q} = \frac{A}{L}\int_{T_1}^{T_2}\frac{k(T)dT}{1 + (T - T_1)C_p / L_v}$$ (37)

which, compared with the conduction integral eq.5, shows that vapor cooling brings to a substantial reduction in heat inleak. Table 14 illustrates the reduction of heat flow obtained by self-sustained helium vapor cooling for selected technical materials.

Table 14
Reduction of heat conduction obtained by self-sustained helium vapor cooling for technical materials.

	Thermal conductivity integral [W cm^{-1}]	Effective thermal conductivity integral [W cm^{-1}]
ETP copper	1620	128
OFHC copper	1520	110
Aluminium 1100	728	39.9
AISI 300 st.steel	30.6	0.92

Comparing the refrigeration characteristics of He and N_2, presented in Table 8, it appears that vapor cooling by nitrogen is less convenient than by helium.

4.7 Neck cooling

We shall now discuss the calculation of the heat inleak from the vapor-cooled neck of an open cryostat. We call A the cross section of the neck, l its length.

The global losses on the cryostat are partitioned between losses from the neck, $\dot{Q}_1$, and from the rest of the environment, $\dot{Q}_R$. Liquid is evaporated by these losses with rate $\dot{m}$. Let us postulate perfect exchange between the walls of the neck and the escaping vapors. Applying Fourier's law between T_1 and T_2 and assuming a linear form for the thermal conductivity of neck's material,

$$k = a + bT \qquad (38)$$

valid for instance for stainless steel, we obtain the relation (31) between the form factor of the neck, $Z = A/l$, and the ratio $\Phi = \dot{Q}_1 / (\dot{Q}_1 + \dot{Q}_R)$.

$$\dot{Q}_1 = \frac{Z\Phi}{C_p\beta}\left\{\left[a + b(T_1 - \frac{\Phi}{\beta C_p})\right]L\left[1 + (T_2 - T_1)\frac{\beta C_p}{\Phi}\right] + b(T_2 - T_1)\right\} \qquad (39)$$

To account for the vapor volume remaining in the cryostat and replacing the evaporated liquid volume, we have applied a correction factor β,

$$\beta = (1 - \frac{\rho_{vap}}{\rho_{liq}})/L \qquad (40)$$

This correction may safely be neglected for most cryogens but helium (~15%), for which the difference between the liquid and vapor densities is small.

By letting Φ vary between 0 and 1, we can calculate $\dot{Q}_1$ and $\dot{Q}_R$ and plot $\dot{Q}_1 + \dot{Q}_R$ as a function of $\dot{Q}_R$. The utility of this approach is best understood with the help of fig. 14. For a particular value of $Z = A/l$, the graph can be used to evaluate if it is useful or not to reduce the residual losses by improving the overall insulation of the cryostat. It also shows that for each Z there is a critical value of $\dot{Q}_R$ such that the gases evaporated by $\dot{Q}_R$ exactly compensate the losses from the neck.
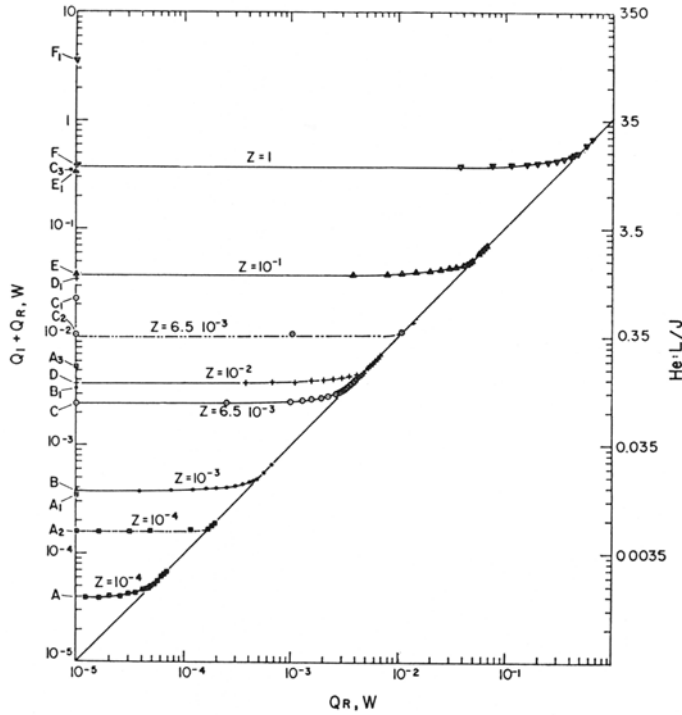
Fig. 8 Losses in a helium vessel with stainless steel neck as a function of $\dot{Q}_R$, for different values of $Z = A/l$ (cm). Solid lines, temperature difference between 77 and 4.2 K. Dashed lines: temperature difference between 300 and 4.2 K. From [11].

4.8 Current lead cooling

Vapor cooling also considerably reduces heat inleaks from electrical conductors feeding high currents into a cryogenic environment. Ensuring a good exchange between the current lead and the escaping vapor, and with appropriate optimization with current I of the aspect ratio l/A, both the heat leaks due to Joule heating and thermal conduction can be minimized.

For this type of calculations, it is always convenient to define the space variable increasing in the direction of heat flow. Heat balance in the elementary volume $A\ dz$ for a current lead of aspect ratio l/A yields:

$$\dot{Q}(z+dz) - \dot{Q}(z) - \frac{\rho I^2}{A}dz = 0 \tag{41}$$

the third term representing Joule heating in the volume. Integrating in $\dot{Q}$ between z and l under the hypothesis of constant ρ, we obtain

$$\dot{Q}(l) - \dot{Q}(z) = \frac{\rho I^2 (l-z)}{A} \tag{42}$$

On the other hand, from Fourier's law ,

$$\dot{Q}(z) = -kA\frac{dT}{dz}$$

which we can plug in eq. 42, integrate a second time between 0 and l and T_c and T_w, to obtain:

$$\dot{Q}(l) = kA\frac{(T_w - T_c)}{l} + \frac{1}{2}\frac{\rho I^2 l}{A} \tag{43}$$

This expression has a minimum as a function of l/A,

$$(\dot{Q}_l)_{min} = I\sqrt{2\rho k(T_w - T_c)} \tag{44}$$

for

$$(l/A)_{min} = \sqrt{2k(T_w - T_c)/\rho I^2} \tag{45}$$

Relaxing the hypothesis of constant ρ and applying Wiedemann-Franz-Lorenz law, $\rho k = L_{Lorenz}T$, we obtain a minimum heat flux $(\dot{Q}_l)_{min} \approx 1$ mW/A almost independently of the conductor's material, for a vapor-cooled current lead operating between 300 K and 4 K. For comparison, a purely conduction cooled current lead would dissipate ~47 mW/A.

5. CONCLUSIONS

Lecture [24] in this same course shall illustrate the way for efficient thermal design of a cryostat for accelerator devices. In high-energy accelerators, however, the cryostat heat inleaks represent only a fraction of the total heat load budget. Table 15 shows the origin of heat loads in superconducting accelerator devices. Large dynamic loads stem from the beam, through synchrotron radiation, beam image currents, beam-gas inelastic scattering and beam spills. Synchrotron radiation is an important issue in leptonic accelerators. In the existing hadronic machines, usually the energy and the luminosity are such that static losses, i.e. the cryostat heat inleaks and the resistive dissipation, dominate over beam-induced losses. In the LHC, however, owing to the high energy and high luminosity of the beam, dynamic losses will largely override the heat inleak from the cryostat itself.

Table 15
Origin of heat inleaks in high-energy accelerators.

Cryostat heat inleak	Resistive dissipation	Beam-induced losses
radiation to cold surface cold mass supports warm-to-cold feedthroughs	superconductor splices wall resistance instrumentation	synchrotron radiation beam-image currents beam-gas inelastic scattering beam losses

6. BIBLIOGRAPHY

6.1 Heat transfer

[1]   W.H. McAdams, Heat Transmission, (McGraw-Hill Int. Editions, 1958).

[2]   W. Frost, Heat Transfer at Low Temperature, (Plenum Press, New York, 1975).

[3]   L. Weil, Elements des echanges thermiques, (Gauthier-Villars, Paris, 1965).

[4]   A. Bejan, Heat Transfer, (J.Wiley & Sons, New York 1993).

[5]   L.C. Thomas, Heat Transfer Professional version, (Prentice Hall, Englewood Cliffs, 1993).

6.2 Cryogenics

[6]   B.A. Hands, Cryogenic Engineering, (Academic Press, London, 1986).

[7]   Handbook of Cryogenic Engineering, J.P.Weisend ed., (Taylor&Francis, Philadelphia 1998).

[8]   S. Van Sciver, Helium Cryogenics, (Plenum Press, New York, 1986).

[9]   R.B. Scott, Cryogenic Engineering, (Van Nostrand, New York, 1959).

[10]   G.G. Haselden, Cryogenic Fundamentals, (Academic Press, London, 1971).

[11]   R. Conte, Elements de Cryogenie, (Masson & Cie, Paris, 1970).

[12]   Ph. Lebrun, Cryogenics, in CAS School Superconductivity in Particle Accelerators, CERN Yellow Report 89-04.

[13]   F. Pobell, Matter and Methods at Low Temperatures, (Springer, Berlin, 1996).

[14]   W.Vinen, The physics of superfluid helium, Proc. CAS School on Superconductivity and Cryogenics for Particle Accelerators and Detectors, Erice, Sicily, 8-17 May 2002.

[14bis] Ph. Lebrun, L. Tavian, The technology of superfluid helium, in this report.

[15]   R.T. Jacobsen, S.G. Penoncello, E.W. Lemmon, Thermodynamic Properties of Cryogenic Fluids, (Plenum Press, New York, 1997).

6.3 Material properties

[16]   Y.S. Touloukian, Thermophysical Properties of Matter, (Plenum Press, New York, 1995).

[17]   G. Hartwig, Polymer Properties at Room and Cryogenic Temperatures (Plenum Press, New York, 1994).

[18]   N.J. Simon, E.S. Drexel, R.P. Reed, Properties of copper and copper alloys at cryogenic temperatures, NIST Monograph 177, (1992).

[19]   V.D. Arp, Electrical and thermal conductivities of elemental metals below 300 K, Thirteenth Symposium on the Thermophysical Properties, June 22- 27, 1997, Boulder Colorado, U.S.A.

6.4 References

[20]   L.J. Salerno and P. Kittel, in Handbook of Cryogenic Engineering, J.P.Weisend ed., (Taylor&Francis, Philadelphia 1998), 164.

[21]   E. Gmelin, M. Asen-Palmer, M. Reuther, R. Villar, J.Phys D: Appl.Phys. <u>32</u> (1999) R19-R43.

[22]   T. Nast, in Handbook of Cryogenic Engineering, J.P.Weisend ed., (Taylor&Francis, Philadelphia 1998), 186.

[23]   Ph. Lebrun, S. Milner, A. Poncet, Adv. Cryog. Eng. <u>31</u> (1986) 543.

[24]   Ph. Lebrun, Design of a cryostat for superconducting accelerator magnet: the LHC main dipole case, in this report.

DESIGN OF A CRYOSTAT FOR SUPERCONDUCTING ACCELERATOR MAGNET: THE LHC MAIN DIPOLE CASE

Ph. Lebrun
CERN, European Organisation for Nuclear Research, Geneva, Switzerland

Abstract
As an application of the lectures on heat transfer, this tutorial presents the simplified thermal design of a cryostat for a superconducting accelerator magnet. Starting from functional requirements and design constraints, and using standard formulae and typical data for heat transfer at low temperatures, we sketch an engineering solution for the cryostat and evaluate its thermal performance. We then present how this design is implemented in a real cryostat, industrially produced in series of 1250 units.

1.   INTRODUCTION

Although an ancillary component, the cryostat housing a superconducting accelerator magnet fulfils several important roles. First of all, it provides adequate thermal insulation for low-temperature operation of the magnet, and in some cases of the associated cryogenic pipework and beam vacuum system. Equally important, the cryostat constitutes the mechanical interface of the superconducting magnet to the outside world. It must therefore rigidly support and precisely position the cold mass with respect to the external alignment fiducials, in a reproducible fashion throughout steady and transient regimes of operation. The cryostat may also perform other functions, such as magnetic screening of the stray field or radiation shielding of the beam halo. It is therefore clear that cryostat design and optimisation must integrate all boundary conditions and constraints set by superconducting magnet, cryogenic and other relevant accelerator systems.

2. FUNCTIONAL REQUIREMENTS AND DESIGN CONSTRAINTS

For the purpose of this tutorial, the basic thermal design and configuration of the LHC main dipole cryostat can be derived from the following simplified set of requirements and constraints.

The cryostat must house a superconducting magnet "cold mass" operating in superfluid helium at 1.9 K.

The cold mass is contained inside a stainless-steel helium vessel with an external diameter of 0.6 m, length 15 m.

The cold mass is 30,000 kg, i.e. 2000 kg/m length.

Due to external space constraints (installation in accelerator tunnel), the outer vessel of the cryostat must have an external diameter not exceeding 1.0 m.

The cold mass must be supported inside the cryostat in a stable and stiff fashion.

The maximum heat load budget at 1.9 K in normal operation is 3 W, i.e. 0.2 W/m length.

In view of possible degradation of the insulation vacuum, a design solution which limits the increase of heat inleak is favoured.

3. HEAT TRANSFER DATA

The laws and formulae of heat transfer by solid conduction, residual gas conduction and radiation are given in the lectures on "Heat transfer" [1].

Typical values for thermal conductivity integrals, emissivity of technical materials and heat fluxes across different insulation systems at low temperatures are recalled respectively in Tables 1, 2 and 3. These Tables should primarily be used to orient design choices; they however have no claim to exhaustivity, and thermal insulation solutions based on other materials, surface finishes and temperature levels may also be considered.

Table 1
Thermal conductivity integrals of selected materials [W/m]

From vanishingly low temperature up to	20 K	80 K	290 K
OFHC copper	11000	60600	152000
DHP copper	395	5890	46100
1100 aluminium	2740	23300	72100
2024 aluminium alloy	160	2420	22900
AISI 304 stainless steel	16.3	349	3060
G-10 glass-fiber/epoxy composite	2	18	153

Table 2
Emissivity of technical materials at low temperatures

	Radiation from 290 K Surface at 77 K	Radiation from 77 K Surface at 4.2 K
Stainless steel, as found	0.34	0.12
Stainless steel, mech. polished	0.12	0.07
Stainless steel, electropolished	0.10	0.07
Stainless steel + Al foil	0.05	0.01
Aluminium, as found	0.12	0.07
Aluminium, mech. polished	0.10	0.06
Aluminium, electropolished	0.08	0.04
Copper, as found	0.12	0.06
Copper, mech. polished	0.06	0.02

Table 3
Typical heat fluxes at vanishingly low temperature between flat plates [W/m^2]

Black-body radiation from 290 K	401
Black-body radiation from 80 K	2.3
Gas conduction (100 mPa He) from 290 K	19
Gas conduction (1 mPa He) from 290 K	0.19
Gas conduction (100 mPa He) from 80 K	6.8
Gas conduction (1 mPa He) from 80 K	0.07
MLI (30 layers) from 290 K, pressure below 1 mPa	1-1.5
MLI (10 layers) from 80 K, pressure below 1 mPa	0.05
MLI (10 layers) from 80 K, pressure 100 mPa	1-2

4. A DESIGN SOLUTION

We present a simplified version of the reasoning which has permitted to roughly size the heat load budget of the LHC [2] and led to the construction of the first superfluid-helium cooled accelerator magnet cryostat [3], thus establishing the cryogenic feasibility of the project.

4.1 A two-dimensional problem

All reasoning will be done per unit length of cryomagnet, which reduces to a two-dimensional problem in the transverse plane. The lumped heat loads, e.g. through the supports, are then calculated as distributed along the length of the cryostat.

4.2 Basic configuration

The mechanical members supporting the 1.9 K cold mass from the room-temperature outer vessel should be such that the heat conduction path is made as long as possible, while still preserving sufficient rigidity, stability and positioning accuracy.

Two basic configurations are considered:

- support posts in compression (Fig. 1.a),
- tie rods in tension (Fig. 1.b)

at regular intervals along the length of the cryomagnet.

The thermal profile along the support members develops over 0.2 m in the first case, and 0.5 m in the second one.
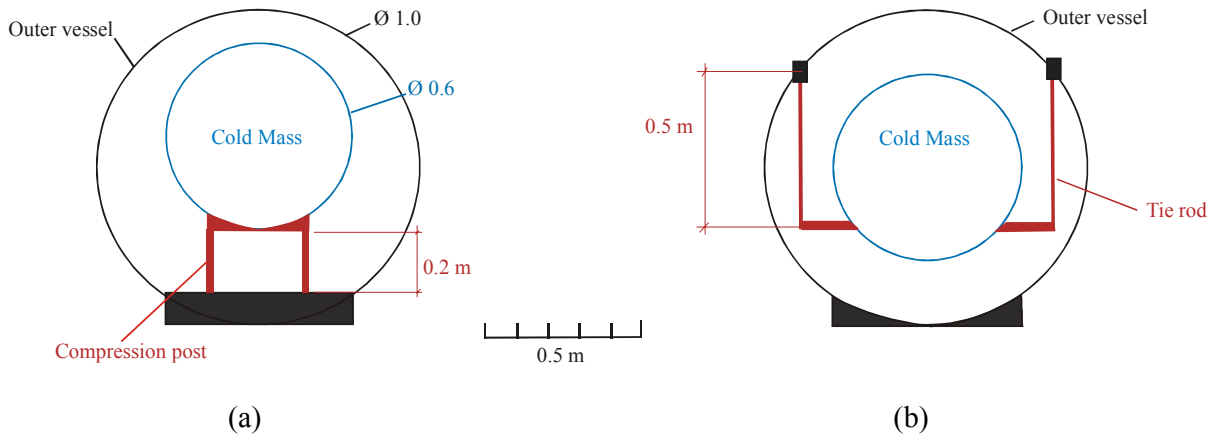
Fig. 1 Basic transverse configurations of cryomagnet,
using compression support posts (a) or tension tie rods (b).

4.3 Does one need intermediate shielding?

Per unit length of cold mass, the lateral cold surface area is

$$\pi \times 0.6 = 1.88 \text{ m}^2$$

Consider only multilayer insulation in good vacuum, for example 30 layers wrapped around the cold mass; the resulting heat load would then be $1.5 \times 1.88 = 2.8$ W, i.e. an order of magnitude too high with respect to the budget of 0.2 W.

57

$\Rightarrow$ The cryostat will feature a thermal shield actively cooled at intermediate temperature, say 80 K which can be provided by liquid nitrogen or gaseous helium. A quasi-cylindrical shield with a diameter of 0.8 m can be fitted in-between cold mass and vacuum vessel, leaving sufficient radial space for thermal insulation and mechanical tolerances.

4.4 Does one still need insulation around the cold mass, in presence of the 80 K shield?

The cold mass surface, made of stainless steel, has an emissivity $\varepsilon_{cm} = 0.12$ (Table 2).

The inner surface of the thermal shield, made of aluminium alloy sheet as found, has an emissivity ε_{ts} of 0.12 (Table 2).

The emissivity factor E for long nested cylinders in the case of diffuse reflection is

$$E = \frac{\varepsilon_{cm} \cdot \varepsilon_{ts}}{\varepsilon_{ts} + \frac{A_{cm}}{A_{ts}} \cdot (1 - \varepsilon_{ts}) \cdot \varepsilon_{cm}}$$

where A_{cm} and A_{ts} are the respective surface areas of cold mass and thermal shield, of emissivity ε_{cm} and ε_{ts}

$$E = \frac{0.12 \times 0.12}{0.12 + 0.75 \times 0.88 \times 0.12} \simeq 0.07$$

The heat inleak by radiation is then:

$$\begin{aligned} \dot{Q}_{rad} &= E\sigma A_{cm}\left(T_{ts}^4 - T_{cm}^4\right) \\ &= 0.07 \times 5.67 \times 10^{-8} \times 1.88 \times 80^4 \\ &= 0.31\,\text{W} \end{aligned}$$

which exceeds the thermal budget.

Consider now an improvement of the emissivity of the cold mass by wrapping one layer of aluminium foil, $\varepsilon_{cm} = 0.01$.

Then $\dot{Q}_{rad} = 0.04$ W within budget.

4.5 What about residual gas conduction?

Let's assume that the residual gas is pure helium, since all other species are condensed at low temperature, with vanishingly low vapour pressure.

Consider only the molecular conduction regime, which prevails at low pressure. In this regime, heat transfer is proportional to residual gas pressure, according to Kennard's law

$$\dot{Q}_{res} = A_{cm}\,\alpha\,\Omega P\left(T_{ts} - T_{cm}\right)$$

with $\Omega = 2.13$ W/m^2.Pa.K for helium and the overall accommodation coefficient α given by:

$$\alpha = \frac{\alpha_{cm} \cdot \alpha_{ts}}{\alpha_{ts} + \alpha_{cm}\left(1 - \alpha_{ts}\right)\frac{A_{cm}}{A_{ts}}}.$$

With a 0.8 m diameter thermal shield,

$$\frac{A_{cm}}{A_{ts}} = 0.75$$

From literature, for helium at 2 K $\quad \alpha_{cm} = 1$
at 80 K $\quad \alpha_{ts} = 0.4$

This yields a value $\alpha = 0.47$.

Then, for 1 mPa residual helium pressure,

$$\dot{Q}_{res} = 0.15 \text{ W}$$

so that the total radiative and gas conductive heat inleak from the 80 K shield to the cold mass wrapped with one layer aluminium foil is

$$\dot{Q}_{rad} + \dot{Q}_{res} = 0.04 + 0.15 = 0.19 \text{ W} \quad \text{within budget.}$$

Consider, however, a 100-fold increase in residual helium pressure (100 mPa). Then

$$\dot{Q}_{res} = 15 \text{ W} \quad \text{which is unacceptable.}$$

A better solution is to wrap the cold mass with a multilayer system, say 10 layers of multilayer insulation. The total heat inleak in good vacuum is then, from Table 3,

$$\dot{Q} = 1.88 \times 0.05 = 0.09 \text{ W.}$$

Under degraded vacuum conditions (100 mPa helium), it still increases significantly

$$\dot{Q} = 1.88 \times 2 = 3.8 \text{ W}$$

however, a factor 4 lower than with the previous insulation system.

$\Rightarrow$ We therefore retain the latter solution of 10 layers multilayer insulation around the cold mass, yielding a distributed heat load of $\boxed{0.09 \text{ W}}$.

4.6 Which type of supporting system? of which material?

The heat load by solid conduction along the supports is given by

$$\dot{Q}_{con} = \int_{T_1}^{T_2} k(T)dT \times \frac{S}{L}.$$

Consider first a low-conductivity metallic material, i.e. austenitic stainless steel, for which a reasonable design stress in compression or tension is 100 MPa. To take the 20 kN weight of the 2000 kg mass, one needs a cross section $S = 2 \times 10^{-4} \text{ m}^2$.

For austenitic stainless steel, from Table 1,

$$\int_{1.9}^{290} k(T)dT = 3060 \text{ W/m}$$

$$\int_{1.9}^{80} k(T)dT = 349 \text{ W/m.}$$

In the case of compression posts, $L = 0.2$ m between the vacuum vessel and the cold mass, so that

$$\dot{Q}_{con} = 3060 \times \frac{2 \times 10^{-4}}{0.2} = 3.06 \text{ W}$$

which is well above budget.

Consider introducing heat interception at 80 K and midlength of the post; then

$$\dot{Q}_{con} = 349 \times \frac{2 \times 10^{-4}}{0.1} = 0.7 \text{ W}.$$

The situation has improved, but insufficiently.

In the case of <u>tension tie-rods</u>, $L = 0.5$ m. In the same fashion as previously

- without heat interception $\dot{Q}_{con} = 1.22$ W
- with 80 K heat interception at mid-length $\dot{Q}_{con} = 0.28$ W.

The latter value, although significantly lower, still remains above budget.

The only practical issue is to make use of an alternative material with lower heat conductivity: consider <u>G-10 glass-fiber/epoxy composite</u>, for which an acceptable design stress in compression is 40 MPa. To take the 20 kN weight, the cross section of G-10 required is thus $S = 5 \times 10^{-4} \text{ m}^2$.

For G-10 glass-fiber/epoxy composite, from Table 1,

$$\int_{1.9}^{290} k(T)dT = 153 \text{ W/m}$$

$$\int_{1.9}^{80} k(T)dT = 18 \text{ W/m}.$$

For a G-10 post without heat interception

$$\dot{Q}_{con} = 153 \times \frac{5 \times 10^{-4}}{0.2} = 0.38 \text{ W}$$

which is still too high.

Introducing 80 K heat interception at midpoint reduces the conductive heat inleak to

$$\dot{Q}_{con} = 18 \times \frac{5 \times 10^{-4}}{0.1} = \boxed{0.09 \text{ W}}$$

which is finally acceptable.

The heat load from 290 K intercepted at 80 K is then

$$135 \times \frac{5 \times 10^{-4}}{0.1} = 0.68 \text{ W}.$$

5. THERMAL DESIGN SUMMARY

$\Rightarrow$ Use a 0.8 m diameter actively-cooled thermal shield at 80 K, wrapped with 30 layers multilayer insulation. Its lateral surface of 2.51 m^2 will receive 3.76 W @ 80 K from the outer vessel.

$\Rightarrow$ Wrap the cold mass with 10 layers multilayer insulation: in good insulation vacuum, it will then receive 0.09 W @ 1.9 K.

⇒ Use compression support posts made of G-10 glass-fiber/epoxy composite, with 80 K heat intercept at midpoint. Solid conduction then yields 0.09 W @ 1.9 K, and 0.68 W @ 80 K.

The transverse cross section of the cryostat which we have designed is sketched in Fig. 2. The corresponding thermal flow scheme is given in Fig. 3. The total heat load budget per meter length in nominal conditions is then:

@ 80 K $3.76 - 0.09 + 0.68 - 0.09 =$ 4.26 W

@ 1.9 K $0.09 + 0.09 =$ 0.18 W
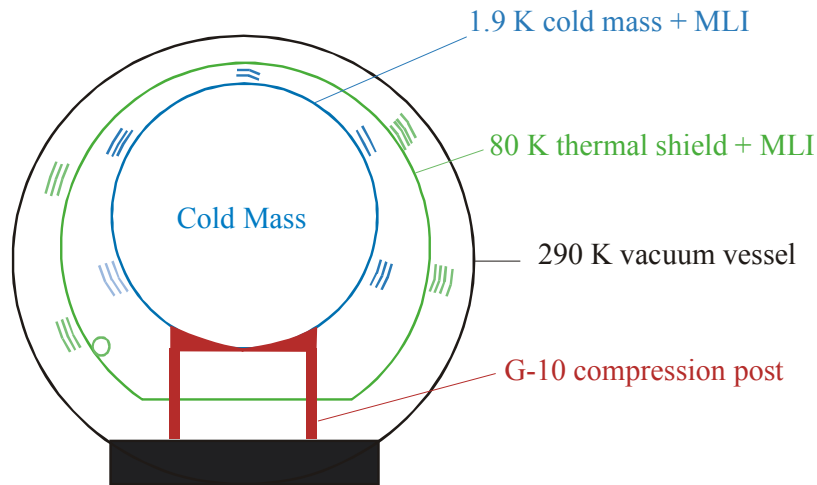
Fig. 2 Sketch of cryostat transverse cross section
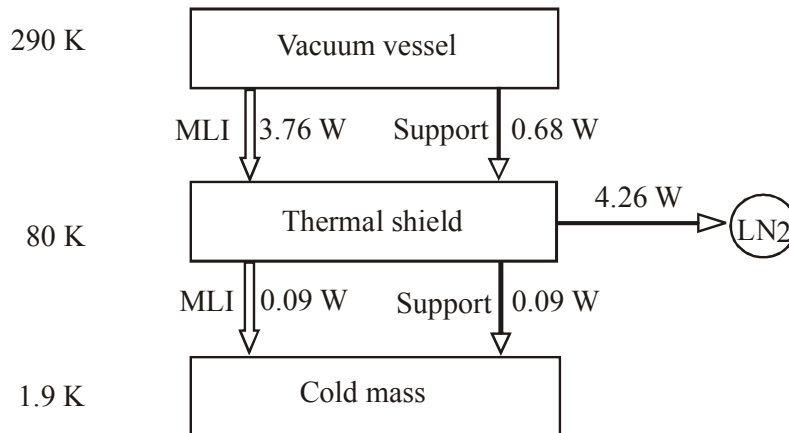
Fig. 3 Thermal flow scheme of cryostat (heat loads per m length)

6. FROM DESIGN TO CONSTRUCTION

The preceding study has permitted to sketch a design solution for the transverse cross-section of the cryostat and estimate its heat load budget. The final LHC dipole cryostat [4] exhibits the main features of the above solution: non-metallic composite support posts, an intermediate temperature thermal shield providing heat interception at the support posts, multilayer reflective insulation around the thermal shield and cold mass (Fig. 4). A difference with the sketched solution resides in the second level of heat interception, using an available 5 K supercritical helium line, on the support posts. This feature enables to reduce further the heat conducted to the 1.9 K plate, from 0.09 W to 0.01 W (per m length of cryomagnet). The LHC support post described in [5], is shown in Fig. 5. Another important difference, which however does not appear on the cross-section, is the use of a forced flow of gaseous helium between 50 and 75 K, instead of liquid nitrogen, to cool the thermal shield. This choice is primarily driven by reasons of safety, to avoid the potential release of large amounts of nitrogen in the underground tunnel, in case of accident, and the resulting oxygen-deficiency hazard.

We shall now address some of the practical issues for constructing such a cryostat.
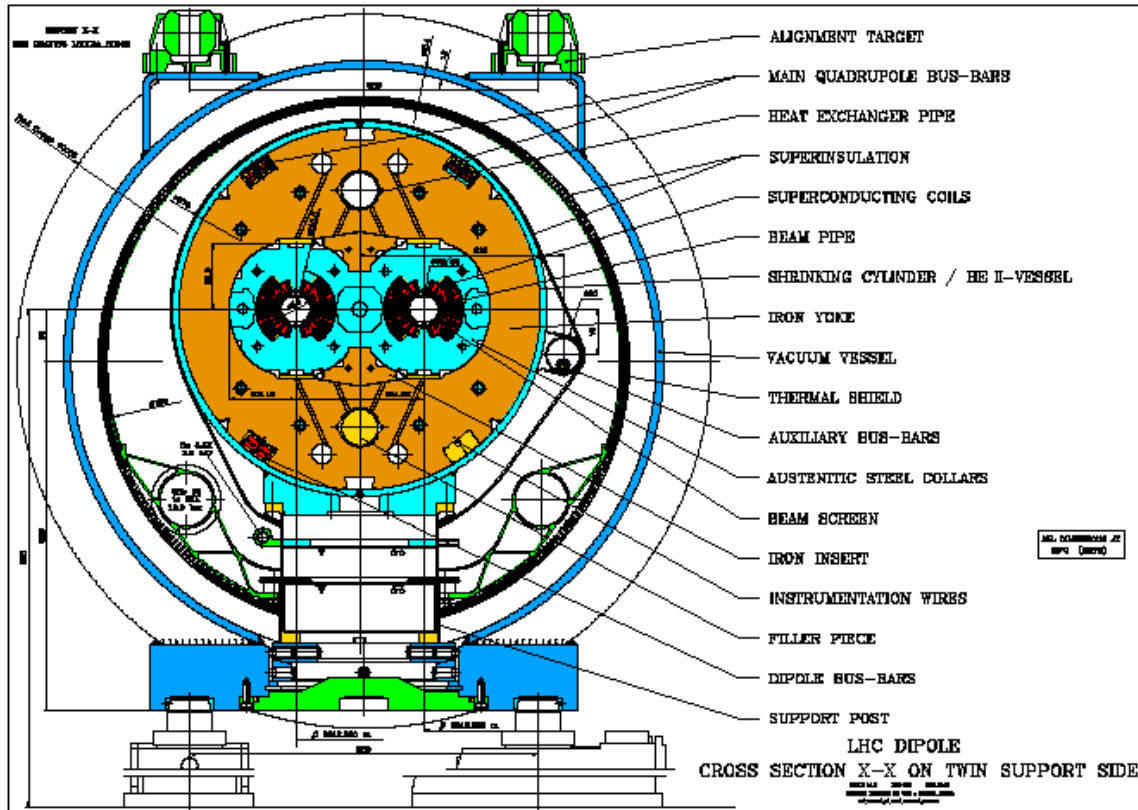
Fig. 4 Transverse cross section of final LHC dipole cryostat

Fig. 5 Non-metallic composite support post for LHC cryomagnet

6.1 The third dimension

The cryomagnet is a 3-dimensional object (Fig. 6): the supporting of the cold mass is performed at precise locations along the length. The maximum spacing, and hence the minimum number of support posts, is given primarily by the flexural rigidity of the cold mass and the allowed sagitta. For the 15-m long LHC dipole, the allowed sagitta of a few tenths of mm imposes to have three support posts. The system composed of the cold mass supported on three points from the vacuum vessel is then hyperstatic. For evident reasons of symmetry, there is a support post at mid-length. The longitudinal positions of the other two are determined by a compromise between considerations of stress (evenly-shared loading) and deformation (displacement and angle of the overhang at the ends of the cold mass).
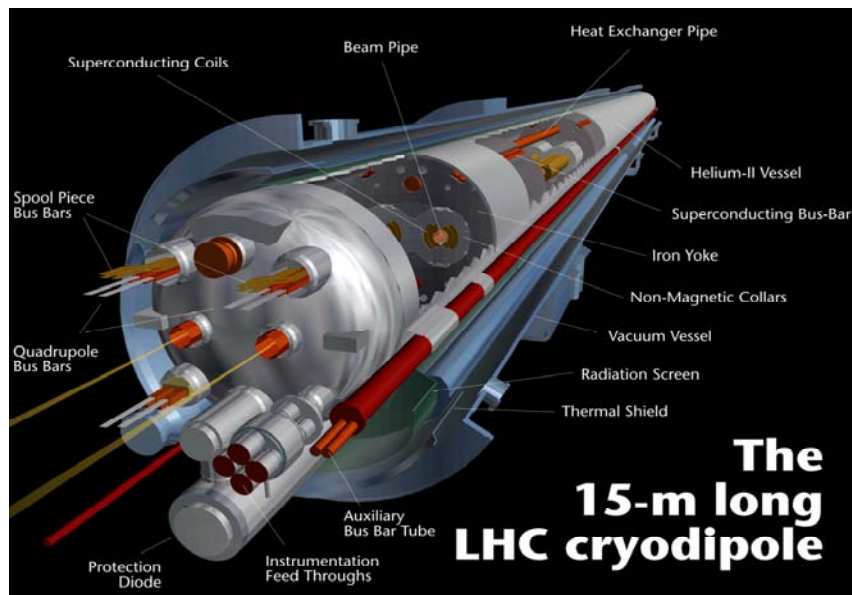
Fig. 6 Artist's perspective of LHC cryodipole

Another issue coming from the longitudinal dimension is that of thermal contraction. Assimilating the cold mass to an austenitic stainless-steel object, its integrated contraction upon cooldown to operating temperature is about 3×10^{-3}, i.e. 45 mm. Two constructional features are needed to cope with this.

- Bellows with sufficient travel, flexibility and resistance must be used to compensate for the contraction between cold masses at the cryomagnet interconnects (Fig. 7). The design optimisation, construction and installation of these several thousands bellows constitute an engineering feat in itself [6].

- To avoid the build-up of shear stresses on the lateral support posts, longitudinal displacement must be allowed between them and the vacuum vessel, thermal shield and/or cold mass. This displacement can be achieved by rolling or sliding, on the room-temperature or the cold end of the support posts. In the LHC cryomagnets, the support posts slide on low-friction surfaces on the vacuum vessel, i.e. under vacuum but at room temperature. Actually, as the cold mass is curved along the particle beam trajectory, the central post, which is fixed longitudinally, can however slide transversely to accommodate the cooldown/warmup displacements.
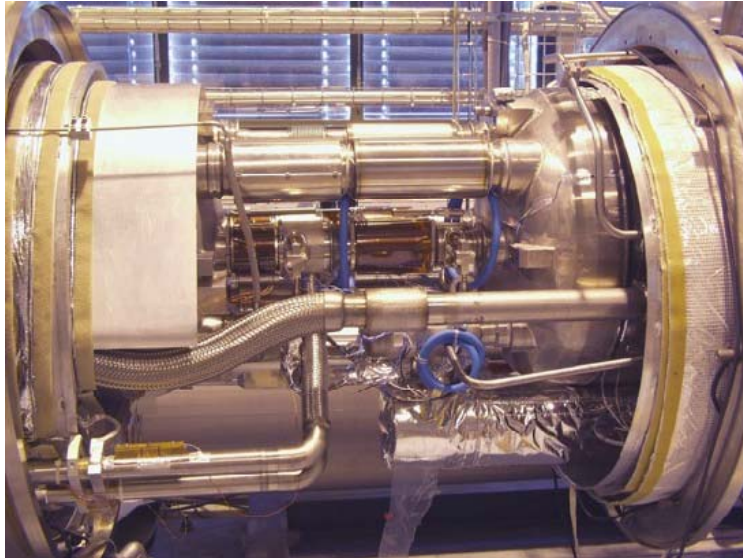
Fig. 7 Cryomagnet interconnect

6.2 Temperature homogeneity of the thermal shield

The thermal shield is a cylindrical shell cooled from one generatrix, along which the cooling tube runs. Its proper operation as a quasi-isothermal horizon surrounding the cold mass imposes that azimuthal thermal gradients developed by heat conduction in the shell remain below a limiting value, say 5 K. This requires selecting a material with high thermal conductivity and proper sizing of the shell.

Assuming a constant heat flux $\dot{q}$ received by the shield, and constant thermal conductivity k in the limited temperature range considered, the temperature profile along the developed circumference is parabolic, and the maximum azimuthal temperature difference is:

$$\Delta T_{azimuth} = \frac{\pi^2}{8} \frac{D^2}{k\,e} \dot{q}$$

with D diameter of thermal shield
        e thickness of thermal shield
        k thermal conductivity of thermal shield.

Let us consider first a 2-mm thick sheet of 2024 aluminium alloy, with an average thermal conductivity in the 50-75 K range of 46 W/m . K

Then, for $D = 0.8$ m
             $\dot{q} = 1.5$ W/m^2

one finds $$\Delta T_{aximuth} = \frac{\pi^2}{8} \frac{0.8^2 \times 1.5}{46 \times 2 \times 10^{-3}} = 12.9 \text{ K}$$

This clearly exceeds the requirement. To stay within the 5 K limit, a sheet thickness of more than 5 mm would be required.

An alternative is to use a 2-mm thick sheet of commercially pure aluminium (1100), which shows an average thermal conductivity of 330 W/m . K

Then, $$\Delta T_{aximuth} = \frac{\pi^2}{8} \frac{0.8^2 \times 1.5}{330 \times 2 \times 10^{-3}} = 1.8 \text{ K}$$

which is acceptable.

With respect to 2024 aluminium alloy, commercially pure aluminium exhibits much weaker mechanical strength: this is however of secondary importance for this application driven by thermal conductivity, provided the rigidity is given by an extruded "bottom tray" which also integrates the cooling channel (Figs 8 and 9).

Fig. 8 Thermal shield extruded "bottom tray" with integrated cooling channel

Fig. 9 Section of aluminium thermal shield around dipole cold mass

6.3 Achieving efficient heat interception

As the thermal flow scheme in Fig. 3 shows, the very low residual heat load at the 1.9 K level rests on the ability to construct heat intercepts which operate as calculated. In practice, these heat intercepts often involve solid-to-solid contacts under vacuum at low temperature, which are known to be difficult to build in an efficient and reproducible manner, preserving their low thermal impedance over time and thermal cycles.

Industrial-type solutions for these intercepts, implemented in the LHC cryodipole construction, include the following.

- The contact between the shell and bottom tray of the thermal shield is ensured by interrupted weld seams covering at least 25% of the length.

- The heat intercept plates on the support posts are made of 10-mm thick aluminium, which ensures their shrink fitting onto the G-10 column, and glued to it.

- The lower heat intercept plate (50-75 K) is connected to the thermal shield bottom tray via flexible aluminium strips, in an all-welded construction (Fig. 5).

- The upper intercept plate (5 K) integrates a 1-mm wall-thickness stainless steel cooling tube, fitted through it at the time of casting (Fig. 5).

6.4 Installing multilayer insulation

The solution retained for the LHC cryomagnets is that of prefabricated multilayer blankets incorporating reflective film, spacer and outer protection net, factory-cut and assembled with the precise geometry, and equipped with VELCRO® fasteners before packaging. Upon assembly of the cryostat, the blankets are easily installed around the cold mass and thermal shield (Fig. 10), and fixed with the VELCRO® fasteners (Fig. 11). It must be noted that the latter show a high emissivity (close to that of a blackbody), and must therefore be covered with aluminium tape, when exposed, or concealed below the internal force of the blanket.

Fig. 10 Prefabricated multilayer insulation blankets upon installation

6.5 The outer vessel

The outer vessel, which constitutes the interface of the cryomagnet with the outside world, combines several functions. First of all, it constitutes the leak-tight enclosure for the insulation vacuum of the cryostat. Equally important, it participates to the supporting and precise positioning of the cold mass, a function specific to accelerator magnet cryostats, which the standard tolerances of sheet-metal work may have difficulty to match. It also performs auxiliary duties, such as magnetic shielding of the stray flux. Finally, in view of its dimensions and mass, it represents the single largest component of the cryostat in terms of cost, and must therefore be optimised also from this point of view.

Fig. 11 VELCRO® fasteners for fixing multilayer insulation blankets

The vacuum vessels of the LHC dipole cryostats are essentially welded steel tubes, with reinforcing rings and precision-machined surfaces at the three locations of the support posts (Fig. 12). In this fashion, the expensive high-precision manufacturing operations are confined to these locations, while the rest of the vessel can be constructed with the tolerances of sheet-metal work. For reasons of cost and magnetic shielding, the vessels are made of low-carbon steel, with stainless steel flanges for interconnects at the ends. They must therefore be painted outside for corrosion protection and sandblasted inside for low outgassing. Locating the external supports at the same longitudinal positions as the support posts suppresses bending moments and corresponding deformations. The vessel wall can then be sized from the standard construction codes applicable for pressure and vacuum vessels.

Fig. 12 Outer vacuum vessels awaiting assembly

7. CONCLUSION

This tutorial will have reached its primary goal if it has convinced the student that cryostats meeting complex and demanding requirements can be conceptually designed from the basic laws of heat transfer and the thermophysical properties of construction materials at low temperature, with the guidance of second-law thermodynamics and – as a consequence – the virtues of temperature staging and heat interception. We hope it will also have demonstrated some of the difficulties of implementing the conceptual design into an engineering product, and illustrated technological solutions to achieve reproducible performance while limiting complexity and cost.

REFERENCES

[1]   G. Vandoni, Heat transfer, in this report.

[2]   G. Claudet, F. Disdier, A. Gauthier, Ph. Lebrun, J. Schmid, Conceptual study of the superfluid helium cryogenic system for the CERN Large Hadron Collider, Proc. ICEC12, Butterworths, Guildford (1988) 497-504.

[3]   M. Granier, Ph. Lebrun, M. Mischiatti, Design and construction of a superfluid helium cryostat for a ten-meter long, high-field superconducting dipole magnet, Cryogenics 30 September supplement (1990) 98-102.

[4]   J.C. Brunet, V. Parma, G. Peón, A. Poncet, P. Rohmig, B. Skoczen and L.R. Williams, Design of the second series of LHC prototype dipole magnet cryostats, Adv. Cryo. Eng. 43A (1998) 435-441.

[5]   M. Castoldi, M. Pangallo, V. Parma and G. Vandoni, Thermal performance of the supporting system for the LHC superconducting magnets, Adv. Cryo. Eng. 45A (2000) 795-802.

[6]   A. Jacquemod, A. Poncet, B. Skoczen, J.-Ph. Tock, The interconnections of the LHC cryomagnets, Proc. PAC2001, IEEE, Piscataway (2001) 616-618.

THE TECHNOLOGY OF SUPERFLUID HELIUM

Ph. Lebrun and L. Tavian
CERN, Geneva, Switzerland

Abstract

The technical properties of helium II ("superfluid" helium) are presented from the user point of view. Its applications to the cooling of superconducting devices, particularly in accelerators, are discussed in terms of heat transfer capability and limitations in conductive and convective modes. Large-capacity refrigeration techniques below 2 K are reviewed, as concerns thermodynamic cycles as well as process machinery. Examples drawn from existing or planned projects illustrate the presentation.

1. INTRODUCTION

Once a curiosity of nature and still today an arduous research topic in condensed-matter physics, superfluid helium[*] has also become a technical coolant for advanced superconducting devices, to the point that it is now implemented in industrial-size cryogenic systems, routinely operated with high reliability. Two classes of reasons call for the use of superfluid helium as a coolant for superconducting devices, namely the lower temperature of operation, and the enhanced heat transfer properties at the solid-liquid interface and in the bulk liquid.

The lower temperature of operation is exploited in high-field magnets [1, 2], to compensate for the monotonously decreasing shape of the superconducting transition frontier in the current density-versus-magnetic field plane, shown in Fig. 1 for superconducting materials of technical interest. In this fashion, the current-carrying capacity of the industrial Nb-Ti superconducting alloys can be boosted at fields in excess of 8 T, thus opening the way for their use in high-field magnet systems for condensed-matter physics [3-5], nuclear magnetic resonance [6, 7], magnetic confinement fusion [8, 9] and circular particle accelerators and colliders [10-12]. In the case of high-frequency superconducting devices, such as acceleration cavities [13], the main drive for superfluid helium cooling is the exponential dependence of the BCS losses on the ratio of operating-to-critical temperature. Accelerators based on this technology, such as medium-energy, high-intensity machines [14, 15] and future high-energy lepton colliders [16-18] operate in the temperature range which minimizes capital costs and overall energy consumption. This issue is schematized in Fig. 2.

The technical heat transfer characteristics of superfluid helium basically derive from peculiar transport properties [19, 20]. Its low bulk viscosity enables superfluid helium to permeate to the heart of magnet windings, while its very large specific heat (typically 10^5 times that of the conductor per unit mass, 2×10^3 per unit volume), combined with excellent heat conductivity at moderate heat flux (10^3 times that of cryogenic-grade OFHC copper) can produce powerful stabilization against thermal disturbances. In order to fully exploit these properties, however, both in steady-state and transient regimes, e.g. for power heat transport over macroscopic distances as well as intimate stabilization of superconductors, an elaborate thermo-hydraulic design of the cooling circuits, conductor, insulation and coil assemblies is required. This often conflicts with other technical or economic requirements of the projects and acceptable trade-offs have to be found.

---

[*] Strictly speaking, we are referring to the second liquid phase of helium, called He II, which exhibits the unusual bulk properties associated with superfluidity and is therefore also called "superfluid". This is not to be confused with the entropy-less component of the phenomenological two-fluid model accounting for the behaviour of He II, which some authors prefer to keep the qualificative "superfluid" for.

In the following, we will only address the specific issues of cryogenic technology pertaining to the use of superfluid helium as a technical coolant, namely different cooling methods as well as processes and machinery for sub-lambda temperature refrigeration [21]. Reference is made to companion lectures for cryogenic techniques which – however important in system design - are not superfluid-helium specific, such as thermal insulation and cryostat design [22, 23].
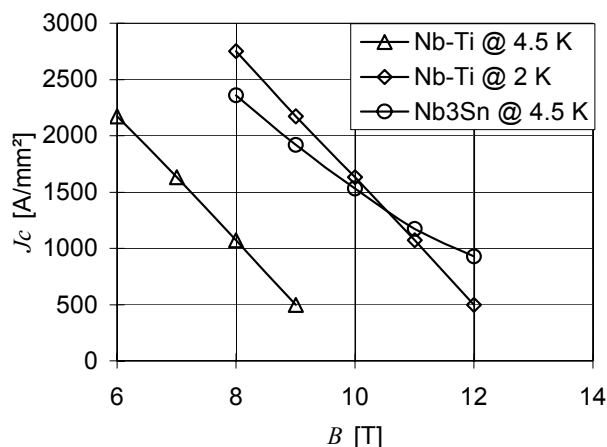

Fig. 1 Critical current density of technical superconductors.
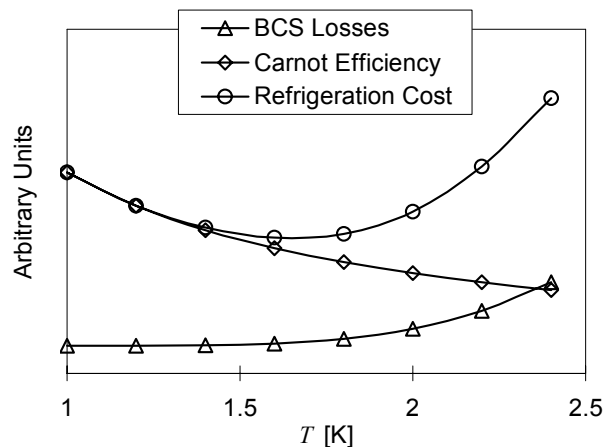
Fig. 2 Optimal operating temperature of RF superconducting cavities.

2. DIFFERENT COOLING METHODS

2.1   Pressurized versus saturated superfluid helium

A look at the phase diagram of helium (Fig. 3) clearly shows the working domains of saturated helium II, reached by gradually lowering the pressure down to below 5 kPa along the saturation line, and pressurized helium II, obtained by subcooling liquid at any pressure above saturation, and in particular at atmospheric pressure (about 100 kPa).

Although requiring one more level of heat transfer and additional process equipment - in particular a pressurized-to-saturated helium II heat exchanger - pressurized helium II cooling brings

several important technical advantages [24]. Avoiding low-pressure operation in large and complex cryogenic systems clearly limits the risk of air inleaks, and resulting contamination of the process helium. Moreover, in the case of electrical devices, the low dielectric strength exhibited by low-pressure helium vapour [25], in the vicinity of the minimum of the Paschen curve (Fig. 4) [26], brings the additional risk of electrical breakdown at fairly low voltage. Operating in pressurized helium II avoids this kind of problem.
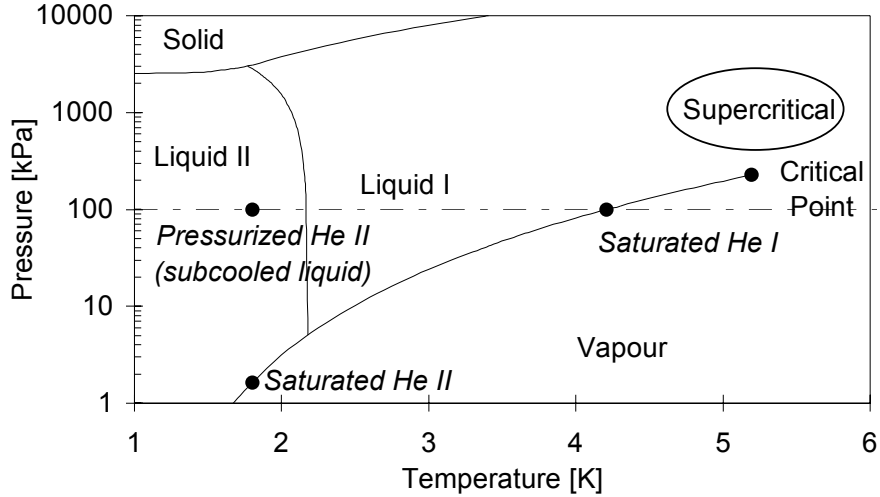
Fig. 3 Phase diagram of helium.
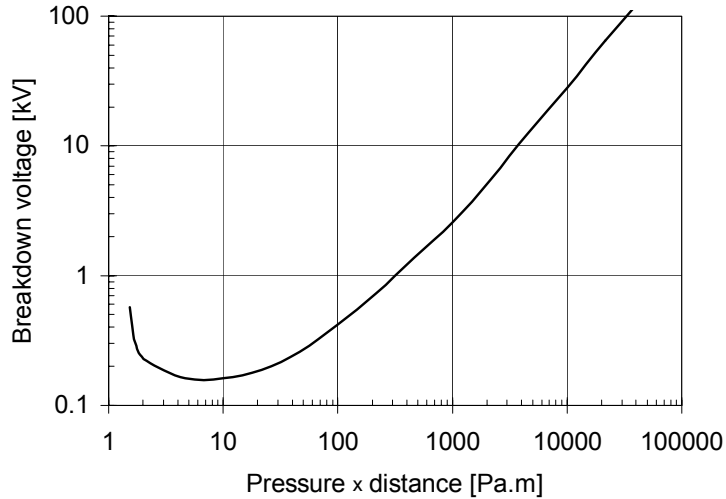
Fig. 4 Paschen curve for helium at 300 K.

However, the most interesting and specific aspect of pressurized helium II in the operation of superconducting devices stems from its capacity for cryogenic stabilization. As a subcooled (monophase) liquid with high thermal conductivity, pressurized helium II can absorb in its bulk a deposition of heat, up to the temperature at which the lambda-line is crossed, and local boiling only then starts due to the low thermal conductivity of helium I. Quasi-saturated helium II, which is in fact slightly subcooled due to the hydrostatic head below the surface of the liquid bath, may only absorb

heat deposition up to the point at which the saturation line is crossed, and change of phase occurs. The enthalpy difference from the working point to the transition line is usually much smaller in the latter case. The argument, developed in reference [27], typically yields an order of magnitude better performance in favour of pressurized helium II.

2.2 Conduction cooling

In the following we shall only consider conductive heat transport in helium II at heat fluxes of technical interest (typically above 1 kW.m^{-2}). For most practical geometries, this means working in the "turbulent" regime with full mutual friction between the components of the two-fluid model [28]. In this regime, helium II exhibits a large, finite and non-linear bulk heat conductivity, the value of which depends both on temperature and heat flux. While the general patterns of this behaviour can be predicted by the Gorter-Mellink [29] theory[*], practical data useful for engineering design has been established in a number of experiments [30-35].

Consider conduction in one dimension, e.g. in a tubular conduit of length L, the ends of which are maintained at temperatures T_C and T_W. The steady-state heat flux $\dot{q}$ is given by:

$$\dot{q}^n \cdot L = X(T_C) - X(T_W)$$ (1)

while the Gorter-Mellink theory contains n = 3, the best experimental fit for n appears to be 3.4, with $X(T)$ a tabulated function of temperature, physically analog to a conductivity integral [30]. A plot of this function reveals that the apparent thermal conductivity of helium II goes through a maximum at around 1.9 K (Fig. 5).
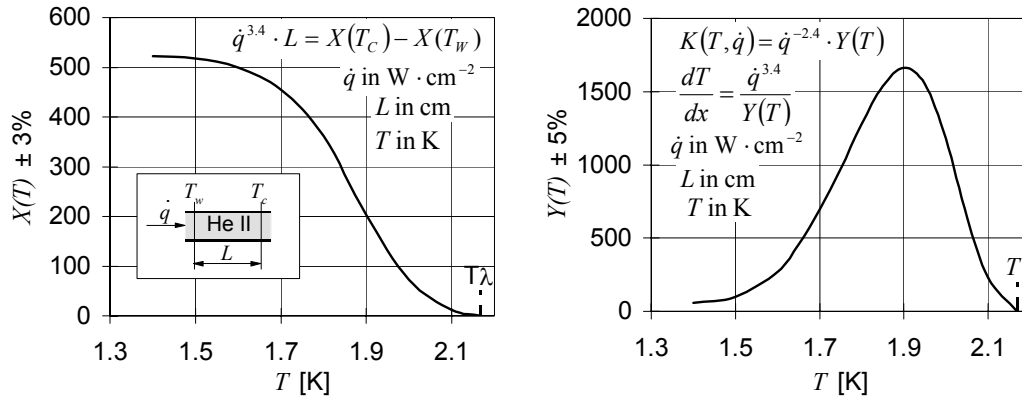

Fig. 5 Thermal conductivity integral and apparent thermal conductivity of pressurized superfluid helium [22].

As an example, the heat flux transported by conduction between 1.9 and 1.8 K in a 1-m long static column of helium II is about 1.2 W.cm^{-2}, i.e. three orders of magnitude higher than what would be conducted along a bar of OFHC copper of the same geometry! The non-linearity with respect to heat flux also results in a much weaker dependence of conduction upon length, or thermal gradient. Fig. 6 shows the steady-state conduction $\dot{Q}$ in superfluid helium between 1.9 and 1.8 K versus the static column length L for different equivalent nominal diameters of the column. This abacus clearly shows that while the heat flux conducted in a solid is directly proportional to the thermal gradient applied, doubling the conduction length in a column of helium II only reduces the heat flux by some 20 %.

---

[*] C.J. Gorter and J.H. Mellink introduced in 1949 the idea of an interaction producing mutual friction between the components of the two-fluid model, to account for the observed transport properties of helium II.
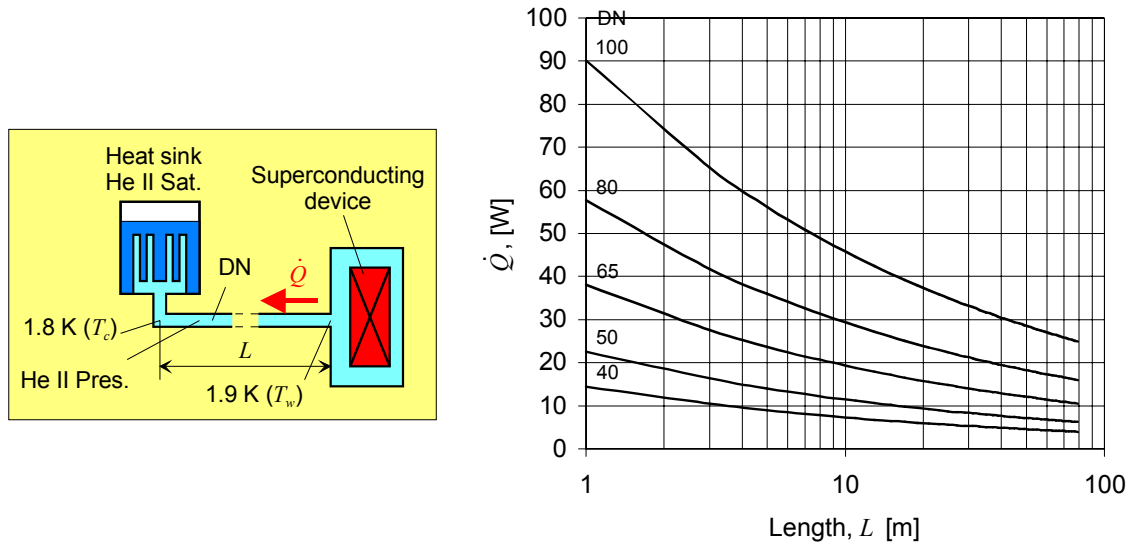
Fig. 6 Steady-state conduction in pressurized superfluid helium.

The variation of *X(T)* also implies that, for each value of the cold boundary temperature T_C, there exists a maximum possible heat flux at which T_W reaches the lambda point, and the helium column ceases to be superfluid. Values of this limiting heat flux, which also weakly depends on *L*, range from a fraction to a few units of W.cm^{-2}, for practical cases of interest. This clearly brings an intrinsic limitation in the applicability of helium II conduction for quasi-isothermal cooling of long strings of superconducting devices in an accelerator. Transporting tens of watts over tens of meter distances would then require several hundred mK temperature difference and a large cross-section of helium, which is both impractical and thermodynamically costly. For a more precise estimate, consider a uniformly heated tubular conduit of length *L*, operating between temperatures T_C and T_W, and apply the helium II steady-state conduction equation to this fin-type geometry. After integration:

$$\dot{q}_{total}{}^n \cdot L = (n+1) \cdot \left[X(T_C) - X(T_W) \right]$$ (2)

where $\dot{q}_{total}$ is the total heat flux flowing through the section at temperature T_C, near the heat sink. Fig. 7 shows the steady-state conduction $\dot{Q}_{tot}$ in superfluid helium of a cryomagnet string with linear heating ξ between 1.9 K (temperature of the warmest magnet) and 1.8 K (temperature at the heat sink). As an example, cooling by conduction a 50-m long cryomagnet string, with a uniform linear thermal load of 1 W.m^{-1}, would require a helium II cross-section of 90 cm^2, i.e. a 10.7-cm diameter conduit. In view of such constraints, the conduction-cooling scheme originally considered for the LHC project [36] was later abandoned.

Conduction through static pressurized superfluid helium however remains the basic process for extraction and local transport of heat from the LHC magnet windings, across their polyimide-wrap electrical insulation. Although the polyimide tape, which constitutes the insulation of the superconducting cable, is wrapped in two layers with half overlap (Fig. 8), in order to achieve sufficient mechanical toughness and dielectric strength, this still preserves sufficient percolation paths for helium II conduction to significantly improve the heat transfer, well above the solid conduction across the sole polyimide [37].
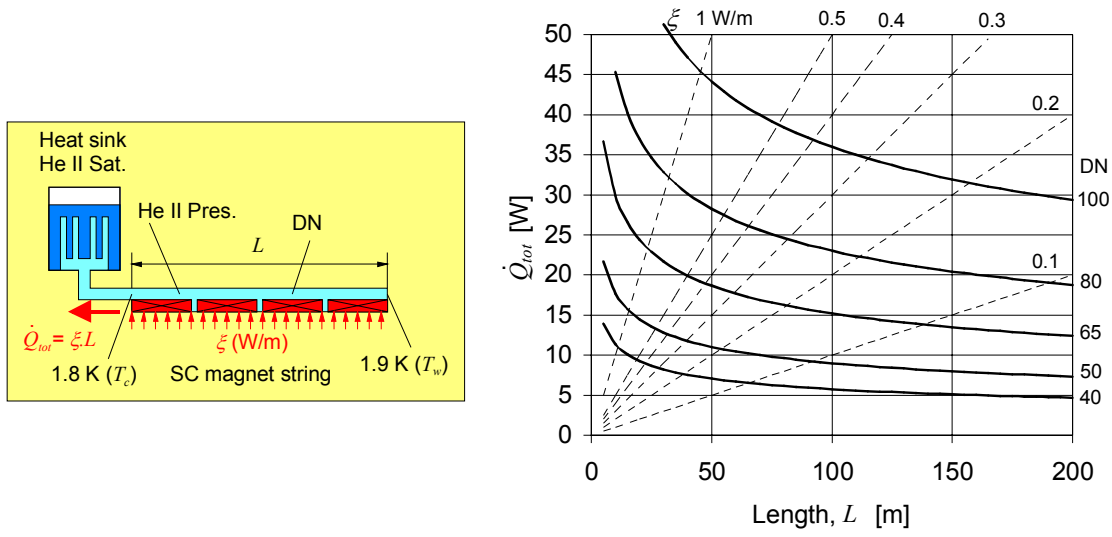
Fig. 7 Steady-state conduction cooling of cryomagnet string with linear applied heat load.
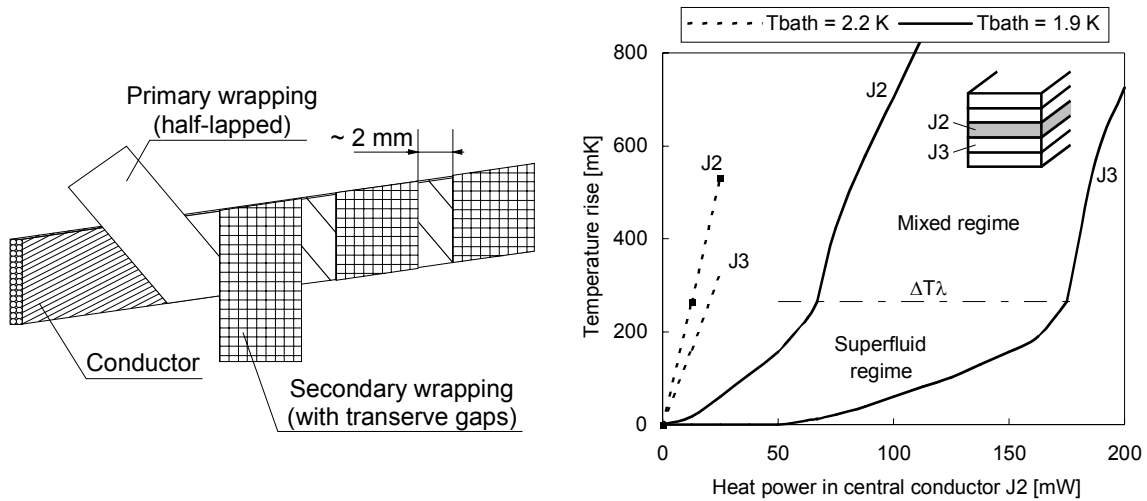

Fig. 8 Heat transfer across polyimide-wrap insulation of superconducting cable.

The high thermal conduction in helium II can also be exploited to ensure quasi-isothermality of helium enclosures of limited spatial extension, such as the helium bath of a superconducting magnet under test. Knowledge of temperature changes at any point in the bath permits to assess enthalpy changes of the system, and thus to perform calorimetric measurements. This technique proves very convenient for measuring minute heat inleaks [38] or substantial energy dissipation [39] such as produced by ramping losses or resistive transitions in superconducting magnets.

2.3 Forced-flow convection of pressurized superfluid helium

To overcome the limited conduction of helium II in long strings of cryogenic devices, the obvious issue is to create a forced circulation of the fluid in a cooling loop, thus relying on convective heat transfer. One can then benefit of an additional control parameter, the net velocity imparted to the bulk

fluid. In the following we shall only discuss convection in channel diameters of technical interest, i.e. typically greater than a few mm. The flow induced by a pressure gradient across an hydraulic impedance is then essentially determined by the viscosity of the bulk fluid. Assuming that internal convection between the components of the two-fluid model is independent of the net velocity, reduces the problem to the behaviour of a flowing monophase liquid with high, non-linear thermal conductivity. The steady-state convective heat transport $\dot{Q}$ between two points 1 and 2 of the cooling loop is then given by the difference in enthalpy H of the fluid flowing with a mass flow-rate $\dot{m}$:

$$\dot{Q} = \dot{m} \cdot (H_2 - H_1) \tag{3}$$

An estimate of the potential advantage of forced convection over conduction can be made, using the same geometry and temperature boundary conditions as described in paragraph 2.2 above. Consider helium II pressurized at 100 kPa, flowing in a heated pipe of length 1 m and cross section 1 cm^2, and assume its temperature increases from 1.8 K at pipe inlet, to 1.9 K at outlet. It is easy to show that for flow velocities above 0.2 m.s^{-1}, convective heat transport exceeds conduction.

The above calculation however neglects pressure drop along the flow. A look at the pressure-enthalpy diagram of helium (Fig. 9) reveals a positive Joule-Thomson effect [40]: the enthalpy of the fluid increases both with increasing temperature and pressure, so that an isenthalpic expansion results in a temperature increase. For example, pressurized helium II flowing across a pressure gradient of 50 kPa will warm up from 1.8 K to 1.9 K, in absence of any applied heat load. The magnitude of this effect requires precise knowledge of the thermohydraulic behaviour of helium II, in order to validate its implementation in long cooling loops [41].
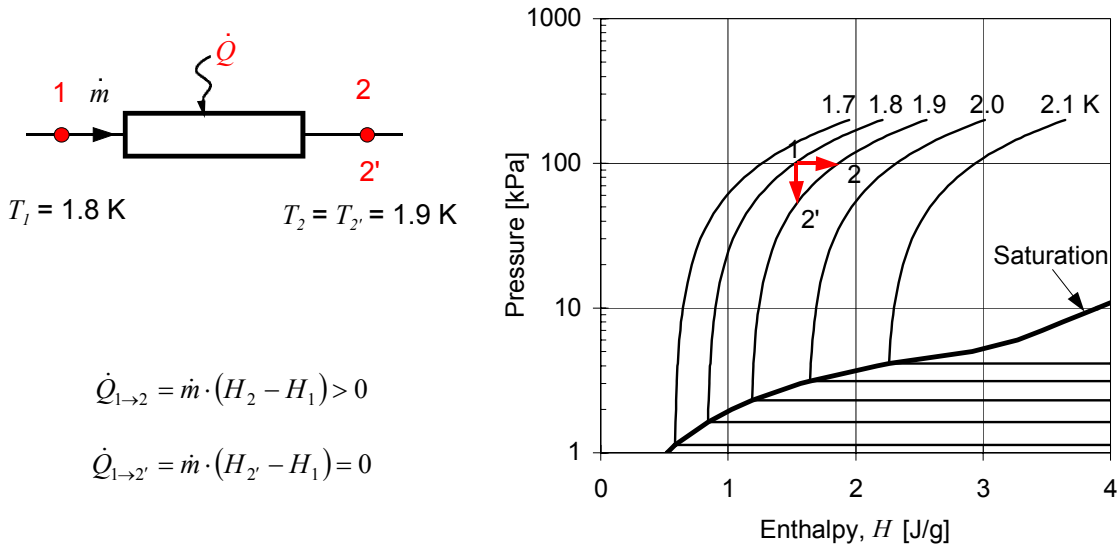

Fig. 9 Pressure-enthalpy diagram and forced-flow convection in superfluid helium.

Following early work [42, 43], several experimental programs have investigated heated flow of pressurized helium II in pipes and piping components [44, 45], culminating with the 230-m long test loop in Grenoble [46, 47] which gave access to high Reynolds numbers and extended geometries characteristic of accelerator string cooling loops. In parallel to that work, mathematical models were developed for calculating combined conductive and convective heat transport processes in complex circuits [48, 49], and validated on experimental results. Pressure drop and heat transfer - both steady-state and transient - in flowing pressurized helium II may now be safely predicted for engineering purposes, using well-established laws and formulae.

The implementation of forced-flow cooling requires cryogenic pumps operating with pressurized helium II. Although most of the experimental work has been performed using positive displacement, i.e. bellows- or piston-pumps originally developed for helium I [50], the thermomechanical effect, specific of the superfluid, may also be used for driving cooling loops by means of fountain-effect pumps [51-54]. In spite of their low thermodynamic efficiency [55], a drawback of limited relevance when using them as circulators which have to produce low pumping work, fountain-effect pumps are light, self-priming and have no moving parts, assets of long-term reliability e.g. for embarked applications in space [56]. At higher heat loads, they have been considered [57] and tested [58] for forced-flow cooling of superconducting magnets: the overall efficiency of the process may then be improved by configuring the cooling loop so as to make use of the heat load of the magnet proper to drive the thermomechanical effect in the pump [59].

2.4 Two-phase flow of saturated superfluid helium

The conductive and convective cooling systems described above both transport heat deposited or generated in the load, over some distance through pressurized helium II, up to a lumped pressurized-to-saturated helium II heat exchanger acting as quasi-isothermal heat sink. This is achieved at the cost of a non-negligible - and thermodynamically costly - temperature difference, thus requiring to operate the heat sink several hundred mK below the temperature of the load.

A more efficient alternative is to distribute the quasi-isothermal heat sink along the length of the accelerator string. In this fashion the conduction distance - and hence the temperature drop - in pressurized helium II is kept to a minimum, typically the transverse dimension of the device cryostat. This leads to the cooling scheme proposed for the LHC at CERN, schematized in Fig. 10: the superconducting magnets operate in static baths of pressurized helium II at approximately atmospheric pressure, in which the heat load is transported by conduction to the quasi-isothermal linear heat sink constituted by a copper heat exchanger tube, threading its way along the magnet string, and in which flowing two-phase saturated helium II gradually absorbs the heat as it vaporizes [11].
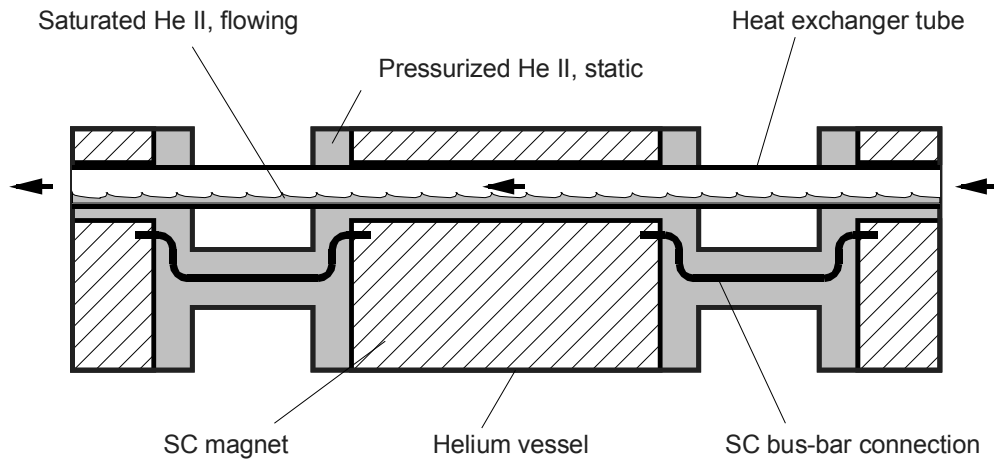

Fig. 10 Principle of the LHC superfluid helium cooling scheme.

Although potentially attractive in view of its efficiency in maintaining long strings of magnets at quasi-uniform temperature, this cooling scheme departs from the well-established wisdom of avoiding long-distance flow of two-phase fluids at saturation, particularly in horizontal or slightly inclined channels. Moreover, no experimental data was originally available on flowing saturated helium II, and very little for other cryogenic fluids in this configuration. Following first exploratory tests [60] which demonstrated the validity of the concept on a reduced geometry, a full-scale thermohydraulic loop [61] permitted to establish the stability of horizontal and downward-sloping helium II flows, to observe partial (but sufficient) wetting of the inner surface of the heat exchanger

tube by the liquid phase, thanks to flow stratification, and to address process-control issues and develop strategies for controlling uniformity of temperature at strongly varying applied heat loads, in spite of the low velocity of the liquid phase. As long as complete dryout does not occur, an overall thermal conductance of about 100 $W.m^{-1}.K^{-1}$ can be reproducibly observed across a DN40 heat exchanger tube, made of industrial-grade deoxidized phosphorus copper.

Once the wetting of the inner surface of the tube is guaranteed, the heat transfer from the pressurized to the saturated helium II is controlled by three thermal impedances in series: solid conduction across the tube wall, and Kapitza resistance at the inner and outer interfaces between tube wall and liquid (Fig. 11). While the former can be adjusted, within technological limits, by choosing tube material and wall thickness, the latter, which finds its origin in the refraction of phonons at the liquid-solid interfaces and is thus strongly temperature-dependent, usually dominates below 2 K [62].
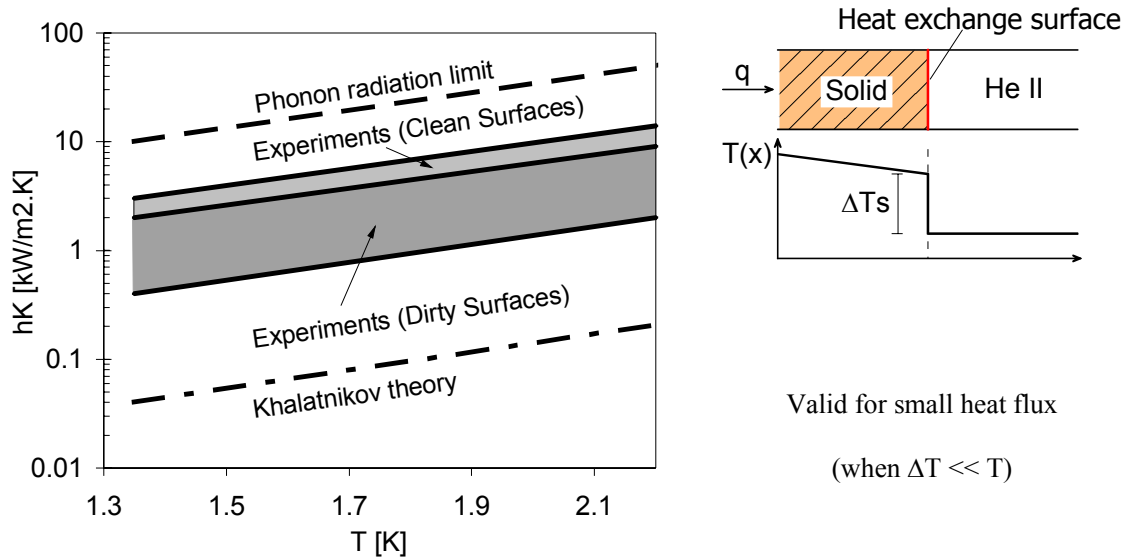

Fig. 11 Kapitza conductance at copper-helium II interface.

The final validation of the two-phase helium II flow cooling scheme for LHC has been performed successfully on a 100-m long test string, equipped with full-scale prototype cryomagnets, operated and powered in nominal conditions [63, 64]. At varying heat loads exceeding 1 $W.m^{-1}$, all magnets in the string were maintained in a narrow range of temperature, a few tens of mK above the saturation temperature of the flowing helium II. Thermal buffering provided by the pressurized helium II baths contributed to limit temperature excursions, at the cost of introducing strong non-linearities and time delays in the system, which must be coped with by elaborate, robust process control [65, 66]. In complement of that applied work, more fundamental experimental studies have been conducted on specially instrumented test loops at CEN-Grenoble, comprehensively equipped with diagnostics and a transparent section for visual observation and interpretation of the flow patterns [67-69]. As long as the vapor velocity remains sufficiently low to maintain stratified flow (up to a few m/s), engineering design of such a cooling scheme rests on a few simple sizing rules [70]. At higher vapor velocity, entrainment and atomization effects, still under investigation, complicate the flow pattern and impact on the heat transfer [71].

This type of cooling scheme may also be used for extracting much higher linear heat loads, typically about 10 $W.m^{-1}$, as present in the low-beta quadrupoles in the high-luminosity insertions of the LHC [72, 73], at the expense of a larger-diameter heat exchanger tube to limit the saturated vapour velocity and thus preserve flow stratification.

3.   REFRIGERATION CYCLES AND EQUIPMENT

The properties of helium at saturation (see Fig. 3) impose to maintain an absolute pressure below 1.6 kPa on the heat sink of a 1.8 K cryogenic system. Bringing the saturated vapour up to atmospheric pressure thus requires compression with a pressure ratio exceeding 80, i.e. four times that of refrigeration cycles for "normal" helium at 4.5 K. Fig. 12 shows the basic scheme for refrigeration below 2 K. A conventional refrigerator produces liquid helium at 4.5 K, later expanded down to 1.6 kPa in a Joule-Thomson expansion stage. The gaseous helium resulting from liquid vaporization is compressed above the atmospheric pressure and eventually recovered by the 4.5 K refrigerator. We will therefore start by presenting the Joule-Thomson expansion stage.

Three types of cycles, sketched in Fig. 12, can be considered [74, 75] for producing refrigeration below 2 K:

- the "warm" compression cycle based on warm sub-atmospheric compressors,

- the "cold" compression cycle based on multistage cold compressors,

- the "mixed" compression cycle based on a combination of cold compressors in series with warm sub-atmospheric compressors.

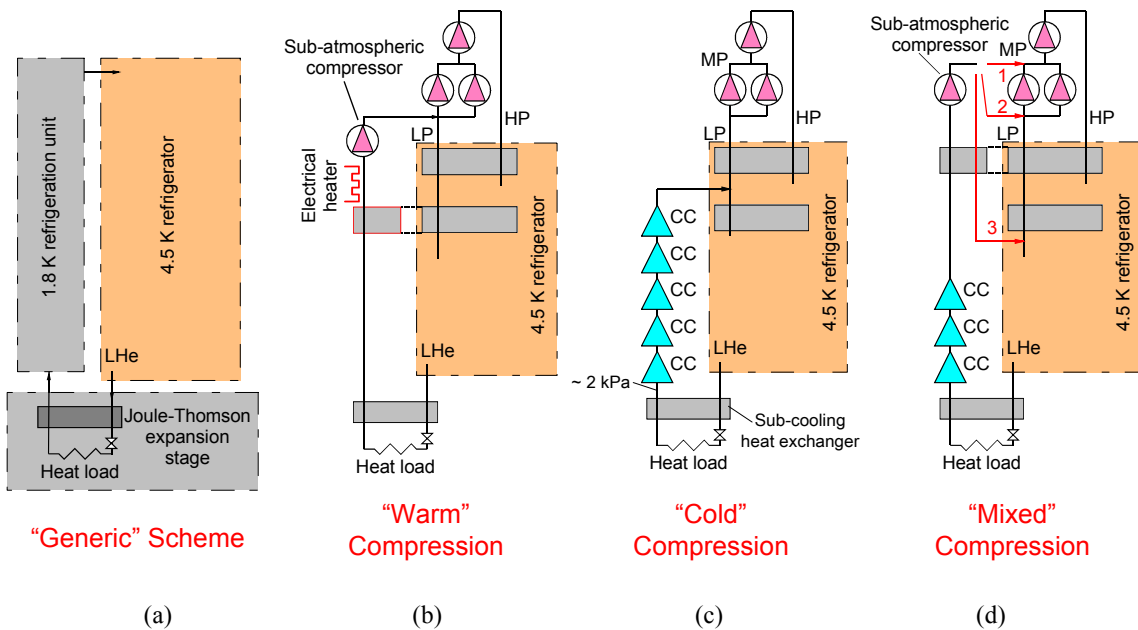We will then proceed to discuss thermodynamics and machinery for these three types of cycle.

"Generic" Scheme	"Warm" Compression	"Cold" Compression	"Mixed" Compression
(a)	(b)	(c)	(d)

Fig. 12 Generic process cycles for refrigeration below 2 K.

3.1 Joule-Thomson expansion stage

The efficiency of the Joule-Thomson expansion of liquid helium, say from 0.13 MPa and 4.5 K, down to 1.6 kPa and 1.8 K, can be notably improved if it is previously subcooled by the exiting very-low-pressure vapour (Fig. 13). This is performed in a counter-flow heat exchanger, subcooling the incoming liquid down to 2.2 K by enthalpy exchange with the very-low-pressure saturated vapour. This heat exchanger has to produce limited pressure drop, particularly in the very-low-pressure stream. A maximum pressure drop of 100 Pa is generally acceptable, corresponding to a few per cent of the absolute saturation pressure. The design of such heat exchangers for large flow-rate [76] is not straightforward, and their qualification impractical. As a consequence, the LHC cryogenic system

features several hundred small-size (5 to 20 g/s) heat exchangers, distributed around the ring. This also avoids transporting subcooled helium over long distances, saving one header in the ring distribution line. Following prototyping, technical validation of different solutions [77, 78] and commercial selection, these heat exchangers are now series-produced by industry.
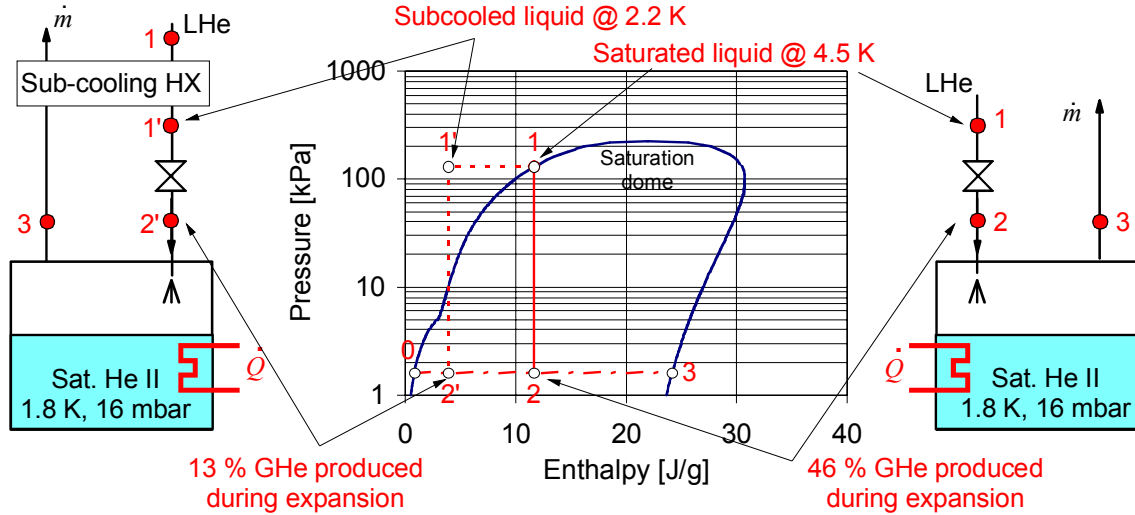

Fig. 13 Efficiency of Joule-Thomson expansion.

3.2 "Warm" compression cycle

For low-power refrigeration, e.g. in small laboratory cryostats, this is achieved by means of standard Roots or rotary-vane vacuum pumps, handling the very-low-pressure gaseous helium escaping from the bath after it has been warmed up to ambient temperature through a heat exchanger and/or an electrical heater. This technology may be pushed to higher flow-rates using liquid-ring pumps, adapted for processing helium by improving the tightness of their casing and operating them with the same oil as that of the main compressors of the 4.5 K cycle [79], or oil-lubricated screw compressors operating at low suction pressure. In any case, compression at ambient temperature is hampered by the low density of the gaseous helium, which results in large volume flow-rates and thus requires large machinery, as well as in costly, inefficient heat exchangers for recovering enthalpy of the very-low pressure stream.

All these compressors are positive-displacement machines having volumetric characteristics. Screw compressors are routinely used in helium refrigeration and their implementation in a 1.8 K cycle therefore follows from current practice. Special attention however has to be paid to the protection against air inleaks: in particular the motor shaft and its rotary sealing must be located on the discharge side to operate above atmospheric pressure.

A first limit to the use of subatmospheric screw compressors stems from volumetric flow requirements: the biggest available machines have a swept volume of about 4600 m^3/h, so that higher flow-rates require parallel arrays. Moreover, the isothermal efficiency - defined as the ratio of isothermal compression work to the effective compression work of the machine - decreases markedly with the suction pressure as shown in Fig. 15, thus precluding their use at very low pressure in efficient process cycles.

(a)   (b)

Fig. 14 Subatmospheric compressors.

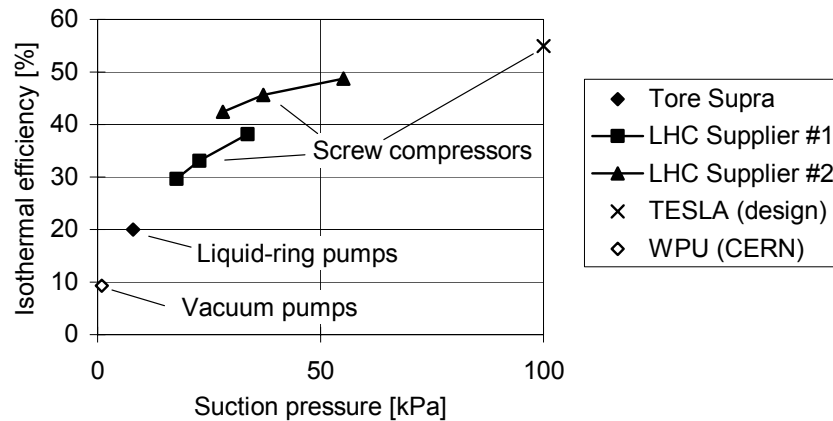(a) combination of Roots and rotary-vane vacuum pumps.   (b) compound screw.

Fig. 15 Isothermal efficiency of warm sub-atmospheric compressors.

3.3   "Cold" compression cycle

The alternative process is to perform compression of the vapour at low temperature, i.e. at its highest density. The pumps and recovery heat exchangers get smaller in size and less expensive, but the work of compression is then injected in the cycle at low temperature, so that the inevitable irreversibilities have a higher thermodynamic weight. Moreover, the pumping machinery which handles cold helium must be non-lubricated and non-contaminating, which seriously limits the choice of technology. Hydrodynamic compressors, of the centrifugal or axial-centrifugal type, have been used in large-capacity systems [80]. Their pressure ratio limited to 2 to 3.5 per stage however imposes to arrange them in multistage configurations [81, 82], thus narrowing the operational range of the system, in particular for startup or off-design modes.

Depending on the operating temperature (2 K or 1.8 K), the "cold" compression cycle requires at least 4 or 5 stages in series in order to perform the overall pressure ratio of 45 to 80. The compressed helium is directly returned to the cold low-pressure (LP) stream of the 4.5 K refrigerator.

The main drawback of this cycle concerns turndown capability. The cold compressor set has to guarantee the same pressure ratio for any load. A typical operating field for hydrodynamic

compressors (Fig. 16) displays the pressure ratio as a function of the reduced flow m^* and the reduced speed N^*. The working area is limited on the left side by the stall line, on the right by the choke line and on top by the maximum rotational speed of the drive. At constant pressure ratio, the compressor can handle a flow reduction of only about 20 % before reaching the stall line. Below 80% of nominal, additional vapour generation by electrical heating must be used to compensate for the load reduction. Such a cycle is therefore not very compliant to turndown, and its operating cost is not optimised for part-load operation.

This led CERN to conduct, in view of the LHC project, a R&D programme on cold compressors, procuring from specialised industry three prototype hydrodynamic compressors of different designs [83-86] to investigate critical issues such as drive and bearing technology, impeller and diffuser hydrodynamics, mechanical and thermal design, as well as their impact on overall efficiency [87]. The choices eventually retained for the LHC series machines [88-90] are 3-phase electrical induction motor drives working at room temperature with rotational speed varying from 200 to 700 Hz, active magnetic bearings working at room temperature, axial-centrifugal (three-dimensional) impellers and fixed-vane diffusers (Figs 17 & 18).

$$m^* = \frac{\dot{m}}{\dot{m}_0} \cdot \sqrt{\frac{Tin}{Tin_0}} \cdot \frac{Pin_0}{Pin}$$

and

$$N^* = \frac{N}{N_0} \cdot \sqrt{\frac{Tin_0}{Tin}}$$

with: $\dot{m}$: mass-flow
Tin: inlet temperature
Pin: inlet pressure
N: rotational speed
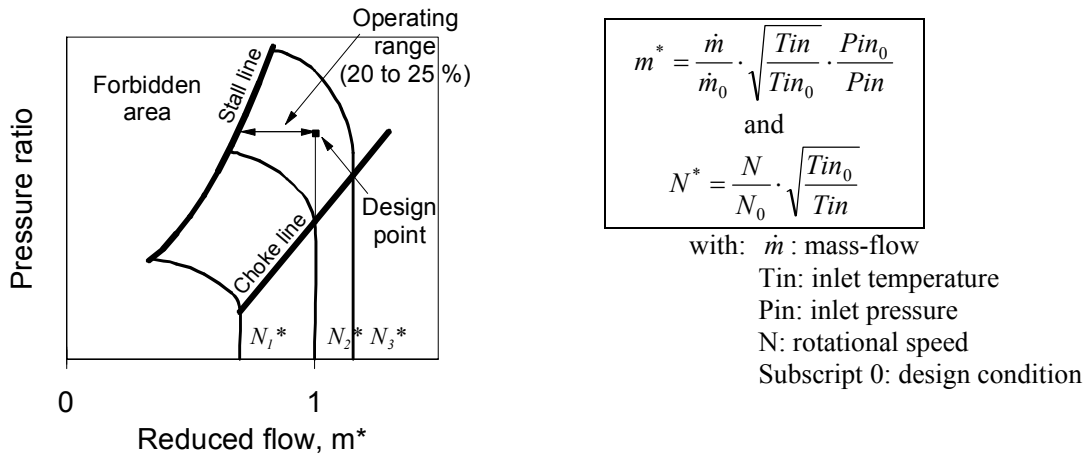Subscript 0: design condition

Fig. 16 Typical operating field of hydrodynamic compressor.
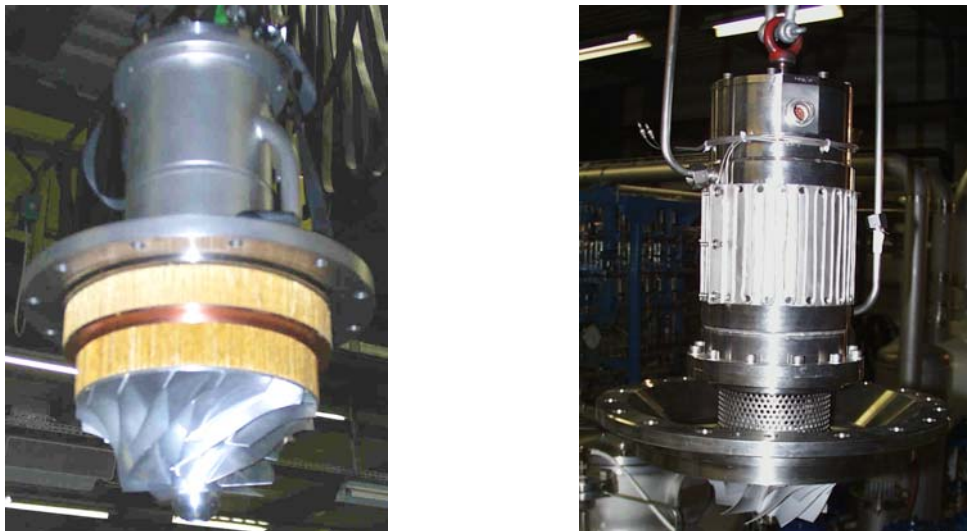

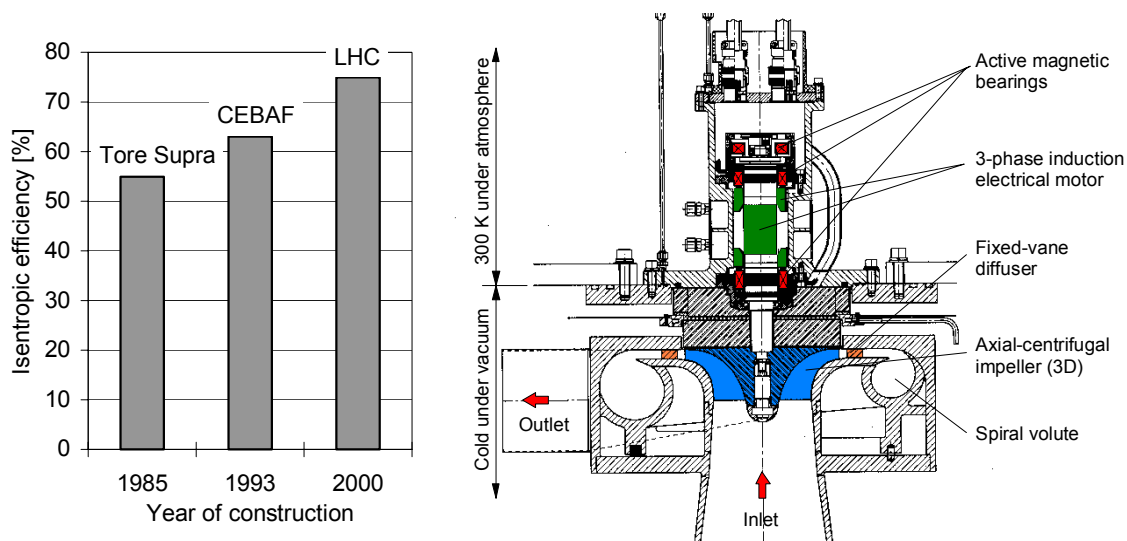Fig. 17 Axial-centrifugal cold compressor cartridges for the LHC.

Fig. 18 Isentropic efficiency and typical cross-section of cold compressors.

Thermodynamic efficiency of cold compressors, determined by hydrodynamic design as well as by limitation of heat inleaks along the drive shaft, has significantly improved (Fig. 18). Here the relevant estimator is isentropic efficiency, defined as the ratio of compression work in the adiabatic, reversible case, to the real one. Recent machines can be expected to reach 75 % isentropic efficiency at their design point.

3.4 "Mixed" compression cycles

For large systems, oil liquid-ring pumps or lubricated screw compressors may be used in series with cold compressors, in "mixed" compression cycles. Cold compressors are well-suited for the lower stages, while the presence of volumetric machines in the upper stages permits independent adjustment of flow-rate or wheel inlet conditions, thus improving load adaptation [91, 92].

In "mixed" compression cycles, the number of cold compressor stages can be reduced to 3, depending on the swept volume and number of warm sub-atmospheric machines. The compressed helium can be returned to the 4.5 K refrigerator at different levels:

- at the warm medium-pressure (MP) side (connection #1 on Fig. 12 d). This requires the use of screw compressors having a sufficient built-in pressure ratio. In this case, the enthalpy of the gas at the outlet of the cold compressors has to be recovered by the heat exchangers of the 4.5 K refrigerator. The main advantage of this solution is that the same oil-removal and final cleaning systems can be used for the warm sub-atmospheric compressors and for the booster stages of the 4.5 K refrigerators, thus minimising the investment cost of the system.

- at the warm low-pressure (LP) side (connection #2 on Fig. 12 d). This solution is compatible with the use of either screw compressors or liquid ring pumps. The enthalpy of the cold gas at the outlet of the cold compressors also has to be recovered by the heat exchangers of the 4.5 K refrigerator. In this case, the warm sub-atmospheric stage requires its own oil-removal system.

- at the cold low-pressure side (connection #3 on Fig. 12 d). This is required when the enthalpy of the cold gas at the outlet of the cold compressors cannot be recovered by the heat exchangers of the 4.5 K refrigerators (LHC case) [88]. In this case, the warm sub-atmospheric stage requires its own oil-removal and final cleaning system (coalescers and charcoal adsorbers), increasing the investment cost.

The main advantage of the "mixed" cycle resides in its turndown capability. With sub-atmospheric compressors having volumetric characteristics, the pressure at the outlet of the cold compressors decreases linearly with the flow-rate, i.e. if the temperature and rotational speed do not change, the reduced flow-rate m* stays constant, thus keeping the working point fixed in the operating field. Such a cycle can then handle a large dynamic range, e.g. 3 for the LHC, without any additional electrical heating. Moreover, the total pressure ratio of the cold compressor train is lowered and the speed of some machines can then be reduced, thus decreasing the total compression power and operating cost.

Another operational advantage concerns the possibility of maintaining the load in cold standby with the cold compressors freewheeling and all compression performed, though at much reduced flow, by the warm machines. This mode allows repair or exchange of a cold-compressor cartridge without helium emptying of the system. In addition, the load adaptation provided by the warm volumetric machines proves very useful during transient modes like cool-down and pump-down, in which the cold compressors operate far from their design conditions.

The only drawback of this cycle concerns the risk of air inleaks due to the presence of sub-atmospheric circuits in air. Helium guards are recommended to prevent pollution of the process helium [93].

3.5 Application range of low-pressure helium compression techniques

The practical ranges of application of the different techniques appear in Fig. 19, setting a *de facto* limit for warm compression above 20'000 $m^3.h^{-1}$, or typically 300 W at 1.8 K. The diagram also illustrates the large span of refrigeration power and diversity of projects using superfluid helium. Investment and operating costs of large superfluid helium refrigeration systems can be assessed from basic thermodynamics and practical scaling laws derived from recent experience [94], thus providing input for technical-economical optimisation of such systems.
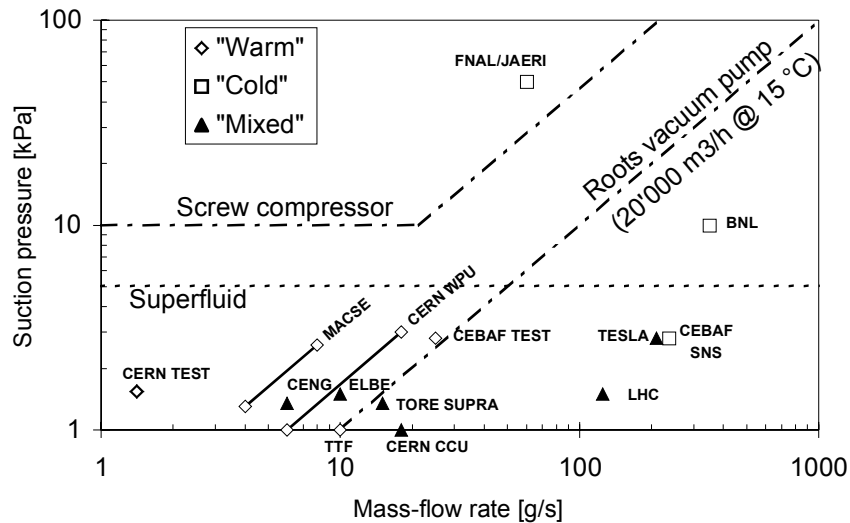

Fig. 19 Range of application of low-pressure helium compression techniques.

4.   CONCLUSION

Operating superconducting devices at 1.8 K, using superfluid helium as a technical coolant, has now become state-of-the-art. The specific aspects of superfluid helium technology addressed in this article can be combined with standard cryogenic practice to design, build and operate complete industrial-

type helium II systems. The particle accelerator projects in construction or in study, however represent major challenges and opportunities for further progress, in view of their large size, complexity and quest for reliability and efficiency.

REFERENCES

[1] G. Claudet & R. Aymar, Tore Supra and helium II cooling of large high-field magnets, Adv. Cryo. Eng. 35A (1990) 55-67.

[2] S.W. van Sciver, He II cooling of large superconducting magnet systems, Cryogenics 32 ICEC Supplement (1992) 320-327.

[3] H.J. Schneider-Muntau & J.C. Vallier, The Grenoble hybrid magnet, IEEE Trans. Mag. 24 (1988) 1067-1069.

[4] J.R. Miller, M.D. Bird, S. Bole, A. Bonito-Oliva, Y. Eyssa, W.J. Kenney, T.A. Painter, H.J. Schneider-Muntau, L.T. Summers, S.W. van Sciver, S. Welton, R.J. Wood, J.E.C. Williams, E. Bobrov, Y. Iwasa, M. Leupold, V. Stejskal & R. Weggel, An overview of the 45-T hybrid magnet system for the new National High Magnetic Field Laboratory, IEEE Trans. Mag. 30 (1994) 1563-1571.

[5] S.W. van Sciver, J.R. Miller, S. Welton, H.J. Schneider-Muntau & G.E. McIntosh, Cryogenic system for the 45 Tesla hybrid magnet, Adv. Cryo. Eng. 39A (1994) 375-380.

[6] W.D. Markiewicz, I.R. Dixon, C.A. Swenson, W.S. Marshall, T.A. Painter, S.T. Bole, T. Cosmus, M. Parizh, M. King, G. Ciancetta, 900 MHz wide-bore NMR spectrometer magnet at NHMFL, IEEE Trans. Appl. Superconductivity 10 (2000) 728-731.

[7] Ultrastabilized™ NMR magnets by Bruker Biospin Corporation, http//www.bruker-biospin.com/nmr/products/ustab.html.

[8] R. Aymar, G. Claudet, C. Deck, R. Duthil, P. Genevey, C. Leloup, J.C. Lottin, J. Parain, P. Seyfert, A. Torossian & B. Turck, Conceptual design of a superconducting tokamak: Tore II Supra, IEEE Trans. Mag. MAG 15-1 (1979) 542-545.

[9] G. Claudet, G. Bon Mardion, B. Jager & G. Gistau, Design of the cryogenic system for the Tore Supra tokamak, Cryogenics 26 (1986) 443-449.

[10] L.R. Evans, LHC accelerator physics and technology challenges, Proc. PAC99, A. Luccio & W.W. MacKay editors, IEEE Piscataway, New Jersey, USA (1999) 21-25.

[11] Ph. Lebrun, Superfluid helium cryogenics for the Large Hadron Collider project at CERN, Cryogenics 34 ICEC Supplement (1994) 1-8.

[12] Ph. Lebrun, Cryogenics for the Large Hadron Collider, IEEE Trans. Appl. Superconductivity, 10 (2000) 1500-1506.

[13] H. Padamsee, Superconducting RF cavity design, Proc. CAS School on Superconductivity and Cryogenics for Particle Accelerators and Detectors, Erice, Sicily, 8-17 May 2002.

[14] C.H. Rode, CEBAF cryogenic system, Proc. PAC95, Am. Phys. Soc. & IEEE Piscataway, New Jersey, USA (1995) 1994-1998.

[15] C. Rode & the JLab SNS team, The SNS superconducting linac system, Proc. PAC2001, P. Lucas & S. Webber editors, IEEE Piscataway, New Jersey, USA (2001) 619-623.

[16] F. Richard, J.R. Schneider, D. Trines & A. Wagner editors, TESLA Technical Design Report, DESY 2001-011 and ECFA 2001-209 (2001).

[17] G. Horlitz, T. Peterson & D. Trines, A 2 Kelvin helium II distributed cooling system for the 2 x 250 GeV e+ e- linear collider Tesla, Cryogenics 34 ICEC Supplement (1994) 131-134.

[18] G. Horlitz, The cryogenic system for the superconducting e+ e- linear collider TESLA, Proc. Symposium on cryogenic systems for large-scale superconducting applications, NIFS-PROC-28, NIFS, Toki, Japan (1996) 85-89.

[19] F. Vinen, Physical properties of superfluid helium - a general review, Proc. Workshop on the stability of superconductors in helium I and helium II, IIF/IIR Bulletin, Commission A1/2, Saclay, 1981/6 (1981) 43-51.

[20] F. Vinen, Physics of superfluid helium, Proc. CAS School on Superconductivity and Cryogenics for Particle Accelerators and Detectors, Erice, Sicily, 8-17 May 2002.

[21] L. Tavian, Large cryogenic systems at 1.8 K, Proc. EPAC 2000, J.L. Laclare, W. Mitaroff, Ch. Petit-Jean-Genaz, J. Poole & M. Regler editors, Austrian Academy of Sciences Press, Vienna, Austria (2000) 212-216.

[22] G. Vandoni, Heat transfer, in this report.

[23] Ph. Lebrun, Design of a cryostat for superconducting accelerator magnet: the LHC main dipole case, in this report.

[24] G. Bon Mardion, G. Claudet, P. Seyfert & J. Verdier, Helium II in low-temperature and superconductive magnet engineering, Adv. Cryo. Eng. 23 (1977) 358-362.

[25] B. Fallou, J. Galand & B. Bouvier, Dielectric breakdown of gaseous helium at very low temperature, Cryogenics 10 (1970) 142-146.

[26] H. Winkelnkemper, Z. Krasucki, J. Gerhold & T.W. Dakin, Breakdown of gases in uniform electric fields, Paschen curves for hydrogen, carbon dioxide and helium, Electra 52 (1977) 67.

[27] B. Rousset & F. Viargues, An alternative cooling scheme for the TeV superconducting linear accelerator project, Cryogenics 34 ICEC Supplement (1994) 91-94.

[28] V. Arp, Heat transport through helium II, Cryogenics 10 (1970) 96-105.

[29] C.J. Gorter & J.H. Mellink, On the irreversible processes in liquid helium II, Physica 15 (1949) 285-304.

[30] G. Bon Mardion, G. Claudet & P. Seyfert, Practical data on steady state heat transport in superfluid helium at atmospheric pressure, Cryogenics 19 (1979) 45-47.

[31] S.W. van Sciver, Heat transfer in superfluid helium II, Proc. ICEC8, C. Rizzuto editor, IPC Science & Technology Press, Guildford, UK (1980) 228-237.

[32] P. Seyfert, Practical results on heat transfer to superfluid helium, Proc. Workshop on the stability of superconductors in helium I and helium II, IIF/IIR Bulletin, Commission A1/2, Saclay, 1981/6 (1981) 53-62.

[33] S.W. van Sciver, Developments in He II heat transfer and applications to superconducting magnets, Adv. Cryo. Eng. 27 (1982) 375-398.

[34] G. Claudet & P. Seyfert, Bath cooling with subcooled superfluid helium, Adv. Cryo. Eng. 27 (1982) 441-449.

[35] P. Seyfert, Results on heat transfer to He II for use in superconducting magnet technology, Proc. ICEC9, K. Yasukochi & H. Nagano editors, Butterworth, Guildford, UK (1982) 263-268.

[36] G. Claudet, F. Disdier, Ph. Lebrun, M. Morpurgo & P. Weymuth, Preliminary study of a superfluid helium cryogenic system for the Large Hadron Collider, Proc. ICFA Workshop on Superconducting Magnets and Cryogenics, BNL 52006, Brookhaven National Laboratory, USA (1986) 270-275.

[37] C. Meuris, B. Baudouy, D. Leroy & B. Szeless, Heat transfer in electrical insulation of LHC cables cooled with superfluid helium, Cryogenics $\underline{39}$ (1999) 921-931.

[38] H. Danielsson, Ph. Lebrun & J.M. Rieubland, Precision heat inleak measurements at 80 K, 4.2 K and 1.8 K, Cryogenics $\underline{32}$ ICEC Supplement (1992) 215-218.

[39] S. Caspi, The use of calorimetry in superfluid He II to measure losses in superconducting magnets, Proc. ICEC9, K. Yasukochi & H. Nagano editors, Butterworth, Guildford, UK (1982) 347-350.

[40] P.L. Walstrom, Joule Thomson effect and internal convection heat transfer in turbulent helium II flow, Cryogenics $\underline{28}$ (1988) 151-156.

[41] G. Claudet, F. Disdier, A. Gauthier, Ph. Lebrun, M. Morpurgo & J. Schmid, Conceptual study of the superfluid helium cryogenic system for the CERN Large Hadron Collider, Proc. ICEC12, R.G. Scurlock & C.A. Bailey editors, Butterworths, Guildford, UK (1988) 497-504.

[42] A. Kashani & S.W. van Sciver, Steady-state forced convection heat transfer in He II, Adv. Cryo. Eng. $\underline{31}$ (1986) 489-498.

[43] A. Kashani & S.W. van Sciver, Transient forced convection heat transfer in He II, Proc. ICEC11, G. & I. Klipping editors, Butterworths, Guildford, UK (1986) 654-658.

[44] P.L. Walstrom & J.R. Maddocks, Pressure drop and temperature rise in He II flow in round tubes, venturi flowmeters and valves, Adv. Cryo. Eng. $\underline{33}$ (1988) 449-456.

[45] P.L. Walstrom, J.G. Weisend II, J.R. Maddocks & S.W. van Sciver, Turbulent flow pressure drop in various helium II transfer system components, Cryogenics $\underline{28}$ (1988) 101-109.

[46] B. Rousset, G. Claudet, A. Gauthier, P. Seyfert, Ph. Lebrun, M. Marquet, R. van Weelderen & J.L. Duchateau, Operation of a forced-flow superfluid helium test facility and first results, Cryogenics $\underline{32}$ ICEC Supplement (1992) 134-137.

[47] B. Rousset, G. Claudet, A. Gauthier, P. Seyfert, A. Martinez, Ph. Lebrun, M. Marquet & R. van Weelderen, Pressure drop and transient heat transport in forced-flow single-phase helium II at high Reynolds numbers, Cryogenics $\underline{34}$ ICEC Supplement (1994) 317-320.

[48] H.A. Snyder & A.J. Mord, Flow of superfluid helium in tubes with heated walls, Adv. Cryo. Eng. $\underline{37A}$ (1991) 81-88.

[49] A.J. Mord, H.A. Snyder & D.A. Newell, End-to-end modelling of helium II flow systems, Cryogenics $\underline{32}$ (1992) 291-299.

[50] G. Morpurgo, Design and construction of a pump for liquid helium, Cryogenics $\underline{17}$ (1977) 91-93.

[51] A. Hofmann, A. Khalil, H.P. Krämer, J.G. Weisend, R. Srinivasan & B. Vogeley, Investigations on fountain-effect pumps for circulating pressurized helium II, Proc. ICEC11, G. & I. Klipping editors, Butterworth, Guildford, UK (1986) 312-316.

[52] S.W.K. Yuan & T.C. Nast, The design of fountain-effect pumps, Adv. Cryo. Eng. $\underline{33}$ (1988) 457-464.

[53] P. Kittel, Operating characteristics of isocaloric fountain-effect pumps, Adv. Cryo. Eng. $\underline{33}$ (1988) 465-470.

[54] A. Hofmann, A. Khalil & H.P. Krämer, Operational characteristics of loops with helium II flow driven by fountain-effect pumps, Adv. Cryo. Eng. <u>33</u> (1988) 471-478.

[55] P. Kittel, Losses in fountain-effect pumps, Proc. ICEC11, G. & I. Klipping editors, Butterworth, Guildford, UK (1986) 317-322.

[56] G. Klipping & H.D. Denner, The thermomechanical effect of superfluid helium and its technical application, Adv. Cryo. Eng. <u>35A</u> (1990) 81-93.

[57] A.J. Mord & H.A. Snyder, Self-driven He II cooling system for the interaction region focusing magnets at SSC, Adv. Cryo. Eng. <u>39A</u> (1994) 797-804.

[58] A. Hofmann, W. Herz, E. Suesser, B. Vogeley, T. Voekel & G. Zahn, Tests results of a large-size thermomechanical pump, Adv. Cryo. Eng. <u>39B</u> (1994) 1813-1820.

[59] A.J. Mord & H.A. Snyder, Comparison of He II cooling systems for superconducting magnets using self-driven mass flow and zero-flow heat pipes, Cryogenics <u>32</u> (1992) 461-465.

[60] J. Casas-Cubillos, A. Cyvoct, Ph. Lebrun, M. Marquet, L. Tavian & R. van Weelderen, Design concept and first experimental validation of the superfluid helium system for the Large Hadron Collider (LHC) project at CERN, Cryogenics <u>32</u> ICEC Supplement (1992) 118-121.

[61] A. Bézaguet, J. Casas-Cubillos, Ph. Lebrun, M. Marquet, L. Tavian & R. van Weelderen, The superfluid helium model cryoloop for the CERN Large Hadron Collider (LHC), Adv. Cryo. Eng. <u>39A</u> (1994) 649-656.

[62] D. Camacho, S. Chevassus, C. Policella, J.M. Rieubland, G. Vandoni & R. van Weelderen, Thermal characterization of the He II LHC heat exchanger tube, Proc. ICEC17, D. Dew-Hughes, R.G. Scurlock & J.P. Watson editors, IoP Publishing (1998) 647-650.

[63] A. Bézaguet, J. Casas-Cubillos, B. Flemsaeter, B. Gaillard-Grenadier, Th. Goiffon, H. Guinaudeau, Ph. Lebrun, M. Marquet, L. Serio, A. Suraci, L. Tavian & R. van Weelderen, The superfluid helium system for the LHC Test String: design, construction and first operation, Adv. Cryo. Eng. <u>41A</u> (1996) 777-784.

[64] A. Bézaguet, J. Casas-Cubillos, H. Guinaudeau, B. Hilbert, Ph. Lebrun, L. Serio, A. Suraci, L. Tavian & R. van Weelderen, Cryogenic operation and testing of the extended LHC prototype magnet string, Proc. ICEC16/ICMC, T Haruyama, T. Mitsui & K. Yamafuji editors, Elsevier Science (1997) 91-94.

[65] B. Flemsaeter, Contribution to the dynamic analysis and optimal control of the superfluid helium cooling loop for the LHC magnet string, Diploma thesis, Norwegian Institute of Technology, Trondheim (1995).

[66] B. Flemsaeter, E. Blanco, J. Casas-Cubillos, C. de Prada & S. Saelid, Applying advanced control techniques for temperature regulation of the LHC superconducting magnets, Proc. ICEC17, D. Dew-Hughes, R.G. Scurlock & J.P. Watson editors, IoP Publishing (1998) 631-634.

[67] B. Rousset, A. Gauthier, L. Grimaud, A. Bézaguet & R. van Weelderen, Thermohydraulic behaviour of He II in stratified co-current two-phase flow, Proc. ICEC16/ICMC, T. Haruyama, T. Mitsui & K. Yamafuji editors, Elsevier Science (1997) 519-522.

[68] B. Rousset, A. Gauthier & A. Grimaud, Stratified two-phase superfluid helium flow : part 1, Cryogenics <u>37</u> (1997) 733-737.

[69]   L. Grimaud, A. Gauthier, B. Rousset & J.M. Delhaye, Stratified two-phase superfluid helium flow : part 2, Cryogenics 37 (1997) 739-744.

[70]   Ph. Lebrun, L. Serio, L. Tavian & R. van Weelderen, Cooling strings of superconducting devices below 2 K: the helium II bayonet heat exchanger, Adv. Cryo. Eng. 43A (1998) 419-426.

[71]   B. Rousset, B. Jager, E. di Muoio, L. Puech, P. Thibaud, R. Vallcorba, R. van Weelderen & P.E. Wolf, He II co-current two-phase flow at high vapor velocities, Adv. Cryo. Eng. 47B (2002) 1311-1318.

[72]   Y. Huang, J. Kerby, T. Nicol & T. Peterson, Cryogenic system and cryostat design for the LHC IR quadrupole magnets, Adv. Cryo. Eng. 43A (1998) 403-410.

[73]   R. Byrns, Y. Huang, J. Kerby, Ph. Lebrun, L. Morrison, T. Nicol, T. Peterson, R. Trant, R. van Weelderen & J. Zbasnik, The cryogenics of the LHC interaction region final-focus superconducting magnets, Proc. ICEC17, D. Dew-Hughes, R.G. Scurlock & J.P. Watson editors, IoP Publishing (1998) 743-746.

[74]   G. Gistau-Baguer, High-power refrigeration at temperatures around 2 K, Proc. ICEC16/ICMC, T Haruyama, T. Mitsui & K. Yamafuji editors, Elsevier Science (1997) 189-194.

[75]   F. Millet, P. Roussel, L. Tavian & U. Wagner, A possible 1.8 K refrigeration cycle for the Large Hadron Collider, Adv. Cryo. Eng. 43A (1998) 387-394.

[76]   E. Kashtanov, V. Pleskatch, K. Polkovnikov, A. Shembel, V. Sytnik, S. Zintchenko, B. Krakovsky, O. Krasnikova, O. Popov, H. Burmeister, B. Petersen & H.O. Roggenbuck, Large low-pressure heat exchanger for the TTF cryogenic system, Proc. ICEC18, K.G. Narayankhedkar editor, Narosa, New Delhi, India (2000) 315-318.

[77]   F. Viargues, G. Claudet & P. Seyfert, Construction and preliminary testing of perforated-plate heat exchangers for use in helium II refrigerators, Cryogenics 34 ICEC Supplement (1994) 325-328.

[78]   P. Roussel, A. Bézaguet, H. Bieri, R. Devidal, B. Jager, R. Moracchioli, P. Seyfert & L. Tavian, Performance tests of industrial prototype subcooling helium heat exchangers for the Large Hadron Collider, Adv. Cryo. Eng. 47B (2002) 1311-1318.

[79]   G.M. Gistau & G. Claudet, The design of the helium refrigerator for Tore Supra, Proc. ICEC10, H. Collan, P. Berglund & M. Krusius editors, Butterworth, Guildford, UK (1984) 288-291.

[80]   G.M. Gistau, J.C. Villard & F. Turcat, Application range of cryogenic centrifugal compressors, Adv. Cryo. Eng. 35B (1990) 1031-1037.

[81]   G.M. Gistau, Y. Pecoud & A.E. Ravex, The 300 W - 1.75 K Tore Supra refrigerator cold centrifugal compressor report, Adv. Cryo. Eng. 33 (1988) 675-681.

[82]   C.H. Rode, D. Arenius, W.C. Chronis, D. Kashy & M. Keesee, 2 K CEBAF cryogenics, Adv. Cryo. Eng. 35A (1990) 275-286.

[83]   L. Decker, K. Löhlein, P. Schustr, M. Vins, I. Brunovski, L. Tucek, Ph. Lebrun & L. Tavian, A cryogenic axial-centrifugal compressor for superfluid helium refrigeration, Proc. ICEC16/ICMC, T Haruyama, T. Mitsui & K. Yamafuji editors, Elsevier Science (1997) 195-198.

[84] L. Decker, A. Kündig, K. Löhlein, W. Pürtschert, B. Ziegler, Ph. Lebrun, L. Tavian, I. Brunovsy & L. Tucek, Operational experience with a cryogenic axial-centrifugal compressor, Adv. Cryo. Eng. 43A (1998) 637-642.

[85] M. Bonneton, L. Tavian, G. Gistau-Baguer, F. Turcat & P. Viennot, A high-reliability gas-driven helium cryogenic centrifugal compressor, Adv. Cryo. Eng. 43A (1998) 643-650.

[86] N. Saji, H. Asakura, S. Yoshinaga, K. Itoh, T. Nogaku, A. Bézaguet, J. Casas, Ph. Lebrun & L. Tavian, A 1 kPa centrifugal cold compressor for the 1.8 K helium refrigeration system, Proc. ICEC17, D. Dew-Hughes, R.G. Scurlock & J.P. Watson editors, IoP Publishing (1998) 295-298.

[87] A. Bézaguet, Ph. Lebrun & L. Tavian, Performance assessment of industrial prototype cryogenic helium compressors for the Large Hadron Collider, Proc. ICEC17, D. Dew-Hughes, R.G. Scurlock & J.P. Watson editors, IoP Publishing (1998) 145-148.

[88] S. Claudet, P. Gayet, B. Jager, F. Millet, P. Roussel, L. Tavian & U. Wagner, Specification of eight 2400 W @ 1.8 K refrigeration units for the LHC, Proc. ICEC18, K.G. Narayankhedkar editor, Narosa, New Delhi, India (2000) 207-210.

[89] B. Hilbert, G.M. Gistau-Baguer & F. Dagut, 2.4 kW @ 1.8 K refrigeration units for the LHC project : the Air Liquide system, Proc. ICEC18, K.G. Narayankhedkar editor, Narosa, New Delhi, India (2000) 211-214.

[90] H. Asakura, J. Boesel, T. Honda, A. Kuendig, K. Kurtcuoglu, A. Meier, M. Mori, A.E. Senn & S. Yoshinaga, Four 2400W/1.8 K refrigeration units for CERN-LHC: the IHI/Linde system, Proc. ICEC18, K.G. Narayankhedkar editor, Narosa, New Delhi, India (2000) 215-218.

[91] J.Ph. Guignard, Contribution à l'étude de la stabilité de fonctionnement et de l'adaptation de charge des compresseurs centrifuges cryogéniques multiétages, Travail d'option "Machines-Energétique", Ecole des Mines de Paris (1993).

[92] M. Kauschke, C. Haberstroh & H. Quack, Safe and efficient operation of multistage cold compressor systems, Adv. Cryo. Eng. 41A (1996) 931-926.

[93] F. Minot, B. Gravil, A. Bocquillon, C. Dugas, D. Henry, J.L. Maréchal, S. Nicollet, P. Prochet, J.P. Serries & R. Simon, Problems encountered with subatmospheric circuits on the Tore Supra cryogenic system, Proc. ICEC17, D. Dew-Hughes, R.G. Scurlock & J.P. Watson editors, IoP Publishing (1998) 609-612.

[94] S. Claudet, Ph. Lebrun & L. Tavian, Towards cost-to-performance optimisation of large superfluid helium refrigeration systems, Proc. ICEC18, K.G. Narayankhedkar editor, Narosa, New Delhi, India (2000) 203-206.

ELEMENTS OF BIBLIOGRAPHY

F. London, Superfluids, Volume II, Macroscopic theory of superfluid helium (John Wiley & Sons, 1954, republished by Dover, New-York, 1964).

J. Wilks, The properties of liquid and solid helium (Clarendon Press, Oxford, 1967).

S.W. van Sciver, Helium cryogenics (Plenum Press, New-York, 1986).

J. Wilks & D.S. Betts, An introduction to liquid helium (Clarendon Press, Oxford, 1987).

Proceedings of the CERN Accelerator School "Superconductivity in particle accelerators", CERN Report 89-04 (1989).

Proceedings of the symposium "A half century of superfluid helium", Adv. Cryo. Eng. <u>35A</u> (1990) 1-93.

Proceedings of the CERN Accelerator School "Superconductivity in particle accelerators", CERN Report 96-03 (1996) .